Astrophysical Plasmas

Steven J. Schwartz, Christopher J. Owen[1], and David Burgess
Astronomy Unit, Queen Mary, University of London
London E1 4NS, U.K.

19 November 2002; last revision 4 January 2004

[1]now at Mullard Space Science Laboratory, Holmbury St. Mary, Surrey, RH5 6NT

Contents

Preface

This book accompanies the MSc course by the same name offered as part of the Queen Mary MSc in Astrophysics. The course consists of 12 two-hour lectures. The material is aimed at a broad audience and, while somewhat theoretical in nature, tries to familiarise students with fundamental plasma processes and their astrophysical applications; some undergraduate mathematics, notably vector calculus, and physics (mechanics, fluids, and electromagnetism) are required, though these are reviewed where they are needed.

The course has evolved over the years from an original one taught by SJS, then taken over by DB, then CJO, before returning to SJS and extended from 6 to 12 lectures. The text and problems originated from printed notes devised by DB which were developed further by CJO during his tenure. SJS is responsible for the additional material and for the present re-drafting of the text and production via LaTeX into an online version. Many figures have become separated from their sources; others have been taken from several good web-sites (e.g., outreach pages of NASA), courses at other universities, the books listed in subsequent pages and/or re-drawn by us. The lack of proper source recognition in this first attempt at an online text is unforgiveable and we apologise most profusely.

In 12 weeks one cannot possibly do justice to the physics which governs 50-95% of the universe (depending on your belief in dark matter!). Perhaps the most serious crime is the non-relativistic treatment of particles, fields, and flows. While this excludes topics such as radiation from plasmas and relativistic jets, most of the important phenomena are well described, at least qualitatively, by this non-relativistic treatment; in many cases the net effect is merely to replace the mass by the relavististic mass. The simplification of most of the derivation allows more topics to be introduced, and enables a rather short course to touch on nearly all topics. Other notable omissions include collision theory and the rich and intriguing area of kinetic plasma astrophysics.

I am indebted to my colleagues for their efforts in drafting the early attempts at a text, and accept full responsibilities for the many errors which will pervade this first translation and enlargement. Many students over the years have posed questions or comments which have contributed to the evolution of the course.

I hope this text succeeds in communicating at least some of the fascination the plasma state holds for astrophysicists. Plasmas are everywhere, and the consequences of electromagnetic effects on particles and flows are omitted at your peril. Perhaps you will gain the insight to pose my favorite and infamous question “But what about the magnetic field ?” at the next seminar you attend and then sit back and watch the speaker’s ensuing angst as they struggle to figure out if you’ve found some fatal flaw!

SJS
August 2002

Chapter 1

Introduction and Overview

This text is a brief introduction to basic plasma physics and its applications to astrophysics. Due to the interests of the authors, there is particular emphasis on solar system plasma physics, although many of the concepts are readily applicable to the wider field. Plasmas are electrified gases in which the atoms have become dissociated into negatively charged electrons and positively charged ions. It is estimated that 99% of the (visible) universe is in the plasma state. In that sense, it is the most important of the 4 states of matter.

SI units will be used throughout, but be warned that much of astrophysical literature is written even now in cgs. This is particularly troublesome for plasma physics because of the frequent appearance of constants like ε_0 and μ_0 (in SI units) which replace the fundamental constant c and geometric factor 4π in the cgs system.

Because of the nature of plasma physics, this text is somewhat theoretical in nature. The mathematics will be kept simple, but some vector calculus will be used. However, most of the concepts do not rely on this level of mathematical ability. Vectors are denoted in **boldface** type, e.g., $\mathbf{B}$, while the magnitude of a vector will be given in normal italic maths type, e.g., $B \equiv |\mathbf{B}|$. Unit vectors are denoted by a carat, e.g., $\hat{b}$.

Additionally, we will need draw on various concepts from general physics, including Newton's Laws of motion, some thermodynamics, fluid dynamics and electrodynamics. It is this interplay between the various (classical) branches of physics that makes plasma physics so interesting.

Other texts abound, and may suit your tastes or interests or otherwise cover material not presented here. If you want one (affordable) book on Plasma Physics then consider Dendy. If you want one book about Space Plasma Physics then try Parks (but it costs about £40) or Kivelson and Russell ($\sim$ £30). Many of the books which have titles such as "Plasma Astrophysics" are, in fact, quite specialized and at an advanced level, and so are only recommended if you wish to study beyond the level we will address here. The following is an out-of-date sampling of good books:

- M.G. Kivelson and C.T. Russell (Editors), Introduction to Space Physics, Cambridge University Press, 1995. Available in paperback.
- G.K. Parks, Physics of Space Plasmas, Addison-Wesley 1991. Quite good. Covers a lot of material, but misses details sometimes. Only available in hardback.
- R.O. Dendy, Plasma Dynamics, Oxford, 1990. Good. Available in paperback.
- P.A. Sturrock, Plasma Physics, Cambridge 1994. Good, but frustratingly in cgs units!. Available in paperback.
- Chen, Introduction to Plasma physics, Plenum 1974. Good, but oriented mainly to laboratory plasmas.

- Cairns, Plasma Physics, Blackie (1985) (avail. in paper back) A bit brief in places, but fairly comprehensive and readable.
- Boyd and Sanderson, Plasma Dynamics, Nelson (sadly out of print, cgs, but very good)
- Clemmow and Dougherty, Electrodynamics of Particles and Plasmas, Addison Wesley 1969 (very thorough and mathematical treatment)
- Nicholson, Introduction to Plasma Theory, Wiley.
- Parker, Cosmical Magnetic Fields, Clarendon Press, 1979. Advanced.
- E.R. Priest, Solar Magnetohydrodynamics, Reidel, 1984. Exactly what the title says, and well-written by the country's leading advocate.
- E.R. Priest (editor), Solar System Magnetic Fields, Reidel, 1985. A nice collection of articles from a summer school and covering a range of topics.
- Schmidt, Physics of High Temperature plasmas, Academic Press, 1966 (covers the right topics, but a bit old now, and biased to laboratory plasmas)
- Choudhuri, Arnab Rai, The physics of fluids and plasmas: an introduction for astrophysicists, Cambridge University Press, 1999. (A thorough treatment of everything from neutral fluids and gas dynamics through turbulence, plasma kinetics, MHD, etc. and aimed at astrophysicists. Suffers only from being in cgs units.)

Chapter 2

Some Basic Concepts

2.1 What is a Plasma?

A plasma is a quasi-neutral gas consisting of positively and negatively charged particles (usually ions and electrons) which are subject to electric, magnetic and other forces, and which exhibit collective behaviour.

Ions and electrons may interact via short range atomic forces (during collisions) and via long range electro-magnetic forces due to currents and charges in the plasma. (Gravitational forces may also be important in some applications.) The long range nature of the electromagnetic forces means that plasma can show collective behaviour, for example, oscillations, instabilities, etc.

Plasmas can also contain some neutral particles (which interact with charged particles via collisions or ionization). Examples include the Earth's ionosphere, upper atmosphere, interstellar medium, molecular clouds, etc.

The simplest plasma is formed by ionization of atomic hydrogen, forming plasma of equal numbers of (low mass) electrons and (heavier) protons.

2.2 Plasmas in the Universe

Most of the (visible) universe is in form of plasma: plasmas form wherever temperatures are high enough, or radiation is strong enough, to ionize atoms. The realm of plasma physics covers a wide range of parameter space. For example, Figure 2.1 shows various plasma populations as a function of electron density and temperature. Note that the density scale covers some 30 orders of magnitude, the temperature scale about 10 orders of magnitude.

Some examples of astrophysical plasmas are listed below:

- Earth's (and other planets') ionosphere (above 60 km) and magnetosphere
- Sun's and other stars' atmospheres, and winds
- Comets
- Cosmic Rays (galactic and extra-galactic energetic particles)
- Interstellar medium
- Jets in active galaxies - radio jets and emission
- Pulsars and their magnetosphere

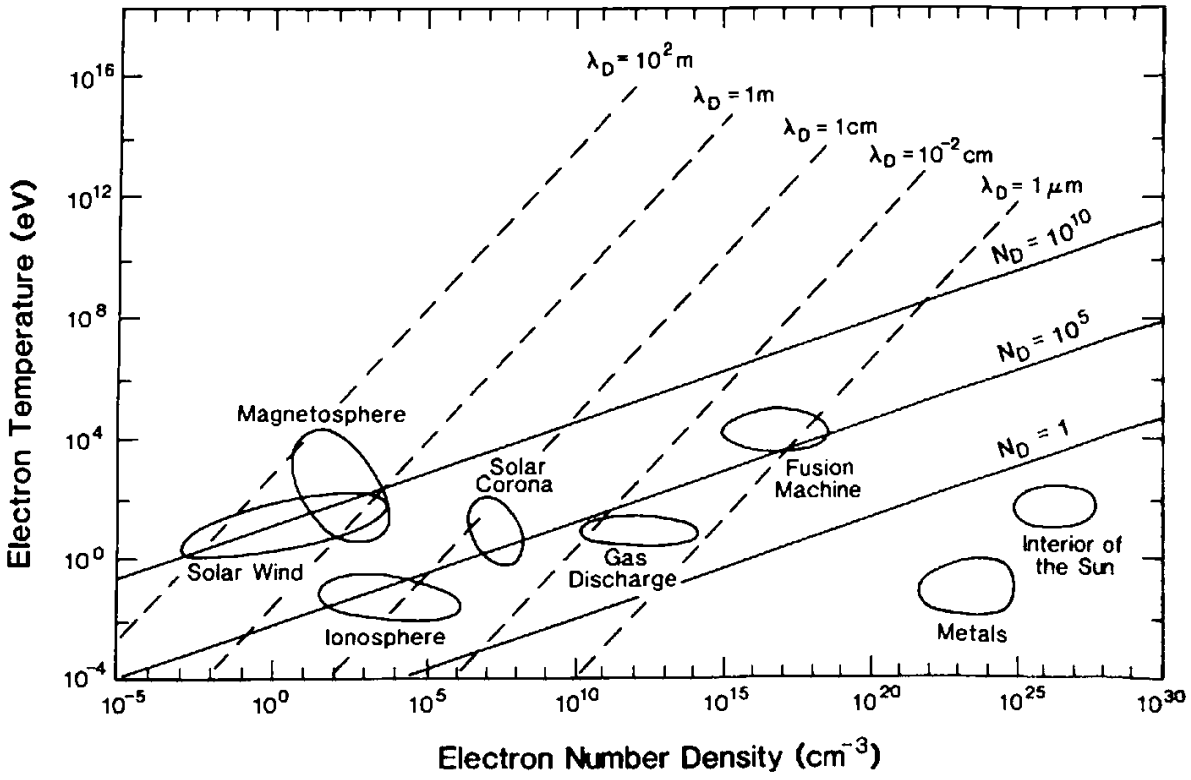

Figure 2.1: The realm of plasma physics.

- Accretion disks around stars

We will be looking at some applications of basic plasma physics to astrophysical plasmas. However, we will concentrate on examples from our "local" corner of the universe! This is because: The Sun is our nearest star and we can study it in great detail; and spacecraft have been exploring the local plasma environment (Earth's magnetosphere, solar wind, magnetospheres of other planets, comets, etc.) for over 30 years. Spacecraft can return in situ observations of an astrophysical plasma (electromagnetic fields, plasma density, temperature, kinetic particle distributions, flows, waves of all sorts and frequencies) - an astrophysical plasma laboratory in our own backyard!

2.3 Different ways of describing plasmas

Exact The most "exact" way to specify the state of a plasma is to give the positions and velocities of all the particles and all the fields at all points in space. For a system of N particles, the particle description would be a phase space of $6N$ dimensions (each position and velocity has 3 components). (Phase space is the combination of configuration space, i.e., ordinary position, and velocity space.) However, N is too large to use this description: $\sim 10^{15}$ in a 1km cube in the interplanetary medium.

Distribution Function The statistical approach is to use a distribution function as a function of position, velocity: $f(\mathbf{x},\mathbf{v})$ in a 6 dimensional phase space (f is also in general a function of time). The number of particles in an elemental volume at position $(\mathbf{x},\mathbf{v})$ in phase space is then given by:

$f(\mathbf{x},\mathbf{v})d^3xd^3v$. The theory of the evolution of the distribution function is known as plasma kinetic theory, and is the best, but most difficult approach to use.

MHD Another (simpler) approach is to treat the plasma as a conducting fluid, and adapt the equations of fluid dynamics to include the effects of electric and magnetic forces. The resulting theory in its simplest (one-fluid) form, is called MagnetoHydroDynamics, or MHD. MHD can be derived from the kinetic theory, in certain limits, but this involves averaging out almost all the interesting kinetic effects. MHD is applicable to most astrophysical plasmas, but many interesting effects cannot be adequately described using MHD and require either a multi-fluid approach or kinetic theory. We will discuss MHD in Chapter 4.

Of course, whatever the description of the plasma matter, we still need to know the electromagnetic fields as functions of time and space.

2.4 Governing Equations

Most astrophysical plasmas are of low density, and so quantum-mechanical effects can be neglected; plasmas are dominated by long range forces.

2.4.1 Maxwell's Equations

$$\nabla\times\mathbf{E} = -\frac{\partial\mathbf{B}}{\partial t} \tag{2.1}$$

$$\nabla\times\mathbf{B} = \mu_0\mathbf{j}+\frac{1}{c^2}\frac{\partial\mathbf{E}}{\partial t} \tag{2.2}$$

$$\nabla\cdot\mathbf{E} = \frac{\rho_q}{\varepsilon_0} \tag{2.3}$$

$$\nabla\cdot\mathbf{B} = 0 \tag{2.4}$$

where $\mu_0\varepsilon_0 = 1/c^2$, ρ_q is the charge density, and $\mathbf{j}$ is the current density.

Maxwell's equations can also be given in terms of electric displacement $\mathbf{D}$ and magnetic induction $\mathbf{H}$. In the case of the plasmas we are considering, individual particles contribute to the charge density and electric currents as though they move in a vacuum, so that $\mathbf{D}=\varepsilon_0\mathbf{E}$ and $\mathbf{B}=\mu_0\mathbf{H}$.

2.4.2 Conservation of Charge

In the absence of ionization or recombination, then one also has:

$$\nabla\cdot\mathbf{j}+\frac{\partial\rho_q}{\partial t}=0 \tag{2.5}$$

2.4.3 Lorentz Force

Force on single particle of charge q and velocity $\mathbf{v}$:

$$\mathbf{F}=q(\mathbf{E}+\mathbf{v}\times\mathbf{B}) \tag{2.6}$$

For an extended medium there is a force density of $\rho_q\mathbf{E}+\mathbf{j}\times\mathbf{B}$

2.4.4 Magnetohydrodynamics (MHD)

The derivation of the MHD equations will be covered in Chapter 4, but reduce to straightforward fluid equations:

$$\frac{\partial \rho}{\partial t} + \nabla \cdot (\rho \mathbf{V}) = 0 \tag{2.7}$$

$$\rho \left(\frac{\partial}{\partial t} + \mathbf{V} \cdot \nabla \right) \mathbf{V} = -\nabla p + \frac{1}{\mu_0} (\nabla \times \mathbf{B}) \times \mathbf{B} \tag{2.8}$$

$$\left(\frac{\partial}{\partial t} + \mathbf{V} \cdot \nabla \right) \left(p \rho^{-\gamma} \right) = 0 \tag{2.9}$$

$$\frac{\partial \mathbf{B}}{\partial t} = \nabla \times (\mathbf{V} \times \mathbf{B}) + \frac{1}{\mu_0 \sigma} \nabla^2 \mathbf{B} \tag{2.10}$$

$$\mathbf{E} + \mathbf{V} \times \mathbf{B} = \mathbf{j}/\sigma \tag{2.11}$$

where σ is the electrical conductivity.

2.4.5 Kinetic Theory

The evolution of the distribution function $f_\alpha(\mathbf{x}, \mathbf{v}, t)$ for particles of species α in space and time in the absence of collisiones is called the Vlasov Equation:

$$\frac{\partial f_\alpha}{\partial t} + \mathbf{v} \cdot \nabla \mathbf{f}_\alpha + \frac{\mathbf{q}_\alpha}{\mathbf{m}_\alpha} (\mathbf{E} + \mathbf{v} \times \mathbf{B}) \cdot \frac{\partial \mathbf{f}_\alpha}{\partial \mathbf{v}} = 0 \tag{2.12}$$

coupled with Maxwell's Equations (Section 2.4.1) in which the charge and current densities are determined from the particle distributions as

$$\rho_q = \sum_\alpha \iiint_V q_\alpha f d^3 v \tag{2.13}$$

$$\mathbf{j} = \sum_\alpha \iiint_V q_\alpha \mathbf{v} f d^3 v \tag{2.14}$$

This multi-dimensional coupled system of integro-partial differential equations is obviously not easy to solve, but does display the scope for a rich variety and complexity of plasma phenomena. This approach is largely beyond the scope of the present text.

2.4.6 Frame transformations

The electric and magnetic fields **E** and **B** are frame dependent quantities and so in order to transform between frames the appropriate (relativistic) Lorentz transformation has to be used.

Consider a 'laboratory' coordinate frame in which the fields are **E** and **B**. Consider now the fields $\mathbf{E}'$ and $\mathbf{B}'$ in another frame which is moving relative to the first at a velocity **u**. Then the fields in the moving frame are given by:

$$\mathbf{E}'_\parallel = \mathbf{E}_\parallel \tag{2.15}$$

$$\mathbf{B}'_\parallel = \mathbf{B}_\parallel \tag{2.16}$$

$$\mathbf{E}'_{\perp} = \frac{\mathbf{E}_{\perp} + \mathbf{u} \times \mathbf{B}}{\sqrt{1-(u^2/c^2)}} \tag{2.17}$$

$$\mathbf{B}'_{\perp} = \frac{\mathbf{B}_{\perp} - \dfrac{\mathbf{u} \times \mathbf{E}}{c^2}}{\sqrt{1-(u^2/c^2)}} \tag{2.18}$$

where $\|$ denotes the component parallel to the transformation velocity $\mathbf{u}$ and $\perp$ the components perpendicular to $\mathbf{u}$. Often $u^2 \ll c^2$, and over sufficiently large scales the natural electrostatic fields are small, and so in this case: $\mathbf{E}' \approx \mathbf{E} + \mathbf{u} \times \mathbf{B}$ and $\mathbf{B}' \approx \mathbf{B}$ (i.e., magnetic fields are approximately absolute, but electric fields are not). In the simple case where $\mathbf{E}$, $\mathbf{B}$, and $\mathbf{u}$ are mutually perpendicular, Equations 2.15 and 2.16 show that this property is retained in the primed frame. Conversely, while it is possible to transform away the perpendicular electric field, say, by choosing $\mathbf{u}$ such that $\mathbf{u} \times \mathbf{B} = -\mathbf{E}_{\perp}$, any component of $\mathbf{E}$ parallel to this $\mathbf{u}$ will remain.

2.5 Some Basic Plasma Phenomena

As a simple introduction to an example of plasma collective behaviour we will consider how a plasma tries to stay charge neutral, over which scales it succeeds, and the associated characteristic frequency.

2.5.1 Plasma oscillations

Consider a plasma with equal numbers of positively and negatively charged particles. At sufficiently large distances this produces a vanishingly small electric field, since all the contributions from positive and negative charges cancel. The compensation is only statistical since all the particles will have random thermal velocities. On small scales one expects there to be local breakdowns in charge neutrality.

But, since plasmas consist of positive and negative charges, and opposite charges attract, then any departure from charge neutrality leads to a restoring force back towards charge neutrality. This restoring force leads to a natural oscillation of the plasma, which are called plasma oscillations and occur at a frequency called the plasma frequency.

In a plasma consisting of electrons and ions, the electrons move much more rapidly than the ions, so they are mostly responsible for this oscillation. In this case consider the following simple model, sketched in Figure 2.2: the ions are fixed, and the electrons have no thermal motion. A single, planar slab (thickness L) of electrons is displaced a distance Δx in the x direction (we assume that $\Delta x \ll L$). If the particle number density is uniform $n_e = n_i = n_0$, then this displacement produces two charge sheets (of opposite sign) with charge per unit area of $\sigma = en_0\Delta x$, separated by distance L. This is like a parallel plate capacitor, with a resulting electric field $E = \sigma/\varepsilon_0 = en_0\Delta x/\varepsilon_0$ (from Poisson's equation).

The electron slab has mass per unit area of $m_e n_0 L$, charge per unit area of $-en_0 L$ and is subject to the electric field E. Thus equation of motion for the displace Δx of the electron sheet is (from $F = ma$):

$$(-en_o L)E = m_e n_0 L \frac{d^2\Delta x}{dt^2} \tag{2.19}$$

or

$$\frac{d^2\Delta x}{dt^2} = -\omega_{pe}^2 \Delta x \tag{2.20}$$

which is equation for simple harmonic motion at an (angular) frequency ω_{pe}^2. The oscillations are called electron plasma oscillations and the frequency is one of the most important characteristic frequencies of a plasma.

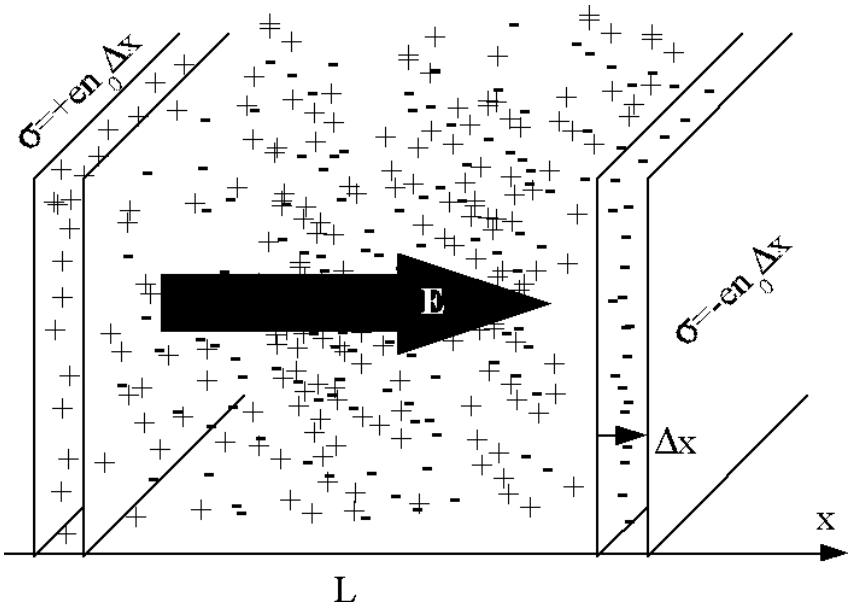

Figure 2.2: The displacement of a slab of electrons establishes an electric field which tries to return the electrons, leading to plasma oscillations.

$$\text{Electron Plasma Frequency} \qquad \omega_{pe}^2 = \frac{n_0 e^2}{m_e \varepsilon_0} \tag{2.21}$$

Plasma oscillations are a direct result of the plasma trying to maintain charge neutrality. They are independent of the "wavelength" L of the oscillation, unlike, e.g., sound or light waves. One finds that $f_{pe}(kHz) \equiv \omega_{pe}/2\pi \approx 9\sqrt{n_e(cm^{-3})}$. In the Solar System f_{pe} changes from many Mhz in the corona, to $\sim$ 50kHz at the orbit of the Earth, to $<$ 1kHz far from the Sun.

Plasma oscillations can be driven by the natural thermal motions of the electrons (thermal noise at the plasma frequency). In this case one can equate the work done by moving the electron sheet through a distance Δx by integrating $\int_0^{\Delta x} eE(x)\,dx = \int_0^{\Delta x} \frac{e^2 n_0 x}{\varepsilon_0}\,dx$ with the average energy in thermal agitation in the x direction

$$\frac{e^2 n_0 \Delta x^2}{2\varepsilon_0} \approx \frac{1}{2} k_b T \tag{2.22}$$

where T is temperature and k_b is Boltzmann constant. Consequently the maximum distance that the electron sheet can move due to thermal agitation is $\Delta x_{max} = \lambda_D$ where:

$$\text{Debye Length} \qquad \lambda_D = \sqrt{\frac{\varepsilon_0 k_b T}{e^2 n_0}} \tag{2.23}$$

The Debye length is the spatial scale over which charge neutrality is violated by spontaneous fluctuations in plasma. In order for a charged gas to show collective behaviour (i.e. to be considered a plasma) the Debye length must be much smaller than the spatial scale of the system (i.e. $\lambda_D \ll L$). In addition, the number of particles, N_D, within the Debye "sphere" (i.e., a sphere of radius λ_D) must be large ($N_D \gg 1$).

Debye Number	$N_D = n_0 \lambda_D^3$	(2.24)

For interplanetary space, λ_D is of the order of a few metres, and a few cm in the solar corona; the number of particles in a Debye sphere, $N_D \sim 10^8$ in each case. Some lines of constant Debye length, λ_D, and number of particles in the Debye sphere, N_D, were plotted in Figure 2.1.

(Note that there is a third condition for a charged gas to be considered a plasma - that the collision frequency with neutral particles is small compared to the plasma frequency. If this is not satisfied the gas behaves as if it were a neutral gas.)

2.5.2 Charge Shielding

One can approach the question of the plasma restoring itself to quasi-neutrality from another direction: namely, by asking how an initially charge neutral plasma responds to a test (fixed) charge, and calculating the electric potential ϕ in the plasma as a result of this additional charge. In vacuum the potential of the charge would just fall off as $1/r$, i.e., ($\phi = q/(4\pi\varepsilon_0 r) = A/r$. However, in a plasma the charge balancing forces result in a redistribution of the plasma charges, so that the potential has the form:

$$\phi = \frac{A}{r} e^{-r/\lambda_D} \tag{2.25}$$

Thus the effect of the test charge (i.e., the electrostatic potential it induces) falls off faster than it would in vacuum. This effect is called charge shielding, and one sees that the test charge is effectively screened out beyond $r \sim \lambda_D$. For charge shielding to be effective there must be sufficient particles in a Debye sphere, i.e., $N_D \gg 1$.

2.5.3 Collisions, Mean Free Path, and Collisionless Plasmas

Neutral particles have quite small collision cross sections (effective size as seen by another particle) because they only interact via short range forces (electron shells have to overlap). But for charged particles the Coulomb force is long range, so collisions in a plasma are in reality a lot of small angle deflections, rather than a few large angle changes.

(What follows are some order of magnitude arguments…)

Consider an ionized hydrogen plasma. Electrical and thermal conductivity is effectively controlled by electrons (because they are so much more mobile - higher thermal speed - than ions), and their interaction frequency with ions. Suppose a plasma has temperature T, and the ions are effectively at rest with respect to the electrons. The thermal energy of an electron is $3k_bT/2$. An electron will be affected by a neighbouring ion if the Coulomb potential is of the order (or more than) the electron thermal energy. This defines a Coulomb interaction distance, r_C:

$$\frac{q^2}{4\pi\varepsilon_0 r_C} \approx \frac{3}{2} k_b T \tag{2.26}$$

And we can define an effective Coulomb cross-section,

$$\sigma_C = \pi r_C^2 \approx \pi \left(\frac{q^2}{6\pi k_b \varepsilon_0} \right)^2 \frac{1}{T^2} \tag{2.27}$$

At $T = 10^6$K (typical of the solar wind plasma) this gives $\sigma_C \sim 10^{-22} m^2$ which is much larger than the nuclear cross-section of $10^{-30} m^2$. (N.B.: this is an order of magnitude estimation only since we haven't taken account of charge shielding!)

Consider a particle A moving at speed v in a gas of particles B which are assumed at rest, with number density n, and σ is the collision cross-section for A on B. Suppose that after a collision A is sent off in a random direction.

The collision frequency is given by $\sigma v n$ (= number of particles in a cylinder of cross sectional area σ and length vt divided by the time t taken to traverse the cylinder) so that the mean time between collisions is simply $1/(\sigma v n)$. So the mean distance travelled by A between collisions, referred to as the mean free path λ_{mfp} is:

$$\lambda_{mfp} = \frac{1}{\sigma n} \tag{2.28}$$

Obviously one can increase λ_{mfp} by decreasing n or (for Coulomb interactions) increasing T. It is possible that λ_{mfp} becomes greater than the size of the system, and in this case the plasma is collisionless, i.e., there is no appreciable energy or momentum transfer via collisions. For example, in the case of solar wind particles they experience only about one collision on their journey from the Sun to the radius of the Earth's orbit.

In many astrophysical systems the plasma is collisionless (because of low densities and high temperatures). The motion of particles is then governed by the behaviour of the particles in the large scale (global) fields.

2.6 Exercises

1. The solar wind at 1AU is a fully ionised proton-electron plasma with density ~ 5 particles/cm^3 and an electron energy ~ 3eV. Calculate the electron temperature in Kelvin, the Debye length λ_d, Debye number N_D, and plasma frequency ω_{pe}. [Be careful with units. We've used traditional units rather than SI ones here. 1eV $\equiv$ 1 electron Volt $= 1.6e^{-19}$ Joules.]

2. A hydrogen plasma consists of protons and electrons with densities $n_p = n_e = n_0$. The electrons can be considered to be free to move while the ions are considered fixed on a uniform grid due to their relatively slower thermal motion. A point test charge q is placed in the plasma and establishes a resulting potential ϕ, the charged shielded Coulomb potential given in Equation 2.25

$$\phi = \frac{A}{r} e^{-r/\lambda_d}$$

If the electron population has temperature T, they can be expected to be distributed in a potential according to the Boltzmann factor $n_e(r) = n_0 e^{-(-e\phi/k_b T)}$. Assuming $|e\phi/k_b T| \ll 1$, expand this expression for $n_e(r)$ to find an expression for the net charge density $\rho_q(r) = e n_p - e n_e(r)$ and use this to show that the potential $\phi(r)$ is consistent with Poisson's equation $\nabla^2\phi = -\rho_q/\varepsilon_0$. (Use the spherical polar form of the Laplacian $\nabla^2\phi = \frac{1}{r^2}\frac{\partial}{\partial r}\left(r^2\frac{\partial\phi}{\partial r}\right) + \frac{1}{r^2\sin\theta}\frac{\partial}{\partial\theta}\left(\sin\theta\frac{\partial\phi}{\partial\theta}\right) + \frac{1}{r^2\sin^2\theta}\frac{\partial^2\phi}{\partial\phi^2}$ with spherical symmetry.)

3. Consider again the plasma oscillation problem posed in Section 2.5.1 and sketched in Figure 2.2 but in which the ions of mass m_i are also free to move. Denoting the electron and ion displacements by Δx_e and Δx_i respectively, find the *net* surface charge density σ due to these displacements. Write down the separate equations of motion for the ion and electron slabs and show that they can be combined to give a single equation of motion for the difference between the two displacements. Find the frequency of oscillation of this difference. Your answer should reduce in the limit $m_i \gg m_e$ to ω_{pe}.

Chapter 3

Individual Particle Motion

3.1 Equation of Motion

Individual particle motion can have direct applications in collisionless plasmas, but it also underlies a lot of the kinetic theory of collective plasma behaviour.

Consider a charged particle, mass m and charge q, moving with velocity $\mathbf{v}$ in a given electro-magnetic field. We will neglect collisions, gravitational and any other forces, and only consider non-relativistic motion $v \ll c$. The equation of motion then follows from the Lorentz force:

$$m\frac{d\mathbf{v}}{dt} = q\left(\mathbf{E} + \mathbf{v} \times \mathbf{B}\right) \tag{3.1}$$

From this simple equation a wide range of behaviours is possible depending on the nature of $\mathbf{E}$ and $\mathbf{B}$ in space and time.

3.2 Motion in uniform, static magnetic field

(In this section we do not solve the equation of motion directly, but use it to determine the type of motion.)

Consider case where $\mathbf{E} = \mathbf{0}$ and $\mathbf{B}$ is uniform (same everywhere in space) and static (unchanging in time). The equation of motion becomes:

$$m\frac{d\mathbf{v}}{dt} = q\mathbf{v} \times \mathbf{B} \tag{3.2}$$

The force on the particle is perpendicular to $\mathbf{v}$ and $\mathbf{B}$, so the magnetic force can do no work on the particle (rate of work done by a force $\mathbf{F}$ in moving something at a velocity $\mathbf{v}$ is $\mathbf{v} \cdot \mathbf{F}$). So, the kinetic energy of the particle must be constant.

Check by dotting with $\mathbf{v}$:

$$m\mathbf{v} \cdot \frac{d\mathbf{v}}{dt} = \mathbf{v} \cdot (q\mathbf{v} \times \mathbf{B}) \quad \Rightarrow \frac{d}{dt}\left(\frac{1}{2}mv^2\right) = 0 \tag{3.3}$$

using $\mathbf{v} \cdot \mathbf{v} = v^2$, and the vector identity $\mathbf{A} \cdot (\mathbf{A} \times \mathbf{B}) = 0$. Hence the kinetic energy $W \equiv \frac{1}{2}mv^2$ is constant in time.

Examine the change in $\mathbf{v}$ by resolving it into two parts: parallel and perpendicular to $\mathbf{B}$:

$$\mathbf{v} = v_{\parallel}\hat{b} + \mathbf{v}_{\perp} \tag{3.4}$$

where $v_\parallel = \mathbf{v}\cdot\mathbf{B}/B$ and $\hat{b}$ is a unit vector in the direction of $\mathbf{B}$. Then the dotting Equation 3.2 with $\hat{b}$ yields

$$m\frac{dv_\parallel}{dt} = 0 \tag{3.5}$$

while the perpendicular part of Equation 3.2 reduces to (recalling $\hat{b}\times\mathbf{B} = \mathbf{0}$)

$$m\frac{d\mathbf{v}_\perp}{dt} = q\mathbf{v}\times\mathbf{B} \equiv q\mathbf{v}_\perp\times\mathbf{B} \tag{3.6}$$

Thus, $v_\parallel = constant$, and from $W = \frac{1}{2}m\left(v_\parallel^2 + v_\perp^2\right) = constant$, it follows that $\mathbf{v}_\perp$ changes only in direction, not magnitude. The acceleration is centripetal, and the particle will execute uniform circular motion in the plane perpendicular to the magnetic field direction.

Suppose that the radius of motion is r_L. Then the radial equation of motion is (balancing radial acceleration for constant speed against the perpendicular magnetic force)

$$\frac{mv_\perp^2}{r_L} = |qv_\perp B| \tag{3.7}$$

so the radius of gyration, known as the Larmor radius

Larmor radius	$r_L = \dfrac{mv_\perp}{\lvert q\rvert B}$	(3.8)

In one gyration the particle travels distance $2\pi r_L$ at speed $v_\perp$, so the angular frequency of gyration is:

Cyclotron (or Gyro-) Frequency	$\Omega_c = \dfrac{qB}{m}$	(3.9)

The cyclotron frequency is one of the most important plasma characteristic frequencies, and is indicative of the field strength and the charge and mass of the particles in the plasma. The cyclotron frequency is independent of the particle energy. A plasma could have several cyclotron frequencies corresponding to the different species of the constituent particles, but all particles of the same q/m ratio have the same cyclotron frequency. [For relativistic particle motion, this is no longer true as the relativistic mass replaces m in Ω_c.]

The cyclotron frequency Ω_c is usually left as a signed quantity, thereby indicating the sense of rotation. The sense of gyration is such that the force $q\mathbf{v}\times\mathbf{B}$ points to the centre of gyration. Particles of opposite signs gyrate in opposite directions. Electrons follow a RH rotation sense with respect to $\mathbf{B}$, as shown in Figure 3.1.

Particles can have cyclotron motion due to their thermal velocities. For a plasma with electrons and ions of similar temperatures the electron Larmor radius is much smaller than the ion Larmor radius, by the ratio $\sqrt{m_e/m_i}$. This is important when deciding whether a phenomenon (with a given scale size) is associated with the electrons or the ions.

Knowing the parallel and perpendicular motion we can now describe the overall motion: In a static, uniform magnetic field, a charged particle moves along the magnetic field direction at uniform speed while gyrating around the field at a frequency Ω_c, with a radius of gyration r_L. This combined motion is a HELIX of constant pitch along $\mathbf{B}$.

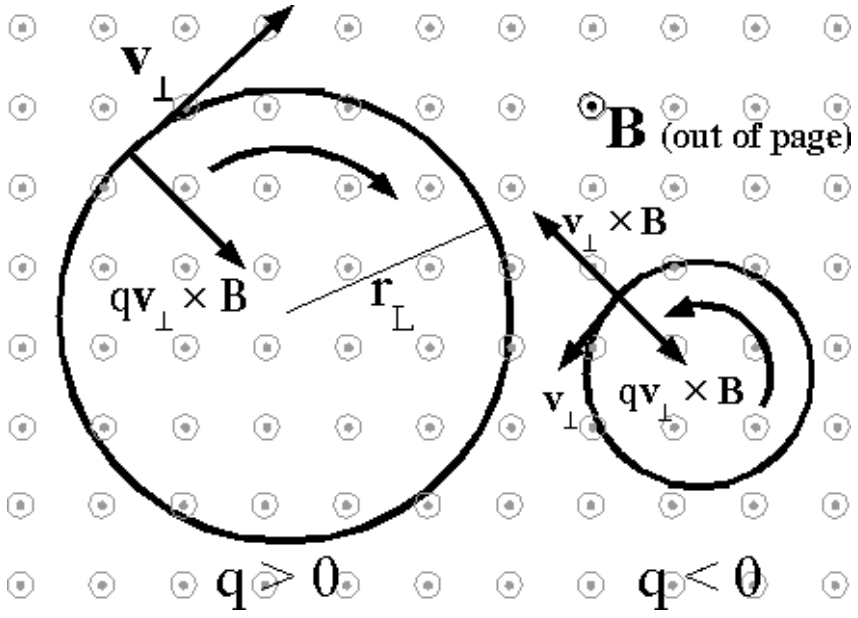

Figure 3.1: Cyclotron motion in a uniform magnetic field for positive and negative charges

3.3 Motion in uniform, static magnetic and electric fields

3.3.1 Qualitative Treatement

In this section we will see the combined effect of a magnetic and electric field. At first we will examine the type of motion, and then we will show a mathematical solution of the equation of motion.

Consider first the motion of the particle associated with the perpendicular (to **B**) components of the electric field, i.e., $\mathbf{E}_\perp$. From the Lorentz transformation (Section 2.4.6) for **E** and **B**, we can transfer to another frame, moving at velocity $\mathbf{v}_D$ perpendicular to **B**, in which the magnetic field is unchanged, but the electric field is given by

$$\mathbf{E}'_\perp = \mathbf{E}_\perp + \mathbf{v_D} \times \mathbf{B} \tag{3.10}$$

This means that by a suitable choice of $\mathbf{v}_D$ we can arrange that $\mathbf{E}'_\perp$ is zero, namely

$$\mathbf{E} \times \mathbf{B} \text{ Drift} \qquad \mathbf{v}_D = \frac{\mathbf{E} \times \mathbf{B}}{B^2} \tag{3.11}$$

(Check by substitution and using the vector identities $(\mathbf{E} \times \mathbf{B}) \times \mathbf{B} = (\mathbf{E} \cdot \mathbf{B})\,\mathbf{B} - (\mathbf{B} \cdot \mathbf{B})\,\mathbf{E}$ and $\mathbf{E} \cdot \mathbf{B} \equiv 0$ here since there is only an $\mathbf{E}_\perp$). We leave the full electric field **E** in Equation 3.11 since any parallel component leaves $\mathbf{v}_D$ unchanged.

In this new frame there is no perpendicular electric field, and so the perpendicular particle motion is just controlled by the magnetic field (which is unchanged by the transformation), and so it is just uniform circular motion, as previously discussed.

Now returning to the original frame, the particle motion will be uniform circular motion about the magnetic field, and a superimposed uniform drift $\mathbf{v}_D$ which has the initially surprising property of being perpendicular to both **E** and **B**. This is known as the **E**-cross-**B** drift velocity, and is sketched in Figure 3.2. Note that particles of opposite charge drift in the same direction at the same speed, a result which follows immediately from the fact that in a frame moving with $\mathbf{v}_D$ the electric field vanishes and

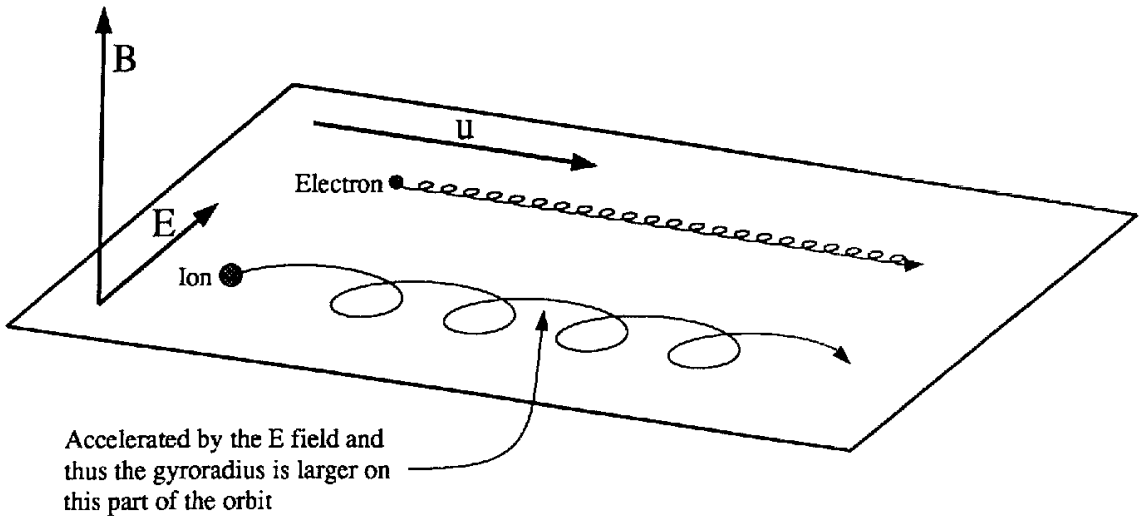

Figure 3.2: $\mathbf{E} \times \mathbf{B}$ drift of particles in steady, uniform electric and magnetic fields

so all particles simply perform cyclotron motion in that frame. The perpendicular motion in the initial frame describes a CYCLOID.

Qualitatively, the $\mathbf{E} \times \mathbf{B}$ drift can be seen without recourse to frame transformations by considering the various portions of the particle gyration around the magnetic field. When a $q > 0$ particle is travelling in roughly the same direction as $\mathbf{E}$ it gets accelerated, increasing its speed. This increasing speed leads to an increasing radius of gyration (see Equation 3.8) over this portion of the orbit (see Figure 3.2). But the magnetic field turns the particle until eventually it is moving against the electric field, so it systematically loses speed and moves in a tighter arc. Over a complete gyration period, the consequence of larger arcs at the top of each orbit shown and smaller arcs around the bottom of each orbit results in a net drift. Negatively charged particles circulate in the opposite sense (Figure 3.1) but *decrease* their speed when moving along $\mathbf{E}$ so perform smaller arcs at the top of each orbit and hence drift in the same direction as $q > 0$ particles. That both categories of particle drift at exactly the same rate is easiest to see via the frame transformation arguments described above.

We now examine the behaviour in detail, to include parallel motion. From our discussion above it seems that the motion can be simplified by splitting the particle motion into two parts: $\mathbf{v} = \mathbf{u} + \mathbf{v}_D$. Then the LHS of the equation of motion 3.1 becomes

$$m\frac{d\mathbf{v}}{dt} = m\frac{d\mathbf{u}}{dt} + m\frac{d\mathbf{v}_D}{dt} \tag{3.12}$$

But the second term is zero, as $\mathbf{v}_D$ is constant, and hence, substituting for $\mathbf{v}$ and $\mathbf{v}_D$, the equation of motion becomes

$$m\frac{d\mathbf{u}}{dt} = q\mathbf{E} + q(\mathbf{u} \times \mathbf{B}) + q\frac{\mathbf{E} \times \mathbf{B}}{B^2} \times \mathbf{B} \tag{3.13}$$

Using the same vector identity as before, $(\mathbf{E} \times \mathbf{B}) \times \mathbf{B} = (\mathbf{E} \cdot \mathbf{B})\mathbf{B} - (\mathbf{B} \cdot \mathbf{B})\mathbf{E}$, this simplifies to

$$\begin{aligned} m\frac{d\mathbf{u}}{dt} &= q\mathbf{E} + q(\mathbf{u} \times \mathbf{B}) + q\left(\frac{\mathbf{E} \cdot \mathbf{B}}{B^2}\right) - q\mathbf{E} \\ &\equiv q(\mathbf{u} \times \mathbf{B}) + q\left(\mathbf{E} \cdot \hat{b}\right)\hat{b} \end{aligned} \tag{3.14}$$

where $\hat{b} \equiv \mathbf{B}/B$ is a unit vector in the direction of **B**. Here the perpendicular components of the **E**-field disappears, leaving only the parallel component via $\mathbf{E} \cdot \mathbf{B}$. We now split **u** into components parallel and perpendicular to **B**

$$m\frac{du_\parallel}{dt} = qE_\parallel \tag{3.15}$$

$$m\frac{d\mathbf{u}_\perp}{dt} = q(\mathbf{u}_\perp \times \mathbf{B}) \tag{3.16}$$

Thus, the first equation implies parallel motion consisting of uniform acceleration driven by the parallel electric field. The second equation, as we have seen already, leads to uniform circular motion perpendicular to the magnetic field.

We can now return to the complete motion described by

$$\mathbf{v} \equiv u_\parallel \hat{b} + \mathbf{u}_\perp + \mathbf{v}_D \tag{3.17}$$

and comprised of, respectively: uniform acceleration parallel to **B** due to any parallel electric field, uniform gyration perpendicular to **B**, and a uniform drift perpendicular to both **E** and **B**.

3.3.2 Mathematical Treatment

We now tackle the same problem by finding a mathematical solution to the equation of motion

$$m\frac{d\mathbf{v}}{dt} = q(\mathbf{E} + \mathbf{v} \times \mathbf{B}) \tag{3.18}$$

Splitting the electric field and velocity into components parallel and perpendicular to **B** one finds

$$m\frac{dv_\parallel}{dt} = qE_\parallel \tag{3.19}$$

$$m\frac{d\mathbf{v}_\perp}{dt} = q(\mathbf{E}_\perp + \mathbf{v}_\perp \times \mathbf{B}) \tag{3.20}$$

Assuming that the magnetic field is aligned with the $\hat{z}$ direction, and that the initial parallel position and speed of the particle are z_0 and $v_{\parallel 0}$, respectively, the solution of the parallel equation of motion is ($v_z \equiv v_\parallel$)

$$v_\parallel = \frac{qE_\parallel}{m}t + v_{\parallel 0} \tag{3.21}$$

and

$$z = \frac{qE_\parallel}{2m}t^2 + v_{\parallel 0}t + z_0 \tag{3.22}$$

This makes it clear how any parallel electric field accelerates particles along the field. Such parallel acceleration is an important mechanism for the acceleration of particles. However, since plasma particles are able to move easily along the field direction, they are able to shield out parallel electric field perturbations. Such electric fields are thus usually small in astrophysical plasmas.

We now solve the perpendicular motion in the case of static, uniform electric and magnetic field. We choose the orthogonal geometry: $\mathbf{B} = (0,0,B)$ and $\mathbf{E} = (E_\perp, 0, 0)$. The equations of motion for x and y

then become

$$\frac{dv_x}{dt} = \frac{\Omega_c E_\perp}{B} + \Omega_c v_y \tag{3.23}$$

$$\frac{dv_y}{dt} = -\Omega_c v_x \tag{3.24}$$

where we have used $\Omega_c = qB/m$. Differentiating the second equation, and using the first, produces

$$\frac{d^2 v_y}{dt^2} + \Omega_c^2 v_y = -\frac{\Omega_c^2 E_\perp}{B} \tag{3.25}$$

This is a second order differential equation which can be solved straightforwardly. (Set RHS to zero to solve for the complementary function, then find the particular integral. The general solution is their sum.)

$$v_y = A\cos(\Omega_c t + \phi) - \frac{E_\perp}{B} \tag{3.26}$$

where A and ϕ are constants specified through the particle initial conditions. Using this expression for v_y in the equation of motion (3.24 one finds:

$$v_x = -A\sin(\Omega_c t + \phi) \tag{3.27}$$

Suppose that the initial velocity ($t = 0$) is $v_\perp = (0, v_{y0})$, then one finds $\phi = 0$, and $A = v_{y0} + E_\perp/B$, yielding

$$v_x = -\left(v_{y0} + \frac{E_\perp}{B}\right)\sin(\Omega_c t) \tag{3.28}$$

$$v_y = \left(v_{y0} + \frac{E_\perp}{B}\right)\cos(\Omega_c t) - \frac{E_\perp}{B} \tag{3.29}$$

One sees that the particle has a gyration motion (set by initial perpendicular velocity) and a uniform drift in the $\hat{y}$ direction, perpendicular to $\mathbf{B}$ and $\mathbf{E}_\perp$, which is the $\mathbf{E} \times \mathbf{B}$ drift. Integrating the equations for v_x and v_y leads to the equations for the particle position.

3.4 Particle Drifts

We have seen that the addition of an electric field (which results in an additional force on the particle) to a magnetic field results in a drift of the guiding centre which is perpendicular to the electric force and the magnetic field. When one considers more general situations, where there is a changing electric field, or non-uniform magnetic fields, one finds that such particle drifts are a very general feature. There are guiding centre drifts associated with gravitational force, electric field, polarization (time-varying electric field), field line curvature, and gradients in the magnetic field strength.

3.4.1 Gravitational Drifts

For example, consider the case where there is a uniform, static magnetic field ($\mathbf{E} = 0$) and the particle is subject to an external force $\mathbf{F}$, e.g., gravity. We can repeat our analysis by defining an effective electric field, $\mathbf{E}_{eff}$, such that

$$\mathbf{F} \equiv q\mathbf{E}_{eff} \tag{3.30}$$

It follows that the motion is again the sum of three parts: acceleration parallel to **B**, gyration perpendicular to **B**, and a uniform drift at velocity $\mathbf{v}_F$ (calculated with $\mathbf{E}_{eff}$), namely

$$\mathbf{v}_F = \frac{\mathbf{F} \times \mathbf{B}}{qB^2} \tag{3.31}$$

since the mathematical equations are identical in form to those presented in Section 3.3.2 The drift is perpendicular to **F** and **B**, and, unlike the $\mathbf{E} \times \mathbf{B}$ drift, depends on the particle charge. So a mixture of particles with different charges, subject an applied force, can produce so-called drift currents because of different drift directions for positive and negative charges.

3.4.2 Curvature Drift

Another type of drift is associated with curvature of the magnetic field lines. In this situation we expect the particle motion to consist of gyration around the field, and motion of the guiding centre along the curved field line, and is illustrated in Figure 3.3. Relative to the field line, the particle feels an effective centrifugal force pushing it away from the centre of curvature. This leads to a drift

$$\mathbf{v}_c = \frac{\mathbf{F_c} \times \mathbf{B}}{qB^2} \tag{3.32}$$

via Equation 3.30.

Now, the centrifugal force is given by

$$\mathbf{F_c} = mv_\parallel^2 \frac{\mathbf{R_c}}{R_c^2} \tag{3.33}$$

where $\mathbf{R_c}$ is the radius of curvature vector (which points away the centre of curvature). If $\hat{b} \cdot \nabla \equiv \partial/\partial s$ is the derivative along a field line, i.e., the rate of change as one moves in the direction $\hat{b} \equiv \mathbf{B}/B$ of **B**, then

$$\begin{aligned} \frac{\mathbf{R_c}}{R_c^2} &= -\frac{\partial}{\partial s}\left(\frac{\mathbf{B}}{B}\right) \\ &= -\frac{1}{B}\frac{\partial \mathbf{B}}{\partial s} + \frac{\mathbf{B}}{B^2}\frac{\partial B}{\partial s} \\ &= -\frac{1}{B^2}(\mathbf{B}\cdot\nabla)\mathbf{B} + \frac{\mathbf{B}}{B^2}\frac{\partial B}{\partial s} \end{aligned} \tag{3.34}$$

We can now substitute this into our expression for the centrifugal force $\mathbf{F_c}$ to yield the following result:

Curvature Drift	$\mathbf{v}_c = \frac{mv_\parallel^2}{qB^4}[\mathbf{B} \times (\mathbf{B}\cdot\nabla)\mathbf{B}]$	(3.35)

where we have changed the order of the cross product to remove the leading minus sign in Equation 3.34 and noted that $\mathbf{B} \times \mathbf{B} = 0$. This drift is in the direction $\mathbf{R_c} \times \mathbf{B}$ for positive particles, and in the opposite direction for negative ones.

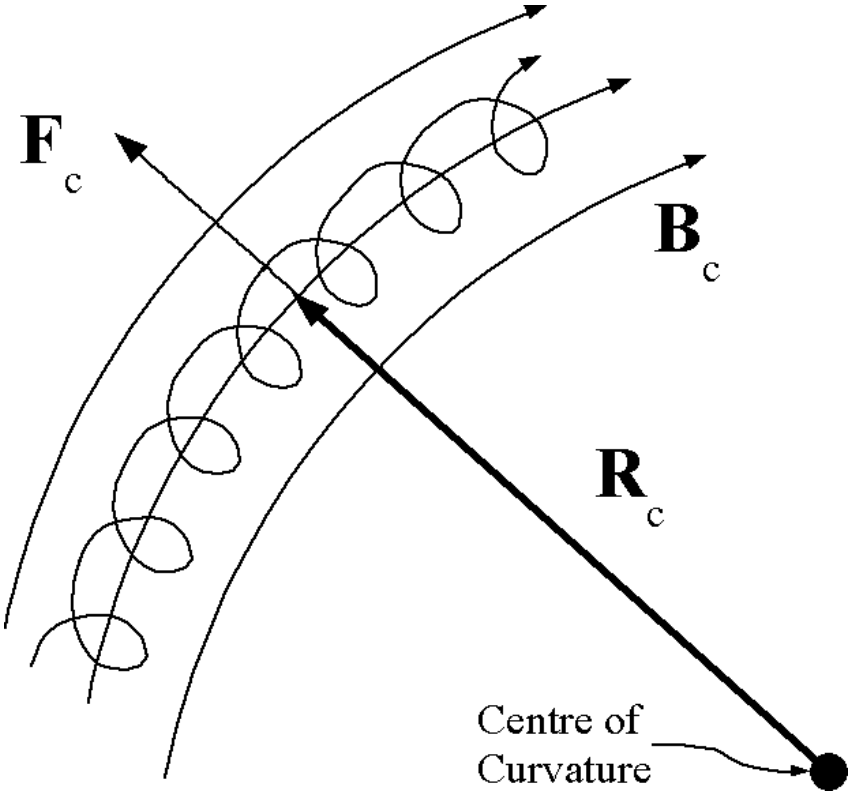

Figure 3.3: Particle motion in a curved magnetic field. The curvature is measured by the radius of curvature, $\mathbf{R}_c$ which points away from the centre of curvature. The particle feels an effective centrifugal force (because there is no explicit centripetal one) and so drifts as if acted upon by $\mathbf{F}_c$.

3.4.3 Gradient Drift

Finally, yet another kind of drift occurs when there is a gradient in the magnetic field in the direction perpendicular to **B**. This is called the gradient drift. (In fact, the gradient and curvature drifts usually occur together since curved field lines are usually associated with perpendicular gradients in the field strength in nature e.g. in a dipole magnetic field). The origin of this drift is clear if we recall that the gyroradius of a given particle is inversely proportional to the magnetic field strength. Hence if the particle is in motion in a region in which the field strength varies across the orbit, the gyroradius also varies, and leads to a drift which is perpendicular to both **B** and to $\nabla\mathbf{B}$, as illustrated in Figure 3.4.

The mathematical derivation of the gradient drift (usually referred to as the "Grad-B" drift) will not be shown here. Essentially, the calculation performs a Taylor expansion of the magnetic field strength and then solves the equation of motion by expansion under the assumption that the Larmor radius is small by comparison with the length scale over which the field varies. The result, cast back from this Cartesian calculation to vector notation, is

Gradient Drift	$\mathbf{v}_{\nabla B} = \dfrac{m v_\perp^2}{2qB^3}(\mathbf{B}\times\nabla\mathbf{B})$	(3.36)

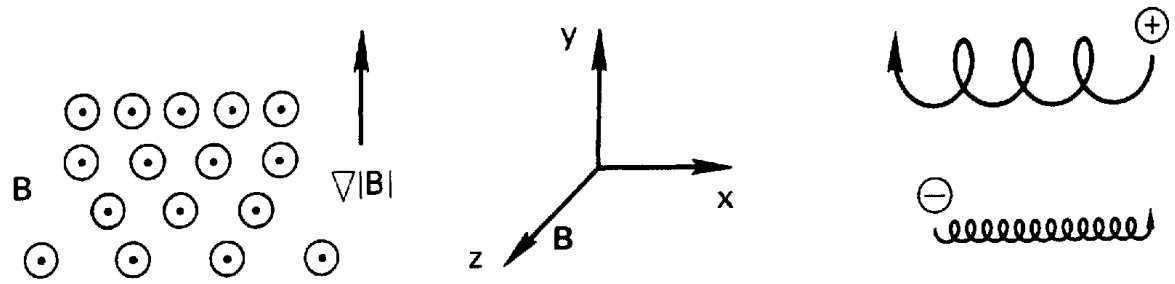

Figure 3.4: Drift of particles across a gradient in the magnitude of the magnetic field.

3.5 Useful Parameters for Describing Particle Motion

3.5.1 Pitch Angle

The pitch angle is the angle between the velocity vector **v** and the magnetic field **B**:

$$\alpha = \tan^{-1} \frac{v_\perp}{v_\parallel} \tag{3.37}$$

Equivalently $v_\parallel = v\cos\alpha$ and $v_\perp = v\sin\alpha$. Particles with small pitch angle are called field aligned, and those with large (i.e., close to 90°) pitch angle are sometimes called gyrating.

3.5.2 Guiding Centre

Particle motion is often decomposed into drifts plus gyration, because often the gyration is on a scale much smaller than the physical system and/or much more rapid than the phenomena of interest. We talk about the motion of the average centre of gyration, known as the "guiding centre." For "slow" changes in the field the motion of the guiding centre is continuous. One way to calculate the guiding centre position is to average the particle position over one cyclotron period (i.e., the time taken to complete one gyration).

3.5.3 Magnetic Moment

Gyration around the magnetic field leads to a current. Consider a charge q circulating with a frequency $\Omega_c/2\pi$. The equivalent current I is then the charge per second passing a given point, i.e.,

$$I = q\frac{1}{2\pi}\frac{qB}{m} \tag{3.38}$$

since the total charge passes in one cyclotron period. The magnetic moment of a current loop is the current carried by the loop times the area of the loop. Thus the corresponding magnetic moment, μ_m, of the gyrating particle is given by $\mu_m = I\pi r_L^2$, or

Magnetic Moment	$\mu_m = \dfrac{mv_\perp^2}{2B} \equiv \dfrac{W_\perp}{B}$	(3.39)

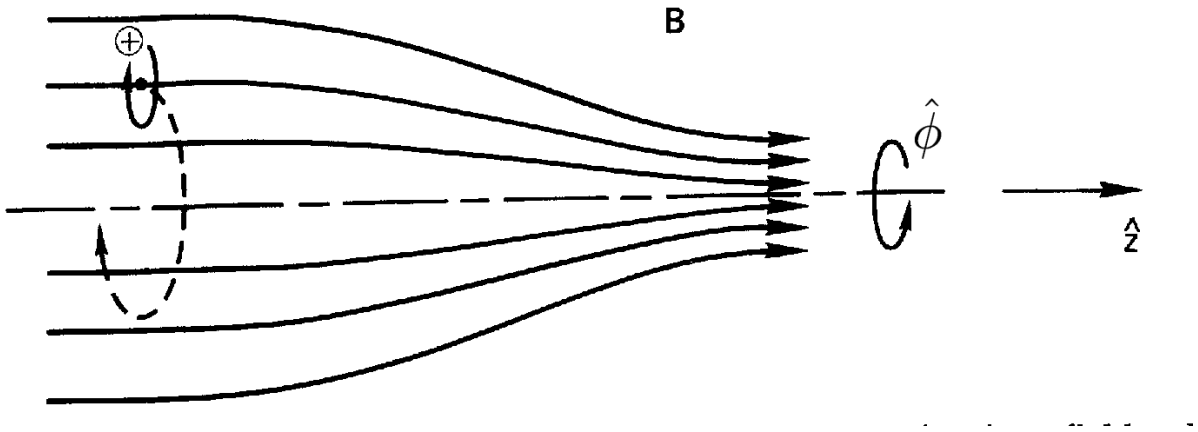

Figure 3.5: Magnetic configuration in which $\nabla B \parallel \mathbf{B}$ - a "magnetic mirror" geometry.

where $W_\perp$ is the kinetic energy of the perpendicular motion. The magnetic moment μ_m is also a measure of the magnetic flux within the particle Larmor radius, a result which follows from its definition and Equation 3.38 which shows that the field and current are linearly related by constants.

3.6 Motion in Static, Non-uniform Magnetic Field: $\nabla B \parallel \mathbf{B}$

Here we examine the motion of a charged particle in the following circumstances:

- a static magnetic field (not time varying)
- a gradient in magnetic field strength in the direction of **B**, thus the field lines converge, without any "twist"
- all gradients are "weak" (i.e. any variation in field experienced by particle is slow compared with cyclotron period)
- zero electric field (therefore, total energy conserved).

This configuration is sketched in Figure 3.5

Assume the magnetic field is mainly in the $\hat{z}$ direction. Since we are working in the guiding centre approximation, the particle motion to lowest order is circular, with cyclotron frequency given by the field strength at the centre of gyration.

The main influence on **B** is via the variation $\dfrac{\partial B_z}{\partial z}$. However, $\nabla \cdot \mathbf{B} = 0$ implies that there must also be variation via $\dfrac{\partial B_x}{\partial x}$ and/or $\dfrac{\partial B_y}{\partial y}$. Here we will use cylindrical polar coordinates (r, ϕ, z), with unit vectors $(\hat{r}, \hat{\phi}, \hat{z})$, in which the magnetic field only has components B_z and B_r (i.e., no twist). The particle motion has constant speed (cf: Equation 3.3 which actually holds as long as $\mathbf{E} = \mathbf{0}$ regardless of any spatial dependence of **B**).

Expressing $\nabla \cdot \mathbf{B} = 0$ in cylindrical coordinates with axial symmetry

$$\frac{1}{r}\frac{\partial}{\partial r}(rB_r) + \frac{\partial B_z}{\partial z} = 0 \tag{3.40}$$

we multiply by r and then integrate with respect to r from $r = 0$ (which we take to be the position of the particle's guiding centre) to $r = r$. Assuming $\dfrac{\partial B_z}{\partial z}$ can be taken as constant over one orbit of the particle, this yields

$$B_r \approx -\frac{r}{2}\frac{\partial B_z}{\partial z} \tag{3.41}$$

Thus $\nabla \cdot \mathbf{B} = 0$ necessarily implies that there is a radial component of $\mathbf{B}$ if the main ($\hat{z}$) component is not constant in magnitude.

This radial field B_r, which is perpendicular to the circular motion, is vital to understanding the motion of the particle. A particle orbiting around the z-axis at $r = r_L$, encounters a finite B_r. So there will be a Lorentz force associated with B_r and v_ϕ. Reference to Figure 3.1 reveals that for all particles, $v_\phi = -\dfrac{q}{|q|}v_\perp$, or $qv_\phi = -|q|v_\perp$, so the force due to the radial field component is

$$\mathbf{F} = -|q|v_\perp\hat{\phi} \times \left(-\frac{r_L}{2}\frac{\partial B_z}{\partial z}\hat{r}\right) \tag{3.42}$$

Since $r_L = mv_\perp/|q|B$, we see that this force is independent of the particle charge q. Rewriting in terms of the magnetic moment $\mu_m = mv_\perp^2/2B$, this is simply

$$\mathbf{F} = -\mu_m\frac{\partial B_z}{\partial z}\hat{z} \tag{3.43}$$

This means that the force is opposite to the field strength gradient, i.e., that it tends to push particles out of stronger field regions.

Using this parallel force (parallel to $\mathbf{B}$, i.e. along $\hat{z}$), the equation of motion becomes

$$m\frac{dv_z}{dt} \approx -\mu_m\frac{\partial B}{\partial z} \tag{3.44}$$

where we have used $B \approx B_z$, i.e., that the field is mainly in the $\hat{z}$ direction. Multiplying both sides by $v_z \equiv \dfrac{dz}{dt}$, and noting that $\dfrac{dv_z^2}{dt} = 2v_z\dfrac{dv_z}{dt}$, we find that

$$\frac{d}{dt}\left(\frac{1}{2}mv_z^2\right) \equiv \frac{dW_\parallel}{dt} = -\mu_m\frac{dB}{dt} \tag{3.45}$$

where the left hand side is just the rate of change of parallel energy ($W_\parallel$), and the right hand side is the rate of change of field strength as seen by the particle.

However, since $\mathbf{E} = \mathbf{0}$, particle energy $W = W_\parallel + W_\perp$ is constant, i.e.

$$\frac{dW_\perp}{dt} = -\frac{dW_\parallel}{dt} = +\mu_m\frac{dB}{dt} = \frac{W_\perp}{B}\frac{dB}{dt} \tag{3.46}$$

where we have used $\mu_m = W_\perp/B$. Therefore

$$\frac{1}{B}\frac{dW_\perp}{dt} - \frac{W_\perp}{B^2}\frac{dB}{dt} \equiv \frac{d}{dt}\left(\frac{W_\perp}{B}\right) = \frac{d\mu_m}{dt} = 0 \tag{3.47}$$

This result implies that the magnetic moment, μ_m, is constant in time (at least in the guiding centre approximation which we have used). This invariance of the particle magnetic moment turns out to be a general property of particle motion for both magnetic fields which change in space (as we have demonstrated) and also in time, provided that the field as felt by the particle varies slowly by comparison with its gyro-motion.

Since μ_m has been shown to be constant the parallel force can be written as

$$F_z = -\frac{\partial(\mu_m B)}{\partial z} \tag{3.48}$$

This shows that for the parallel motion, $\mu_m B$ behaves like a potential. By analogy, there can be regions where $\mu_m B$ is high enough to exclude certain particles. The consequence is that some particles moving towards regions of high B will be excluded, so that their parallel motion will reverse. This is known as a magnetic mirror, and the above force is known as the mirror force.

Since the total energy W is also an invariant of the particle motion,

$$W_{\parallel} = W - \mu_m B \tag{3.49}$$

so that as B increases, $W_{\parallel}$ decreases. Since $W_{\parallel}$ can never become less than zero, the particle ceases its parallel progress when the parallel energy reduces to zero. At this point the particle has a pitch angle of 90° and all its energy is in the perpendicular motion, $W = W_{\perp}$. It does not rest here, however, since Equation 3.48 ensures that there is a parallel force which repels ("reflects") it away from the higher field region; the particle thus reverses its parallel motion. This behaviour is known as "magnetic mirroring." Note that particles with similar total energy, but smaller pitch angles have smaller $W_{\perp}$ and hence smaller μ_m. These particles therefore penetrate to regions where B has increased to a greater value before being mirrored, if indeed they reach fields of sufficient magnitude to mirror them at all.

Consider particles with speed v, and pitch angle α_0 at a position where $B = B_0$. By definition $v_{\perp} = v\sin\alpha$ and therefore $\dfrac{\mu_m}{W} = \dfrac{\sin^2\alpha}{B} = \dfrac{\sin^2\alpha_0}{B_0}$ is a constant for the particles. The mirror point is where $\sin\alpha = 1$, i.e., where

$$B_m = \frac{B_0}{\sin^2\alpha_0} \tag{3.50}$$

If a particle is in a region of space between two high field regions, then the particle may be reflected at one, travel towards the second, and also reflect there. Thus the particle motion is confined to a certain region of space, bouncing back and forth between the regions of high field; this process is known as "magnetic trapping."

3.7 Conservation of Magnetic Moment

The conservation of magnetic moment is equivalent to the statement that it is a constant (or invariant) of the motion, just as the total kinetic energy is an invariant (for zero electric field). The concept of invariants is extremely powerful in describing the possible types of particle motion without having to solve the detailed equations of motion. We have seen that conservation of magnetic moment is valid when the fields seen by the particle change "slowly" i.e., slower than the gyration of the particle. This means that magnetic moment conservation is a so-called "adiabatic invariant."

It can be shown that whenever the particle motion has a certain periodicity, and provided that the fields change on a time scale slower than this periodicity, then there is an associated adiabatic invariant. The magnetic moment is the first adiabatic invariant, associated with gyration. For a particle in a magnetic trap there is a second adiabatic invariant associated with the particle's bounce period. For

particles in a dipole field there is a third adiabatic invariant associated with the periodic curvature drift of the particle around the dipole. These invariants allow you to draw many important conclusions about the particle motion, such as which regions are accessible to the particle, the partition of energy between the particle's degrees of freedom, and hence what the properties of particles at a given location might be, etc., without solving a single equation of motion!

3.8 Comment on Relativistic Motion

So far we have only considered non-relativistic motion, but the exact equation of motion is quite straightforward

$$\frac{d}{dt}\left(\frac{m_0\mathbf{v}}{\sqrt{1-(v^2/c^2)}}\right) = q\left(\mathbf{E}+\mathbf{v}\times\mathbf{B}\right) \tag{3.51}$$

A full discussion of the resultant motion can be found in various text books, but we just mention that for $\mathbf{E}=\mathbf{0}$, one finds gyrational motion as before, but now the gyro-frequency is a function of the relativistic energy (i.e.,. the gyro-frequency reduces as the particle motion becomes more relativistic)

$$\Omega_c = \frac{qB}{m_0}\sqrt{1-(v^2/c^2)} \tag{3.52}$$

3.9 Applications of Particle Motion

There are a wide variety of astrophysical environments where conecpts from single particle motion play a key role. These include

Particle Trapping due to magnetic mirroring in the Earth's "van Allen" radiation belts and energetic electrons confined in solar coronal magnetic loops

Particle Transport of energetic particles (galactic cosmic rays, solar energetic particles, ultra-relativistic particles from extra-galactic sources) is governed by the variety of particle drifts and adiabatic invariants discussed in the present chapter. Note that in many regimes, particle transport is not controlled by collisional, diffusive processes due to the long collision mean free paths, but is instead controlled by single particle motion. The rate of Coulomb collisions between charged particles decreases strongly with increasing particle energy.

Particle Acceleration due to parallel electric fields, as found in pulsar magnetospheres and solar flares. Magnetic mirroring due to either stochastic motion of high field regions, or systematic motion between converging mirrors in the vicinity of shock waves, leads to Fermi acceleration of particles.

Radiation given off by relavistic gyrating particles (synchrotron radiation) or accelerating particles (brehmstralung) often provides vital information about the fields and energy content of distant sources.

3.10 Exercises

1. Calculate the Larmor radius and gyrofrequencies for the following particles

   (a) A 10 keV electron moving with a pitch angle of 45° with respect to the Earth's magnetic field of 30,000nT [nanoTeslas].

(b) A solar wind proton moving at 400 km/s perpendicular to a field of 5nT.

(c) A 1 keV He^+ ion in the solar atmosphere near a sunspot where $B = 5 \times 10^{-2}$T ($v_\parallel = 0$).

2. The magnetic field strength in the Earth's magnetic equatorial plane is given by

$$B = B_0 \left(\frac{R_e}{r} \right)^3$$

where $B_0 = 0.3 \times 10^{-4}$T, R_e is the Earth radius ($\sim$ 6400km), and r is the geocentric distance. Derive an expression for the drift period (the time for 1 orbit of the Earth) of the particle under the influence of the ∇B drift. Evaluate this period for both a proton and an electron of 1keV at a distance $5R_e$ from the Earth. Compare the answer to (a) the drift induced by the force of gravity on the same particles and (b) the orbital period of an uncharged particle at the same position. (The mass of the Earth is 6×10^{24}kg).

3. (a bit harder) A non-relativistic particle of mass m and charge q moves in a steady, axially symmetric magnetic field of a sunspot, which is taken to be uniform below the solar surface and falls off with height, h, above the surface as

$$B = B_0 \frac{H^3}{H^3 + h^3}$$

for $h > 0$, where H is a constant and B_0 is the value of the field at and below the surface. [In effect, the field is roughly dipolar for large h].

(a) Sketch the field lines in this model of a sunspot field

(b) If particles of speed v are produced at the surface with an isotropic distribution (i.e., they move equally likely in all directions), and conserve their magnetic moments μ_m, show that as they move to successively greater heights h the particles possess a smaller range of pitch angles, $\alpha \equiv \arccos\left(v_\parallel / v\right)$. [Hint: Draw a picture of a spherical shell in $(v_\parallel, v_\perp)$ space, and consider those particles with pitch angles near 90°.]

(c) Hence explain how this process of "magnetic focussing" produces a "beam-like" particle distribution. How narrow is this beam in angular spread (i.e., pitch angle) at $h \sim 2H$?

4. A cosmic ray proton is trapped between 2 moving magnetic mirrors in which the field strength increases by a factor of 5. It has an initial kinetic energy $W = 1keV$ and $v_\perp = v_\parallel$ in the mid-plane between the two mirrors. Each mirror is moving towards this mid-plane with velocity $V_m =$ 10km/s. Initially the mirrors are separated by a distance $L = 10^{10} km$.

(a) Using the invariance of μ_m find the energy to which the proton will be accelerated before it escapes the system.

(b) How long will it take to reach that energy?

Hints:

(a) Treat the mirrors as flat pistons and show that $v_\parallel$ increases by $2V_m$ at each bounce.

(b) Compute the number of bounces needed

(c) Accuracy to a factor of 2 is sufficient.

Chapter 4

MagnetoHydroDynamics - MHD

4.1 One-fluid MHD Equations

The magnetohydrodynamic (MHD) equations describe the plasma as a conducting fluid with conductivity σ[1] which experiences electric and magnetic forces. The fluid is specified by a mass density ρ, a flow velocity $\mathbf{V}$, and a pressure p, which are all functions of space and time. For an electron-proton plasma the mass density ρ is related to the number density n by $\rho = n(m_i + m_e)$. Perhaps the most elegant derivation of the MHD equations, which reveals the many assumptions, is by taking moments of the Vlasov Equation (see Section 2.4.5), i.e., weighting by successive powers of $\mathbf{v}$ and integrating over all velocity space. See, for example, the treatment in the book by Boyd and Sanderson listed in the Introduction (p9). Here, we shall simply draw on the ordinary equations of hydrodynamics. The equation of motion has an additional force per unit volume $\mathbf{j} \times \mathbf{B}$ due to the net magnetic force on the plasma particles. On fluid scales ($\gg \lambda_D$) the plasma is overall charge neutral, so that the net electric force is neglibly small. The MHD equations represent the conservation of mass, the conservation of momentum, and some equation of state (i.e., an energy relationship). Thusly we reach:

$$\frac{\partial \rho}{\partial t} + \nabla \cdot (\rho \mathbf{V}) = 0 \tag{4.1}$$

$$\rho \left(\frac{\partial}{\partial t} + \mathbf{V} \cdot \nabla \right) \mathbf{V} = -\nabla p + \mathbf{j} \times \mathbf{B} \tag{4.2}$$

$$\left(\frac{\partial}{\partial t} + \mathbf{V} \cdot \nabla \right) (p \rho^{-\gamma}) = 0 \tag{4.3}$$

$$\tag{4.4}$$

The operator

$$\frac{d}{dt} \equiv \left(\frac{\partial}{\partial t} + \mathbf{V} \cdot \nabla \right) \tag{4.5}$$

is called the *convective derivative* (or total or substantial or Lagrangian derivative). It measures the rate of change as seen by a parcel of the fluid. This parcel sees any instrinsic time variation, and additionally sees variations which arise because it is moving (or "convecting") to other regions where, due to spatial gradients, the fluid parameters are different.

There are a number of assumptions behind the above equations: The energy equation is the adiabatic equation of state with γ being the ratio of specific heats ($\gamma = 5/3$ for a monatomic gas); there are other

[1] Sometimes the resistivity $1/\sigma$ is used, and denoted η. However, we shall reserve η for the magnetic diffusivity, which is $1/(\mu_0 \sigma)$

possible choices for an energy equation such as isothermal ($\gamma = 1$), etc. Ohmic heating $\mathbf{j} \cdot \mathbf{E}$ has been ignored, i.e., assumed to be less important than the plasma's thermal energy; radiative or other heat losses are also neglected (or modelled in an ad hoc fashion by playing with the value of γ). We have also assumed that the pressure is isotropic which is not generally true when the magnetic field can impose different kinds of motion on the particles parallel and perpendicular to the field direction. Any possible heat flux has been ignored, and there is no relative flow between the different species in the plasma, so that the one fluid description is valid. While the conductivity is usually large due to the mobile electrons, the absence of collisions has the opposite impact on other transport processes such as viscosity, which we have also therefore neglected.

In addition to the equation for the fluid, one also has Maxwell's equations for the fields:

$$\nabla \times \mathbf{E} = -\frac{\partial \mathbf{B}}{\partial t} \tag{4.6}$$

$$\nabla \times \mathbf{B} = \mu_0 \mathbf{j} \tag{4.7}$$

$$\nabla \cdot \mathbf{B} = 0 \tag{4.8}$$

where $\mu_0 \varepsilon_0 = 1/c^2$.

Note that the displacement current term in the $\nabla \times \mathbf{B}$ equation has been dropped because we are interested in low frequency (gross fluid) behaviour (see Section 2.4.1). Furthermore, the Poisson equation for $\nabla \cdot \mathbf{E}$ has been dropped since we are treating the plasma as a single, charge neutral fluid. These approximations are discussed later. Chapter 8 relaxes the one-fluid assumption.

While the fluid equations effectively add the mass densities, forces, etc., for all the plasma constituents, the plasma's conducting properties require some understanding of the differences between positive and negative species to determine the current density. This results in an Ohm's Law relating the electric field to the current density:

One Fluid MHD Ohm's Law $$\mathbf{E} = -\mathbf{V} \times \mathbf{B} + \frac{\mathbf{j}}{\sigma} \tag{4.9}$$

This simply says that in the frame moving with the fluid (see Section 2.4.6) the fluid behaves like a simple conductor with $\mathbf{E}' \propto \mathbf{j}$. The term $-\mathbf{V} \times \mathbf{B}$ is called the motional electric field, and is a consequence of the motion of the fluid and the rule for transforming electric field between frames. Chapter 8 develops the two fluid approach and derives the generalized Ohm's Law (Equation 8.17) which includes terms due to finite electron inertia, so-called Hall effects, thermoelectric fields, and other proesses. The one-fluid MHD Ohm's Law is a simplification of this more general result when two-fluid effects are ignored.

4.1.1 The Induction Equation

Combining the fluid and field equations one can find the governing equation for the evolution of the magnetic field and thereby eliminate the electric field $\mathbf{E}$. Taking the curl of Equation 4.9 gives

$$\nabla \times \mathbf{E} = -\nabla \times (\mathbf{V} \times \mathbf{B}) + \frac{1}{\sigma} \nabla \times \mathbf{j} \tag{4.10}$$

assuming σ is constant. Substituting for $\mathbf{j} = \nabla \times \mathbf{B}/\mu_0$ from Ampere's law and using the law of induction Equation 4.6 yields

$$-\frac{\partial \mathbf{B}}{\partial t} = -\nabla \times (\mathbf{V} \times \mathbf{B}) + \frac{1}{\mu_0 \sigma} \nabla \times (\nabla \times \mathbf{B}) \tag{4.11}$$

The double curl can be expanding with the help of the vector identity A.13 to give

$$-\frac{\partial \mathbf{B}}{\partial t} = -\nabla \times (\mathbf{V} \times \mathbf{B}) + \frac{1}{\mu_0 \sigma} \nabla (\nabla \cdot \mathbf{B}) - \frac{1}{\mu_0 \sigma} \nabla^2 \mathbf{B} \tag{4.12}$$

The middle term is zero by Maxwell's equation for $\nabla \cdot \mathbf{B}$ and so the law of induction in a plasma reduces to

$$\boxed{\text{MHD Induction Equation} \qquad \frac{\partial \mathbf{B}}{\partial t} = \nabla \times (\mathbf{V} \times \mathbf{B}) + \frac{1}{\mu_0 \sigma} \nabla^2 \mathbf{B}} \tag{4.13}$$

This equation, together with the fluid mass, momentum and energy equations 4.1-4.3 form a close set of equations for the MHD state variables $(\rho, \mathbf{V}, p, \mathbf{B})$.

4.1.2 Ideal MHD

The case where the conductivity is high $(\sigma \to \infty)$, such that the electric field is $\mathbf{E} = -\mathbf{V} \times \mathbf{B}$ (i.e., motional electric field only), is known as ideal magnetohydrodynamics.

4.2 Magnetic Field Behaviour in MHD

We now examine the form of the induction equation in two extreme cases, depending on which of the two terms on the RHS is dominant.

4.2.1 $\nabla \times (\mathbf{V} \times \mathbf{B})$ Dominant - Convection

In this case, corresponding to the infinite conductivity limit dubbed Ideal MHD, the flow and the field are intimately connected. We shall see that the field lines convect with the flow; conductors do not allow new fields to penetrate them, and retain any internal fields they possess. Plasma physicists refer to this as "flux freezing", which we shall explore more below. The flow in turn responds to the field via the $\mathbf{j} \times \mathbf{B}$ force.

4.2.2 $\frac{1}{\mu_0 \sigma} \nabla^2 \mathbf{B}$ Dominant - Diffusion

In this case the induction equation takes the form of a diffusion equation: the field lines diffuse through the plasma down any field gradients, so as to reduce field gradients. There is no coupling between the magnetic field and fluid flow.

4.2.3 The Magnetic Reynold's Number

Now consider the relative sizes of the two RHS terms in the Induction Equation, by using dimensional arguments. We replace ∇ by $1/L$ where L is the characteristic scale length, and let V denote the characteristic (i.e. typical) speed. Then the ratio of the convection term to the diffusion term can be expressed by the dimensionless number

$$\boxed{\text{Magnetic Reynold's Number} \qquad R_m \equiv \frac{VB/L}{B/\mu_0 \sigma L^2} = \mu_0 \sigma V L} \tag{4.14}$$

If R_m is large then convection dominates, and the magnetic field is frozen into the plasma. Else if R_m is small then diffusion dominates. In the solar system, and in astrophysics generally, R_m is very large, e.g., 10^8 in a solar flare, and 10^{11} in the solar system and planetary magnetospheres. We shall see that R_m is not large everywhere; thin boundary layers form where $R_m \sim 1$ and ideal MHD breaks down. As in most branches of physics, these boundary layers mediate the global dynamics by controlling the rate of transport of mass, momentum, and energy through the system.

4.3 Flux Freezing

In 1942 Alfvén showed that the induction equation for ideal MHD is equivalent to the statement that the "field is frozen into the fluid" or that the "matter of the plasma is fastened to the lines of magnetic force."

This is an extremely important concept in MHD, since it allows us to study the evolution of the field, particularly the topology of the field lines, by finding out about the plasma flow. Of course, the principle also works in the other direction: If we know how the magnetic field lines evolve, then we can deduce the plasma fluid flow.

To establish this Flux Freezing Law we begin with the Ideal MHD Induction Equation

$$\frac{\partial \mathbf{B}}{\partial t} = \nabla \times (\mathbf{V} \times \mathbf{B}) \tag{4.15}$$

and then show that the magnetic flux through a closed loop which moves with the fluid is constant in time.

The magnetic flux through a closed loop ℓ is

$$\Phi_B \equiv \oint_\ell \mathbf{B} \cdot \hat{n}\, dS \tag{4.16}$$

where dS is the area element of any surface which has ℓ as a perimeter. The quantity Φ_B is independent of the specific surface chosen, as can be proved from $\nabla \cdot \mathbf{B} = 0$ and Gauss' Theorem. The Flux Freezing Law we are trying to establish is then expressed as:

$$\frac{d\Phi_B}{dt} = 0 \tag{4.17}$$

where we use the total derivative $\dfrac{d}{dt}$ to indicate that the time derivative is calculated with respect to fluid elements moving with the flow.

The quantity Φ_B is not locally defined, so we have to follow an explicit calculation for its time derivative. Figure 4.1 sketches all the necessary components.

Consider a loop of fluid elements ℓ at two instants in time, t and $t + \Delta t$. The two surfaces S_1 and S_2 have $\ell(t)$ and $\ell(t + \Delta t)$ as perimeters. There is also a "cylinder" S_3 generated by the fluid motion between the two instants of the elements making up ℓ. Let Φ_B be the flux enclosed by ℓ and Φ_{B1} be the flux through surface S_1, and similarly for S_2 and S_3. The normal vectors to S_1 and S_2 are chosen to lie on the same side of the surfaces, relative to the fluid flow.

Then,

$$\frac{d\Phi_B}{dt} = \lim_{\Delta t \to 0} \left(\frac{\Phi_{B2}(t + \Delta t) - \Phi_{B1}(t)}{\Delta t} \right) \tag{4.18}$$

From $\nabla \cdot \mathbf{B} = 0$ the net flux through the three surfaces at any time is zero, so

$$-\Phi_{B1}(t + \Delta t) + \Phi_{B2}(t + \Delta t) + \Phi_{B3}(t + \Delta t) = 0 \tag{4.19}$$

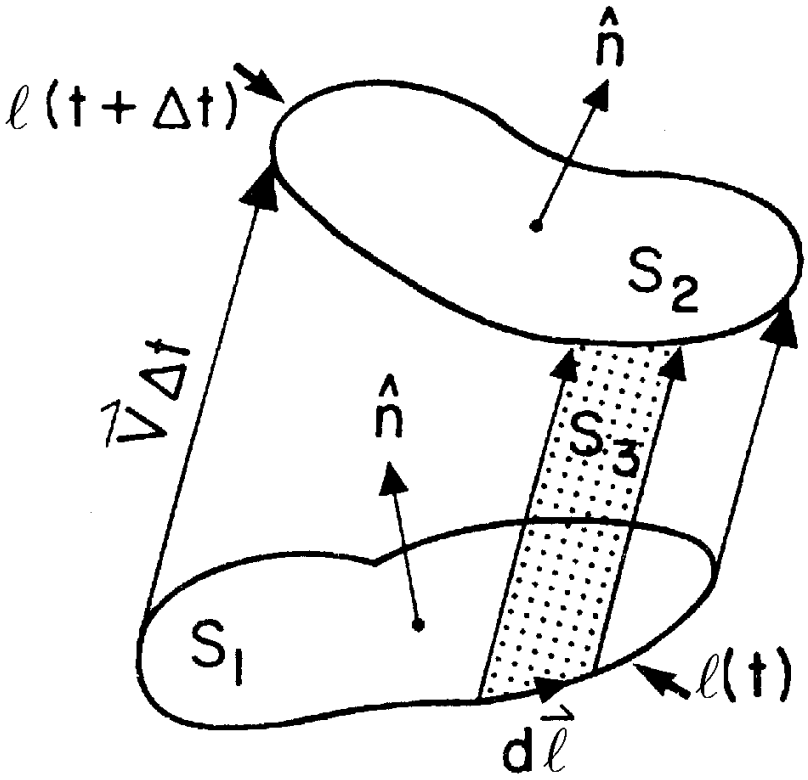

Figure 4.1: Generalized cylinder formed by the motion of a closed line ℓ "frozen" to the fluid.

(Note negative sign on first term to account for normal pointing inward into the volume, rather than outward.) We can thus eliminate $\Phi_{B2}(t+\Delta t)$, and at the same time use the definition of flux in expressing Φ_{B1} and Φ_{B3}

$$\frac{d\Phi_B}{dt} = \lim_{\Delta t\to 0}\frac{1}{\Delta t}\left[\iint_{S_1}(\mathbf{B}(t+\Delta t)-\mathbf{B}(t))\cdot\hat{n}\,dS - \iint_{S_3}\mathbf{B}\cdot\hat{n}\,dS\right] \tag{4.20}$$

The first term is nothing more than

$$\iint_{S_1}\frac{\partial\mathbf{B}}{\partial t}\cdot\hat{n}\,dS \tag{4.21}$$

Also we can convert the surface integral over S_3 to one over S_1 by noting that the area element for S_3 can be written $\hat{n}dS = \mathbf{d}\ell\times\mathbf{V}\Delta t$, where $\mathbf{d}\ell$ is a line element of the loop of fluid elements. Thus

$$\iint_{S_3}\mathbf{B}\cdot\hat{n}\,dS = \oint_{\ell(t)}\mathbf{B}\cdot(\mathbf{d}\ell\times\mathbf{V})\Delta t = \oint_{\ell(t)}(\mathbf{V}\times\mathbf{B})\cdot\mathbf{d}\ell\,\Delta t \tag{4.22}$$

Then, by using Stokes Theorem to convert the line integral to a surface integral

$$\iint_{S_3}\mathbf{B}\cdot\hat{n}\,dS = \iint_{S_1}\nabla\times(\mathbf{V}\times\mathbf{B})\cdot\hat{n}\,dS\Delta t \tag{4.23}$$

And so, finally putting these results into Equation 4.20

$$\frac{d\Phi_B}{dt} = \iint_{S_1}\left[\frac{\partial\mathbf{B}}{\partial t}-\nabla\times(\mathbf{V}\times\mathbf{B})\right]\cdot\hat{n}\,dS = 0 \tag{4.24}$$

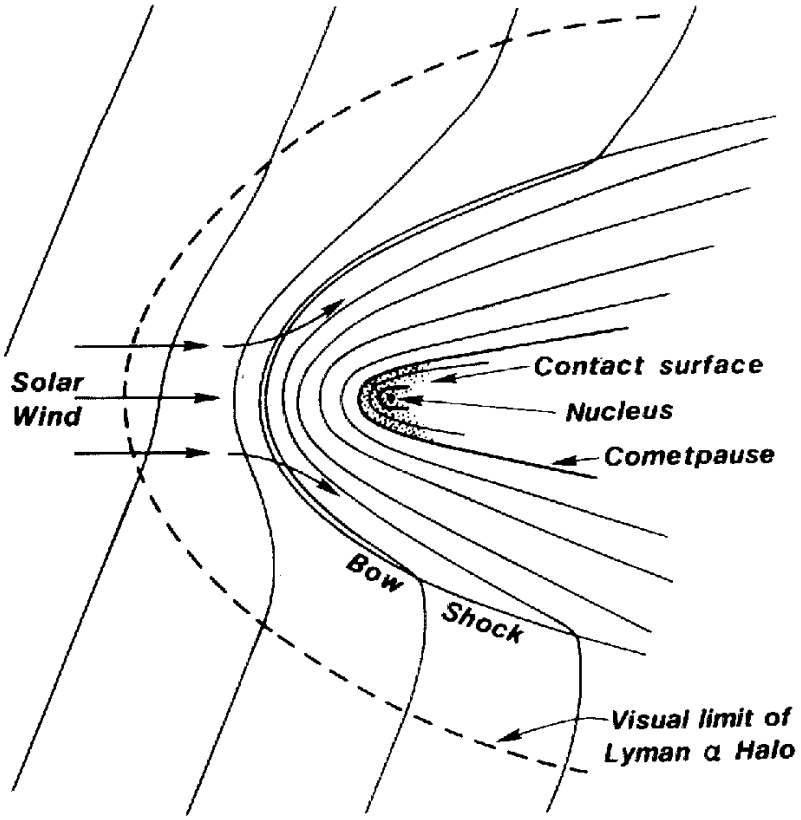

Figure 4.2: Sketch of Solar Wind - Comet interaction illustrating field line draping.

which establishes the Flux Freezing Theorem.

The most important implication of this theorem is that it imposes constraints on the allowable motion of the plasma. We can, for example, define a magnetic flux tube: Take a closed loop and move it parallel to the field it intersects. The surface thus created has zero flux through it, and consequently the fluid elements that form the flux tube at one moment, form the flux tube at all instants. If two fluid elements are linked by a field line (defined as the intersection of two flux tubes) at one instant, then they are always so linked. If the conductivity σ, is not infinite (equivalently, R_m is small), then the flux "thaws" and then slippage of the the field relative to the flow is possible.

4.3.1 Example - Field Line Draping

Consider a flowing plasma with, say, the field lines initially perpendicular to the flow. Suppose that there is some region where the flow is slowed, or even stopped, by some kind of obstacle for example as shown in Figure 4.2. Outside of this region the flow continues unabated taking its field lines with it. But at the obstacle the field lines are slowed, effectively caught up by the obstacle. This has the effect of stretching out the field lines behind the obstacle, creating a "tail" in the magnetic field behind the region of slowed flow. In the tail the field reverses direction, so there will be a current sheet at the centre of the tail. All of the objects visited by spacecraft have been observed to have some kind of magnetic tail: the Earth, other planets, comets, etc.

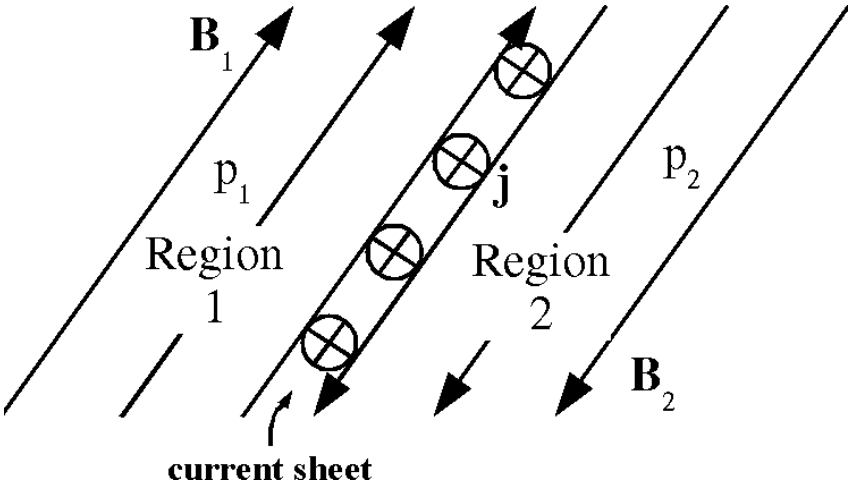

Figure 4.3: Separation of fields and plasmas of different sources by thin boundary layers (current sheets).

4.4 The Plasma Cell Model of Astrophysical Plasmas

A central question is the following: If R_m is large can we neglect the effects of magnetic diffusion completely?

Large R_m means no cross field plasma mixing: particles are tied to the same field line. Astrophysical plasmas generally come from different sources, such as stellar winds, or clouds of interstellar gas. But what happens when plasmas from different sources, carrying different magnetic fields, come in contact? Figure 4.3 illustrates such a contact between two different plasma regions.

In ideal MHD the lack of plasma mixing means the formation of a thin boundary layer separating the two different plasma and field systems. The location of the boundary layer is determined by pressure balance. The boundary layer must also be a current sheet, since the magnetic field changes across it.

Thus we can make the following general model of the plasma universe: Astrophysical plasma systems become divided into separate cells containing field and plasma from different sources, separated by current sheets. This is illustrated in Figure 4.4

Observations in the Solar System, where we can actually measure thin layers, indicate that this is an excellent approximation. As an example we can cite the existence of well defined planetary magnetospheres where boundary layers have thickness of order $100-1000$km in a system with an overall size of 100,000km.

But there is a problem: The magnetic Reynold's number (Equation 4.14) was calculated from the over all length scale L of the system. On the other hand the behaviour of the thin boundary layers is described by a much smaller R_m. Thus we conclude that diffusion will probably be important at boundary layers, and, indeed, will be the mechanism of mass and momentum transfer between the two plasma systems.

4.5 Electromagnetic forces in MHD

Previously we only retained the magnetic force term $\mathbf{j}\times\mathbf{B}$ in the one fluid MHD equations. We now examine the validity of this assumption.

Generally the equation of motion for the fluid will be of the form

$$\rho\left(\frac{\partial}{\partial t}+\mathbf{V}\cdot\nabla\right)\mathbf{V}=-\nabla p+(\text{e.m. forces})+(\text{viscous forces})+\ldots \tag{4.25}$$

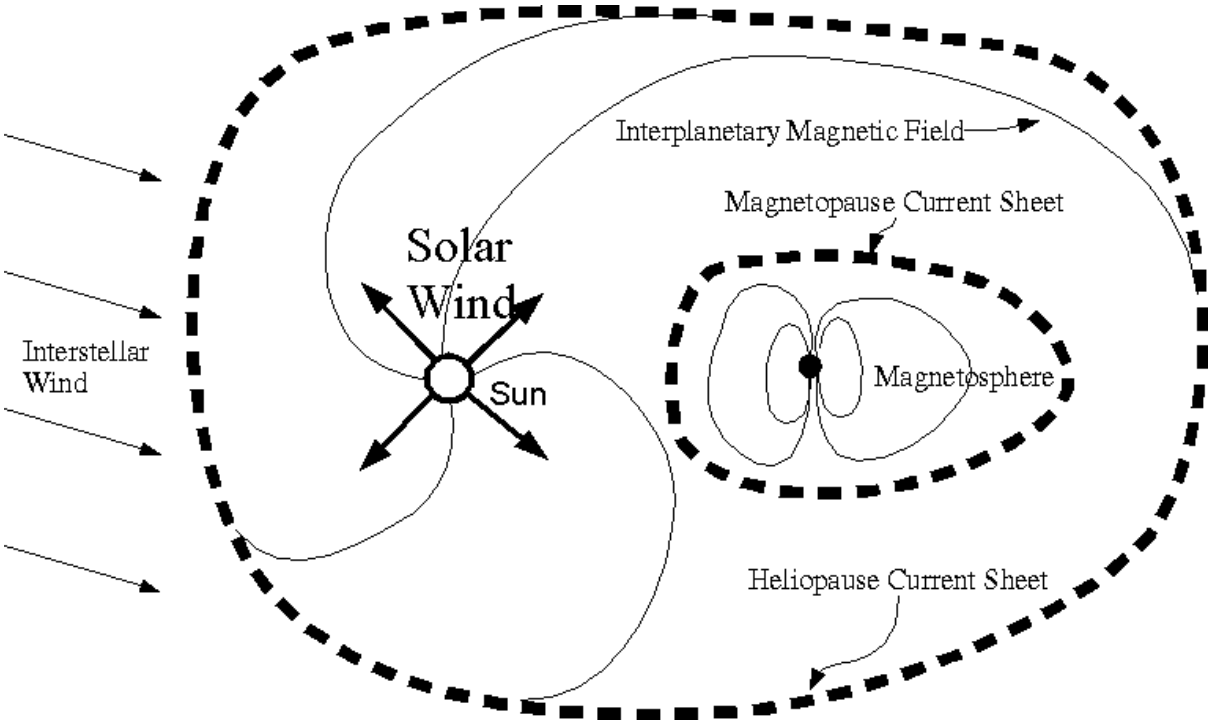

Figure 4.4: Cartoon illustrating the plasma cell model of the solar system (items NOT to scale!).

Then, treating the plasma as two interpenetrating fluids, one of singly ionised ions and one of electrons (a model we shall explore further in Chapter 8), we can write the electromagnetic forces as

$$\begin{aligned} \mathbf{F}_{e.m.} &= (n_i - n_e)\, e\mathbf{E} + (n_i \mathbf{v}_i - n_e \mathbf{v}_e)\, e \times \mathbf{B} && (4.26)\\ &= \rho_q \mathbf{E} + \mathbf{j} \times \mathbf{B} && (4.27)\\ &= \rho_q \mathbf{E} + \frac{1}{\mu_0}\left[(\nabla \times \mathbf{B}) \times \mathbf{B}\right] - \varepsilon_0 \frac{\partial \mathbf{E}}{\partial t} \times \mathbf{B} && (4.28) \end{aligned}$$

where we have used Maxwell's equations to substitute for $\mathbf{j}$.

We can now compare the relative magnitude of the three terms in the expression for the electromagnetic force in (4.28), using dimensional arguments, i.e., substituting $\nabla \Rightarrow 1/L$, $\dfrac{\partial}{\partial t} \Rightarrow 1/T$, $L/T \Rightarrow V$ and $E \Rightarrow VB$ where all the quantities (length, time, velocity) are now the characteristic values for the system under consideration.

Taking the ratio of the middle to last terms

$$\frac{B^2/L\mu_0}{\varepsilon_0 V B^2/T} \sim \frac{T}{\mu_0 \varepsilon_0 L V} \sim \frac{c^2}{V^2} \gg 1 \qquad (4.29)$$

Thus, we can neglect the $\dfrac{\partial \mathbf{E}}{\partial t}$ term, i.e., the displacement current term, provided that the fluid flows are much less than the speed of light.

Now consider the ratio of the first to middle terms

$$\frac{\varepsilon_0 E^2/L}{B^2/L\mu_0} \sim \frac{V^2}{c^2} \ll 1 \qquad (4.30)$$

where we have used Poisson's Equation (2.3), i.e., $\nabla \cdot \mathbf{E} = \rho_q/\varepsilon_0$ to evaluate ρ_q. So, again for fluid velocities much less than the speed of light, the magnetic term dominates over the electrostatic force term. This completes the justification of using only the magnetic force term in the one fluid MHD equation of motion (4.2). But we now go further, and find an interesting way of splitting the magnetic force. Using a vector identity (A.9) we can write

$$\mathbf{F}_M = \frac{1}{\mu_0}\left[(\nabla \times \mathbf{B}) \times \mathbf{B}\right] = -\nabla\left(\frac{B^2}{2\mu_0}\right) + \frac{1}{\mu_0}(\mathbf{B}\cdot\nabla)\mathbf{B} \tag{4.31}$$

We write $\mathbf{B} = B\hat{b}$, so that $\hat{b}$ is the unit vector in the direction of the magnetic field. Then, the operator $\hat{b}\cdot\nabla \equiv \partial/\partial s$ represents the derivative along the direction of the magnetic field where s is a distance parameter along a field line. Then the last term in (4.31) can be written (e.g., by re-arranging Equation 3.34)

$$(\mathbf{B}\cdot\nabla)\mathbf{B} = \hat{b}\frac{\partial}{\partial s}\left(\frac{B^2}{2}\right) - B^2\frac{\mathbf{R_c}}{R_c^2} \tag{4.32}$$

where $\mathbf{R}_c$ is the vector from the centre of curvature of the field as sketched in Figure 3.3 We now return to the expression for $\mathbf{F}_M$ in (4.31) and split the gradient operator into two parts, one parallel and one perpendicular to $\mathbf{B}$. The parallel term is just the gradient in the direction of $\hat{b}$ so that this decomposition is

$$\nabla = \nabla_\perp + \hat{b}\frac{\partial}{\partial s} \tag{4.33}$$

Thus we can bring things together (cancelling the parallel gradient terms) to arrive at

MHD Magnetic Forces	$\mathbf{F}_M = -\nabla_\perp\left(\frac{B^2}{2\mu_0}\right) - \frac{B^2}{\mu_0}\frac{\mathbf{R}_c}{R_c^2}$	(4.34)

This equation shows that the magnetic force can be resolved into two, conceptually simple, components: a force perpendicular to the magnetic field which behaves like a pressure (i.e., it is the gradient of a scalar quantity, $B^2/2\mu_0$), and a force towards the instantaneous centre of curvature which depends on the curvature and the field magnitude. This is the physical equivalent of a tension force B^2/μ_0 acting along the field lines. To summarise: Forcing the field lines together results in an opposing perpendicular pressure force. Trying to bend the field lines results in an opposing tension force. These different kinds of forces, illustrated in Figure 4.5 lead to different kinds of dynamics.

4.6 MHD Waves, Equilibria and Instabilities

It is from the two kinds of restoring force due to the magnetic field that one can find a number of wave modes in MHD, and also investigate the equilibria (and instabilities!) of various MHD situations.

4.6.1 MHD waves

From an analysis of the linear wave modes we shall find that, in place of the sound waves associated with a classical gas, there are three distinct MHD waves:

Alfvén waves In this case the restoring force is due entirely to the tension associated with the field lines; the wave is transverse and essentially magnetic, with no compression of the matter.

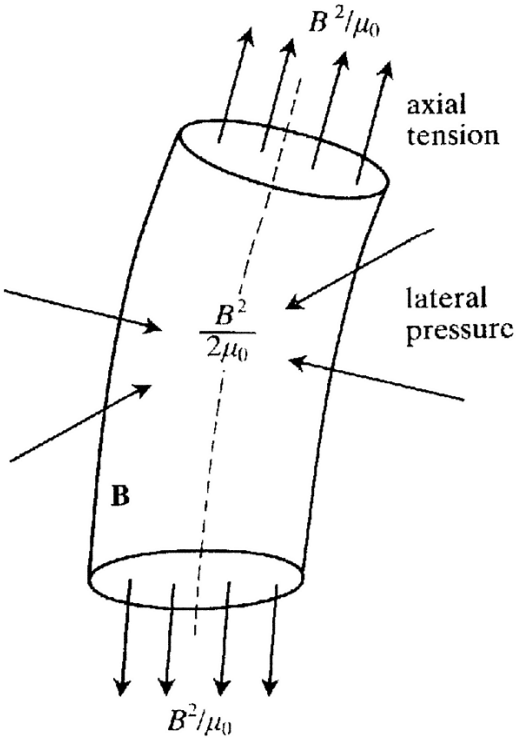

Figure 4.5: Magnetic pressure and tension forces acting on a magnetic flux tube

Fast mode waves The field magnitude and gas pressure both vary. In the fast mode their variation is in phase, and the waves propagate faster than an Alfvén wave.

Slow mode waves The field magnitude and gas pressure both vary. In the slow mode their variation is out of phase, and the waves propagates slower than an Alfvén wave.

We will investigate the MHD equations for small amplitude, plane wave solutions. Appendix B reviews the basic mathematics and conepts related to plane wave analysis which we employ here. Into the MHD equations we substitute:

$$\mathbf{B} = \mathbf{B}_0 + \mathbf{B}_1 \tag{4.35}$$
$$\mathbf{V} = \mathbf{V}_0 + \mathbf{V}_1 \equiv \mathbf{V}_1 \tag{4.36}$$
$$\rho = \rho_0 + \rho_1 \tag{4.37}$$
$$p = p_0 + p_1 \tag{4.38}$$

where quantities with subscript "1" represent small, linear perturbations from the values (subscript "0") obtained from an equilibrium solution of the MHD equations. Higher order perturbations are ignored. As noted in (4.36) we will work in a frame where $\mathbf{V}_0 = \mathbf{0}$. The equilibrium is assumed to be uniform, with $\rho_0 = constant$, $\mathbf{B}_0 = constant$, and $p_0 = constant$. Then we linearize by substituting into the MHD equations (see Section 2.4.4), cancel the terms which appear in the equilibrium solutions to obtain

$$\frac{\partial \rho_1}{\partial t} + \rho_0 \nabla \cdot \mathbf{V}_1 = 0 \tag{4.39}$$

$$\rho_0 \frac{\partial \mathbf{V}_1}{\partial t} = -\nabla p_1 + \frac{1}{\mu_0}(\nabla \times \mathbf{B}_1) \times \mathbf{B}_0 \tag{4.40}$$

$$\frac{\partial \mathbf{B}_1}{\partial t} = \nabla \times (\mathbf{V}_1 \times \mathbf{B}_0) \tag{4.41}$$

$$p_1 = c_s^2 \rho_1 \tag{4.42}$$

where c_s is the sound speed, $c_s^2 = \gamma p_0/\rho_0$. Now we look for plane wave solutions of the form

$$Q_1 = \delta Q e^{i(\mathbf{k}\cdot\mathbf{x} - \omega t)} \tag{4.43}$$

where Q_1 represents one of the fluid perturbation quantities defined above, and where $\mathbf{k}$ is the wave vector (wavelength $\lambda = 2\pi/|\mathbf{k}|$), and ω is the angular frequency of the oscillation. Substituting and equating coefficients of the same exponent will simply give the same result as the following substitution in the original equations: $\nabla \Rightarrow i\mathbf{k}$ and $\partial/\partial t \Rightarrow -i\omega$.

So the equations for the perturbations become

$$-\omega\delta\rho + \rho_0 \mathbf{k}\cdot\delta\mathbf{V} = 0 \tag{4.44}$$

$$-\rho_0\omega\delta\mathbf{V} = -\mathbf{k}\delta p + \frac{1}{\mu_0}(\mathbf{k}\cdot\mathbf{B}_0)\,\delta\mathbf{B} - \frac{1}{\mu_0}(\delta\mathbf{B}\cdot\mathbf{B}_0)\,\mathbf{k} \tag{4.45}$$

$$-\omega\delta\mathbf{B} = (\mathbf{k}\cdot\mathbf{B}_0)\,\delta\mathbf{V} - (\mathbf{k}\cdot\delta\mathbf{V})\,\mathbf{B}_0 \tag{4.46}$$

$$\delta p = c_s^2 \delta\rho \tag{4.47}$$

This gives us 4 equations containing 4 unknowns. Combining (4.44) and (4.47) gives

$$\delta p = \frac{\rho_0 c_s^2}{\omega}\mathbf{k}\cdot\delta\mathbf{V} \tag{4.48}$$

Now substitute (4.48) for δp and (4.46) for $\delta\mathbf{B}$ into (4.45), in order to get an equation for $\delta\mathbf{V}$

$$\begin{aligned} -\rho_0\omega\delta\mathbf{V} = & -\frac{\rho_0 c_s^2}{\omega}(\mathbf{k}\cdot\delta\mathbf{V})\,\mathbf{k} \\ & -\frac{1}{\mu_0}(\mathbf{k}\cdot\mathbf{B}_0)\left[\frac{(\mathbf{k}\cdot\mathbf{B}_0)}{\omega}\delta\mathbf{V} - \frac{(\mathbf{k}\cdot\delta\mathbf{V})}{\omega}\mathbf{B}_0\right] \\ & +\frac{1}{\mu_0}\left[\frac{(\mathbf{k}\cdot\mathbf{B}_0)}{\omega}(\mathbf{B}_0\cdot\delta\mathbf{V})\,\mathbf{k} - \frac{(\mathbf{k}\cdot\delta\mathbf{V})}{\omega}B_0^2\mathbf{k}\right] \end{aligned} \tag{4.49}$$

This can be written in matrix form, $\boldsymbol{A}\cdot\delta\mathbf{V} = \mathbf{0}$, where the matrix $\boldsymbol{A}$ is a function of $(\mathbf{k}, \omega, \mathbf{B}_0, \rho_0, p_0)$. In order for this equation to have a non-trivial solution we require $\det\boldsymbol{A} = 0$. This gives a relationship between $\mathbf{k}$ and ω, which is called the dispersion relation. The corresponding $\delta\mathbf{V}$ is an eigenvector, and gives the polarization and other characteristics of the wave. While this approach provides the complete solution to waves in MHD plasmas, we shall content ourselves here to begin by considering in more detail a few special cases related to choices of the orientation of the wave-vector $\mathbf{k}$ with respect to $\mathbf{B}_0$.

Waves propagating parallel to $\mathbf{B}_0$

Let $\mathbf{B}_0 = B_0\hat{z}$ and $\mathbf{k}$ be along the z-direction. First, consider only the z-component of (4.49); both terms in the square brackets vanish, and one is left with:

$$\omega^2\delta V_z = k^2 c_s^2 \delta V_z \tag{4.50}$$

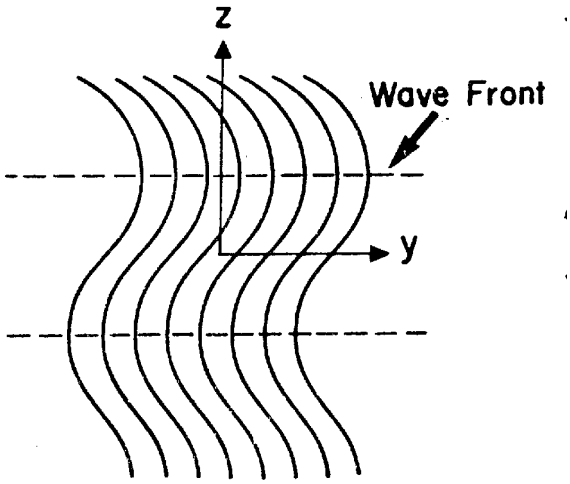

Figure 4.6: An Alfvén wave propagating parallel to the background magnetic field.

And for $\delta V_z \neq 0$ this implies $\omega^2 = k^2 c_s^2$ which is the dispersion relation for sound waves. One finds that $\delta V_x = 0 = \delta V_y$ and so $\delta \mathbf{V} \parallel \mathbf{k}$, i.e. the waves are longitudinal, with a phase speed of

Sound Wave Dispersion Relation	$\omega/k = \pm c_s$	(4.51)

.

Now consider the transverse component of (4.49):

$$-\rho_0 \omega \delta \mathbf{V}_\perp = \mathbf{0} - \frac{kB_0}{\mu_0}\left[\frac{kB_0}{\omega}\delta \mathbf{V}_\perp\right] + \mathbf{0} \tag{4.52}$$

so that, for $\delta \mathbf{V}_\perp \neq \mathbf{0}$,

Alfvén Wave Dispersion Relation	$\omega^2 = k^2 v_A^2$	(4.53)

where $v_A^2 = B_0^2/(\mu_0 \rho_0)$ is the square of the Alfvén speed. This is the dispersion relation for Alfvén waves. The perturbation $\delta \mathbf{V}$ is perpendicular to $\mathbf{k}$ and $\mathbf{B}_0$, so that the wave is called a transverse, or shear wave. The phase speed $\omega/k = \pm v_A$. For the Alfvén wave, from (4.46)

$$\delta \mathbf{B}_\perp = -\frac{kB_0}{\omega}\delta \mathbf{V}_\perp \tag{4.54}$$

i.e., the field perturbation and velocity perturbations are parallel to each other. The waves are like waves on a string, and are due to the field line tension, as sketched in Figure 4.6. Equations (4.44) and (4.48) tell us that $\delta\rho = 0 = \delta p$, so there is no compression of the plasma and the Alfvén wave is thus essentially magnetic.

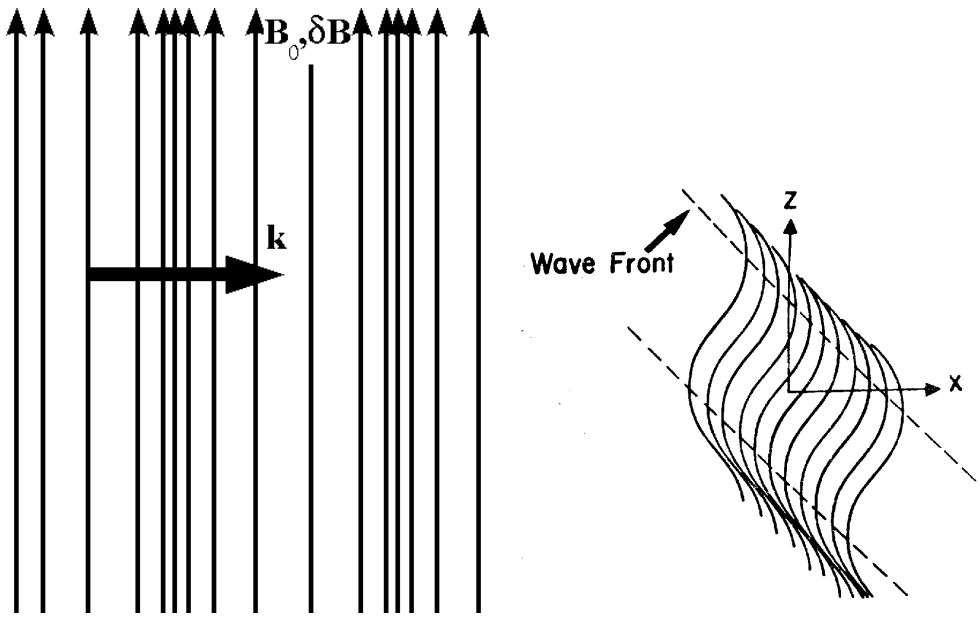

Figure 4.7: Fast magnetosonic wave propagating perpendicular ($\mathbf{k} \perp \mathbf{B}_0$) (left) and obliquely (right) to $\mathbf{B}_0$.

Waves propagating perpendicular to $\mathbf{B}_0$

From (4.49), $\mathbf{k} \perp \mathbf{B}_0$ gives $\delta V_z = 0$, and the perpendicular component of (4.49) gives

$$-\rho_0 \omega \delta \mathbf{V}_\perp = -\frac{\rho_0 c_s^2}{\omega} (\mathbf{k} \cdot \delta \mathbf{V}_\perp) \mathbf{k} - \mathbf{0} - \frac{(\mathbf{k} \cdot \delta \mathbf{V}_\perp)}{\mu_0 \omega} B_0^2 \mathbf{k} \tag{4.55}$$

Hence $\delta \mathbf{V}_\perp$ is parallel to $\mathbf{k}$, and thus

$$\omega^2 \delta V_\perp = k^2 \left(c_s^2 + v_A^2\right) \delta V_\perp \tag{4.56}$$

For a non-trivial solution for $\delta V_\perp$ we therefore reach the dispersion relation

Fast Magnetosonic Dispersion Relation $\qquad \omega^2 = k^2 \left(c_s^2 + v_A^2\right)$	(4.57)

These are termed *fast mode magnetosonic* waves. Both B and p show compression ($\delta\rho \neq 0$, $\delta p \neq 0$, $\delta \mathbf{B} \neq \mathbf{0}$ from (4.44), (4.48) and (4.46)). In this case of perpendicular propagation, the fast mode propagates with a phase velocity

$$\omega / k \equiv v_f = \sqrt{c_s^2 + v_A^2} \tag{4.58}$$

. Figure 4.7 shows the fast magnetosonic mode propagating both perpendicular and obliquely to $\mathbf{B}_0$ and reveals the compression in the field.

General Case: $\mathbf{k} \cdot \mathbf{B_0} = kB_0 \cos\theta$

In the general case the wave vector $\mathbf{k}$ is oblique to $\mathbf{B}_0 \equiv B_0 \hat{z}$, with θ being the angle between the two. Now there are three waves, essentially because there are three restoring forces: magnetic tension, mag-

netic pressure, and thermal pressure. The dispersion relations for these three modes are

Alfvén Wave	$\omega^2 = k^2 v_A^2 \cos^2\theta \equiv k_z^2 v_A^2$	(4.59)

The Alfvén wave is purely transverse, does not compress the plasma ($\delta\rho = 0 = \delta p$) and carries energy along the background field (the group velocity $\partial\omega/\partial\mathbf{k} = v_A\hat{z}$)

Fast and Slow Magnetosonic Waves	$\omega^2 = k^2 \frac{c_s^2 + v_A^2}{2}\left[1 \pm \sqrt{1 - \frac{4c_s^2 v_A^2 \cos^2\theta}{\left(c_s^2 + v_A^2\right)^2}}\right]$	(4.60)

One way to visualise these waves is to imagine dropping a pebble into a plasma "pond" and watching the resulting ripples. Unlike simple water waves, which propagate at the same speed in all directions and therefore have circular ripples, the waves in an MHD plasma propagate at different speeds, and these speeds depend on the direction of propagation. The resulting "ripples" are shown in the Friedrichs Diagrams in Figure 4.8.

4.6.2 MHD Equilibria

Since there are restoring forces associated with both field line compression and field line bending, there is the possibility of storing energy in both kinds of field perturbations. This means that, if we consider an MHD system, we can ask the question: Is the system in equilibrium? Depending on whether the system is in an energy minimum, or at an energy maximum, we say that it is in a stable or unstable equilibrium, respectively. Solar prominences are a spectacular example of MHD systems in a quasi-stable equilibrium. Prominences are enormous tubes of cool dense material, held up high in the corona, presumably by twisted magnetic fields. We say "quasi-stable" because they are sometimes observed to last for weeks, or months. Sometimes prominences are observed to "erupt", i.e., to appear to burst upwards, disappearing rapidly, in the space of a few hours. Such eruptive prominences are obviously due to some large scale (MHD?) instability. The reason for the transition from stability to instability is not completely clear, but is probably due to a rearrangement of the magnetic fields at the base of the corona.

We can set $\partial/\partial t = 0$ in the MHD equations, and then examine the resulting solutions which are called magnetohydrostatic (MHS) equilibria. Since much of these studies are concerned with coronal structures we include the gravitational term:

$$\nabla p - \rho\mathbf{g} = \frac{1}{\mu_0}(\nabla \times \mathbf{B}) \times \mathbf{B} \tag{4.61}$$

$$p = \frac{k_b}{m}\rho T \tag{4.62}$$

$$\nabla \cdot \mathbf{B} = 0 \tag{4.63}$$

Along the magnetic field there is no contribution from the magnetic force, and so we have a hydrostatic balance between pressure gradients and gravity. Comparing the gas pressure p to the magnetic pressure $B^2/2\mu_0$ defines the plasma beta

Plasma Beta	$\beta = \frac{p}{B^2/2\mu_0} = \frac{2}{\gamma}\frac{c_s^2}{v_A^2}$	(4.64)

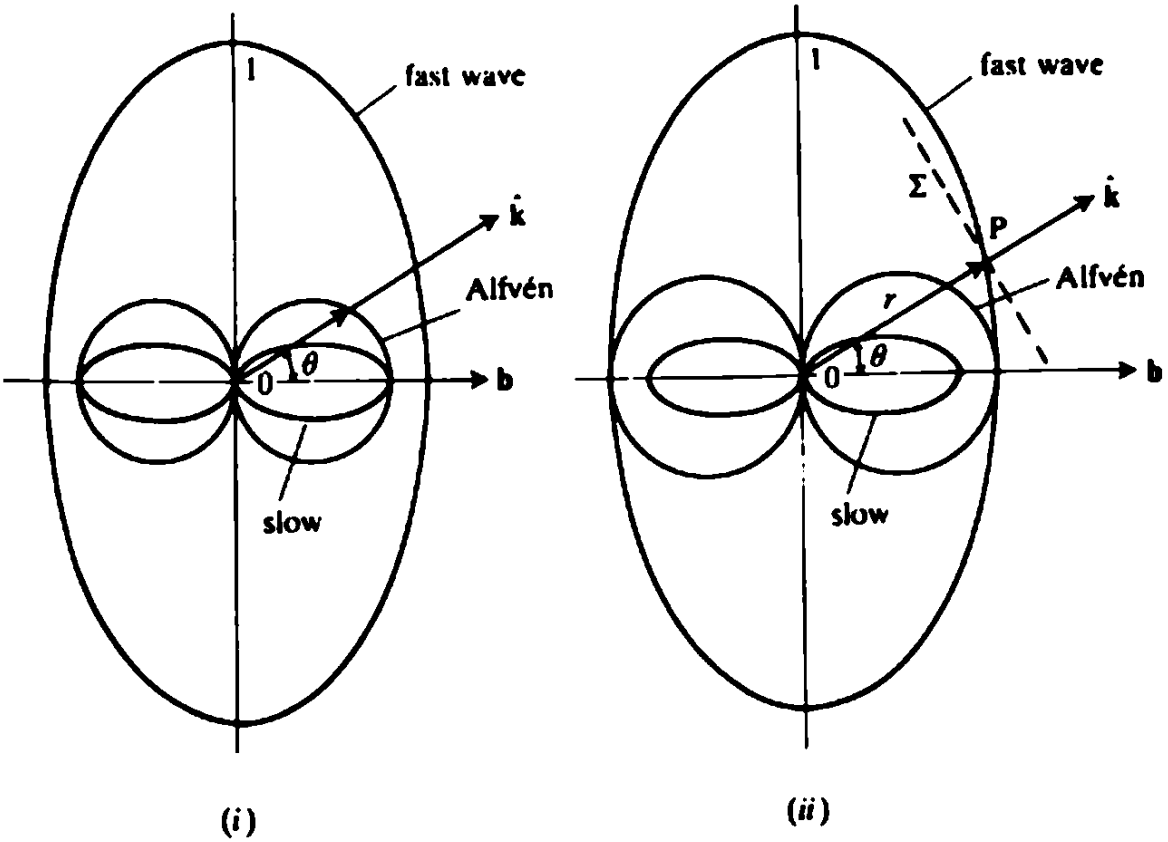

Figure 4.8: Friedrichs Diagram showing MHD wave mode phase speeds as a function of angle between **k** and $\mathbf{B}_0$. The distance r to a point P in the direction of **k** is proportional to the phase speed of the waves propagating in that direction. The case on the left corresponds to $c_s^2 \gg v_A^2$ for which the fast mode is essentially a modified sound wave (in the limit $v_A^2 \to 0$ the Alfvén and slow modes shrink to the origin and the fast mode "ripple" becomes circular). The case on the right corresponds to $v_A^2 \gg c_s^2$.

For $\beta \gg 1$ the magnetic field behaviour is dominated by the gas pressure, and the Lorentz force can be neglected. For $\beta \ll 1$ the magnetic field dominates, and the pressure may be neglected (this is case for solar corona, usually). When $\beta \ll 1$ and L the typical scale length of any structures is such that $L < h$ where h is the pressure scale height (the distance over which the pressure falls by a factor e due to gravity), then the gravitational force can be neglected. In this case (typical of active regions on the Sun) one finds so called force-free equilibrium where

$$\boxed{\text{Force Free Equilibrium} \qquad (\nabla \times \mathbf{B}) \times \mathbf{B} = \mathbf{0}} \tag{4.65}$$

A more restrictive case is when one further specifies that there is zero current. Such current-free equilibria obey

$$\nabla \times \mathbf{B} = \mathbf{0} \tag{4.66}$$

A second solution exists to (4.65) in which the electric current **j** is parallel to the magnetic field **B**. The force-free equilibrium equation in this case is deceptively simple, especially when it is noted that it is

equivalent to

$$\nabla \times \mathbf{B} = \alpha \mathbf{B} \tag{4.67}$$

where $\alpha = \alpha(\mathbf{r})$. In fact a major area of research is finding suitable solutions for α. Of course when $\alpha = constant$, the force-free equilibrium equation becomes much easier to solve.

MHS Example: Cylindrically Symmetric Flux Tube

The subject of MHD equilibria is too vast to go into too much detail here. Various texts are devoted to the subject, and textbooks which deal with the solar atmosphere are useful starting points.

For now, let us just explore briefly the nature of equilibria by considering a cylindrically symmetric flux tube. We work in (r,ϕ,z) coordinates and assume the magnetic field to be of the form $\mathbf{B} = (0, B_\phi(r), B_z(r))$ while the gas pressure $p = p(r)$ is similarly only a function of the radial distance. Our choice of $\mathbf{B}$ satisfies $\nabla \cdot \mathbf{B} = 0$ without further ado (see Equation A.19), so the MHS equations, ignoring gravity, reduce to just

$$\frac{d}{dr}\left[p + \frac{B_\phi^2 + B_z^2}{2\mu_0}\right] + \frac{B_\phi^2}{\mu_0 r} = 0 \tag{4.68}$$

The first term behaves like a pressure gradient, and the second like a tension. It is clear that an isolated flux tube, in which one expects the total pressure to decrease from the interior, requires an azimuthal field B_ϕ to have any chance of an equilibrium. Thus magnetic flux tubes tend to be "twisted". Equation 4.68 is only one equation for three unknowns, therefore we have the freedom to specify two of them, and solve for the third.

4.6.3 MHD Instabilities

Instabilities arise when an equilibrium represents a system possess free energy in the sense that, for some small perturbation, the perturbation grows and the system departs further from the equilibrium state toward one of lower energy.

There are many different kinds of MHD instabilities. They include the following: interchange modes, in which field lines are wrapped around plasma in a concave manner; Rayleigh-Taylor instability, in which plasma is supported by a field against gravity, which may create structure in prominences; sausage and kink modes of a flux tube; Kelvin-Helmholtz instability, in which plasma flows over a magnetic surface; resistive modes of a sheared magnetic field, which drive reconnection (see Chapter 6); convective instability when a temperature gradient is too large, which can concentrate flux tubes in the photosphere; radiative instability, which creates cool loops and prominences up in the corona; and magnetic buoyancy instability of a magnetic field in a stratified medium in which the density decreases with height. Buoyancy causes flux tubes to rise through the solar convection zone.

In each case, the question of nonlinear development and saturation of the instability is important (and difficult). In general, instability calculations proceed by linearising the governing equations, as we did in Section 4.6.1 except now the background state is not uniform. The resulting dispersion relation gives rise to complex frequencies $\omega = \omega_r + i\gamma$ which results in growing solutions for $\gamma > 0$. [In the MHD equations, in fact, it is possible to show that $\omega_r \equiv 0$.]

4.7 Dynamos

Magnetic fields abound in most, if not all, astrophysical environments. So the obvious question is "Why?". Two answers spring to mind: Either the universe was born with "primordial" magnetic fields, which have been decaying ever since, or else something is generating them. In fact, it is possible that primordial fields are still lurking around, but there is ample evidence that fields can be generated. In the

laboratory, simple circuits and currents give rise to magnetic fields due to Ampere's Law (Equation 2.2). In plasmas, however, fields are more often induced via electromotive effects embodied in the induction equation (4.13). This forms the basis for investigations into the generation of magnetic fields, generally known as "the dynamo problem."

$$\frac{\partial \mathbf{B}}{\partial t} = \nabla \times (\mathbf{V} \times \mathbf{B}) + \eta \nabla^2 \mathbf{B} \tag{4.69}$$

where we have introduced the magnetic diffusivity $\eta \equiv 1/(\mu_0 \sigma)$ to emphasize the role of this term. As we saw in Section 4.2 the last term in this equation represents the magnetic diffusion while the middle term the convection of the field by the plasma bulk flow. Then the decay of the magnetic field due to diffusion (which also leads to dissipation of the field) gives rise to a characteristic decay time τ found from (4.69) as

$$\frac{B}{\tau} \sim \eta \frac{B}{L^2} \tag{4.70}$$

Using standard (collisional) values to evaluate τ gives long, but not infinite, timescales. In the Earth's core, $\tau \sim 3 \times 10^5$ years; in the Sun, $\tau \sim 10^{11}$years, only marginally longer than the age of the Sun. This simple calculation suggests that the Earth needs something to replenish its magnetic field, but perhaps the Sun doesn't. However, we know that the Sun's field reverses on a short timescale (11 years), as does the Earth's, though not nearly so frequent nor regular. Thus some active process is generating these fields. Dynamos really do exist. The only problem is explaining them from our mathematical and plasma physical understanding.

4.7.1 The Dynamo Problem

The full dynamo problem consists of using the MHD equations to show how fluid motions **V** and magnetic fields **B** can be self-consistent and self-maintaining. The motion induces magnetic fields via the induction equation given above, while the fields in turn influence the motion through the MHD momentum equation (4.2). This problem is highly nonlinear and difficult to treat, even numerically. Even the induction equation (4.69) on its own is complicated by the nonlinear convective term.

A compromise to this full problem is to consider the *kinematic dynamo* problem in which the flow is prescribed and the consequences for the magnetic field explored. This makes (4.69) linear in the unknown field behaviour and enables some progress to be made which, hopefully, sheds light on the full dynamo problem.

Known astrophysical fields tend to be dipolar in structure and aligned roughly with a symmetry/rotational axis, so it would be natural to seek solutions with these properties. Unfortunately, a result due to Cowling, known as *Cowling's Theorem*, intervenes. Cowling showed that no steady, axisymmetric solution for a dynamo with laminar fields and flows is possible! Since Cowling's theorem applies to the exact field, it is possible that there are solutions for which some average field and flow are axisymmetric. This has spawned a considerable body of literature on the subject of mean field electrodynamics, in which the properties of fluctuations due to turbulence are inserted and investigated. We shall return to this subject in Section 4.7.3.

4.7.2 Qualitative Dynamo Behaviour

Although the mathematics of dynamo behaviour quickly becomes complicated, the qualitative process can be illustrated rather simply and consists of the following sequence of operations, sketched in Figure 4.9:

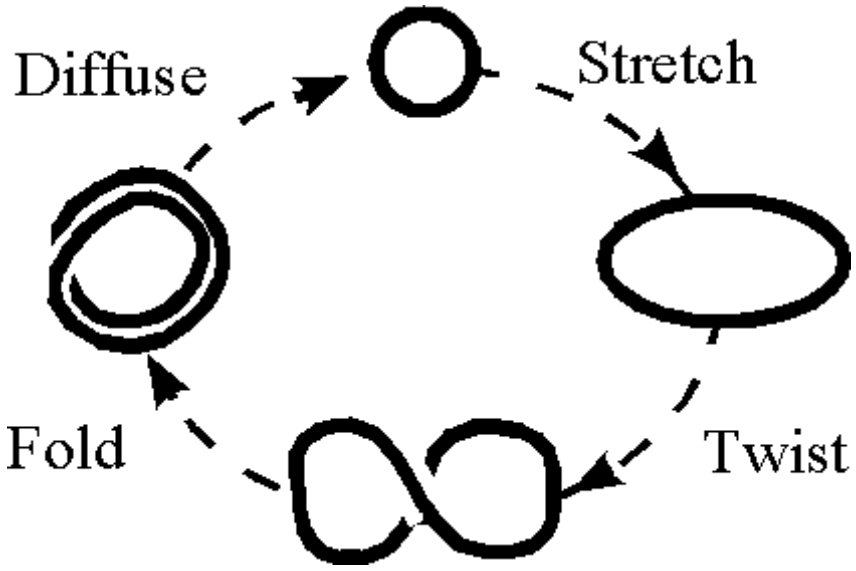

Figure 4.9: Steps in the idealised steady dynamo process

Stretch the field lines to lengthen them. This process does work on the field, transfering flow energy to the magnetic energy density.

Twist the stretched field, to change the direction of the stretched field toward that of the original field. Further twists or folds then amplify the original field. This is the key step.

Diffuse the field across the small scales which are imposed in the above steps to return the system toward its starting point.

4.7.3 Mean Field Kinematic Dynamos

We restrict ourselves here to perhaps the simplest mathematical formulation of the dynamo problem. This is a pure kinematic approach, in which the velocity field is prescribed and we seek the resulting magnetic field by looking at the induction equation. We proceed by decomposing all quantities into their mean values (subscripted "0") and their fluctuations (subscripted "1"). Thus we write

$$\mathbf{B} = \mathbf{B}_0 + \mathbf{B}_1 \tag{4.71}$$
$$\mathbf{V} = \mathbf{V}_0 + \mathbf{V}_1 \tag{4.72}$$

where $\mathbf{B}_0 \equiv < \mathbf{B} >$, the average being over space, time, or ensemble (we shall not need to distinguish amongst these) so that $< \mathbf{B}_1 >= \mathbf{0}$. This is reminiscent of the linearisation we performed in Section 4.6.1 except that here there is no assumption that the fluctuating quantities $\mathbf{B}_1$, $\mathbf{V}_1$ are small. Substitution into the induction equation (4.69) leads to

$$\frac{\partial}{\partial t}(\mathbf{B}_0 + \mathbf{B}_1) = \nabla \times [(\mathbf{V}_0 + \mathbf{V}_1) \times (\mathbf{B}_0 + \mathbf{B}_1)] + \eta \nabla^2 (\mathbf{B}_0 + \mathbf{B}_1) \tag{4.73}$$

Taking the average of this equation leads to the following equation which governs the mean magnetic field $\mathbf{B}_0$:

$$\frac{\partial \mathbf{B}_0}{\partial t} = \nabla \times (\mathbf{V}_0 \times \mathbf{B}_0) + \nabla \times (< \mathbf{V}_1 \times \mathbf{B}_1 >) + \eta \nabla^2 \mathbf{B}_0 \tag{4.74}$$

Thus we can see that the fluctuations in $\mathbf{V}$ and $\mathbf{B}$ give rise to an extra electromotive force $\boldsymbol{\mathcal{E}} \equiv < \mathbf{V_1} \times \mathbf{B_1} >$ which can contribute to the inducted magnetic field. The details of $\boldsymbol{\mathcal{E}}$ depend on the nature of the fluctuations, usually assumed to be turbulent. In particular, if the mean fields are axisymmetric, the fluctuations cannot be in order to avoid the constraints of Cowling's Theorem. An exposition of the momentum equation (to determine $\mathbf{V}_1$) and difference between (4.73) and (4.74) (to determine $\mathbf{B}_1$) is beyond the scope of this text. However, rather general arguments lead to the conclusion that $\boldsymbol{\mathcal{E}}$ is of the form

$$\boldsymbol{\mathcal{E}} = \boldsymbol{\alpha} \cdot \mathbf{B}_0 + \boldsymbol{\beta} : \nabla \mathbf{B}_0 + \ldots \tag{4.75}$$

Taking the simplest case, in which the tensor $\boldsymbol{\alpha}$ is isotropic and $\boldsymbol{\beta}$ is a scalar constant leads to

$$\frac{\partial \mathbf{B}_0}{\partial t} = \nabla \times (\mathbf{V}_0 \times \mathbf{B}_0) + \nabla \times (\alpha \mathbf{B}_0) + (\eta + \eta_T) \nabla^2 \mathbf{B}_0 \tag{4.76}$$

where we have introducted the turbulent diffusivity η_T which results from the $\boldsymbol{\beta}$ term in $\boldsymbol{\mathcal{E}}$. Given the typically long decay times based on classical diffusivity, this role for the turbulence in the medium is essential if a balance between field generation and dissipation is to be reached. Equation 4.76 forms the starting point for many investigations of dynamo action. In terms of the dynamo steps depicted in Figure 4.9, the first term on the right hand side embodies the stretching of the field by the mean flow, while the second term contains the "α-effect" twisting due to the helicity in the turbulence.

4.7.4 $\alpha - \omega$ Solar Dynamo

The solar dynamo represents a key challenge for any dynamo theory. The simplest mathematical approach begins with (4.76) and makes the following further simplifications/assumptions:

- The mean fields $\mathbf{B}_0$ and $\mathbf{V}_0$ are axisymmetric, i.e., they have no ϕ dependence in a spherical polar representation. In particular, we take $\mathbf{B}_0 = \mathbf{B}_0(r, \theta)$
- The mean velocity field is a radially dependent, differentially rotating fluid, i.e., $\mathbf{V}_0 = \omega(r, \theta) r \sin\theta \hat{\phi}$

The first term on the right hand side of (4.76) can be expanded by using (A.7) into four terms. Note firstly that $\nabla \cdot \mathbf{B}_0 = 0$ thanks to maxwell and that $\nabla \cdot \mathbf{V}_0 = 0$ using (A.23) with the knowledge that $\mathbf{V}_0$ has only a $\hat{\phi}$ component and is independent of ϕ. The remaining two terms combine using (A.26) to give

$$\nabla \times (\mathbf{V}_0 \times \mathbf{B}_0) = \hat{\phi} \sin\theta \left[r B_r \frac{\partial \omega}{\partial r} + B_\theta \frac{\partial \omega}{\partial \theta} \right] \tag{4.77}$$

This result may also be obtained more directly by first evaluating $\mathbf{A} \equiv \mathbf{V}_0 \times \mathbf{B}_0$ and then using (A.24) followed by some re-arrangement making use of $\nabla \cdot \mathbf{B}_0 = 0$ as evaluated in spherical polars.

The result of all this is

$$\frac{\partial \mathbf{B}_0}{\partial t} = \hat{\phi} \sin\theta \left[r B_r \frac{\partial \omega}{\partial r} + B_\theta \frac{\partial \omega}{\partial \theta} \right] + \nabla \times (\alpha \mathbf{B}_0) + (\eta + \eta_T) \nabla^2 \mathbf{B}_0 \tag{4.78}$$

The first term on the right hand side embodies the ω-effect, which winds up an initial poloidal field to generate a toroidal ($\hat{\phi}$) one. The second term describes the α-effect, in which the turbulent motions result in a twisting of the field. In the solar case, a net twist (as opposed to equal and cancelling twists) is accomplished by the coriolis effect on rising flux in the stratified solar atmosphere that is not symmetric with that on falling flux tubes. These effects are illustrated in Figure 4.10.

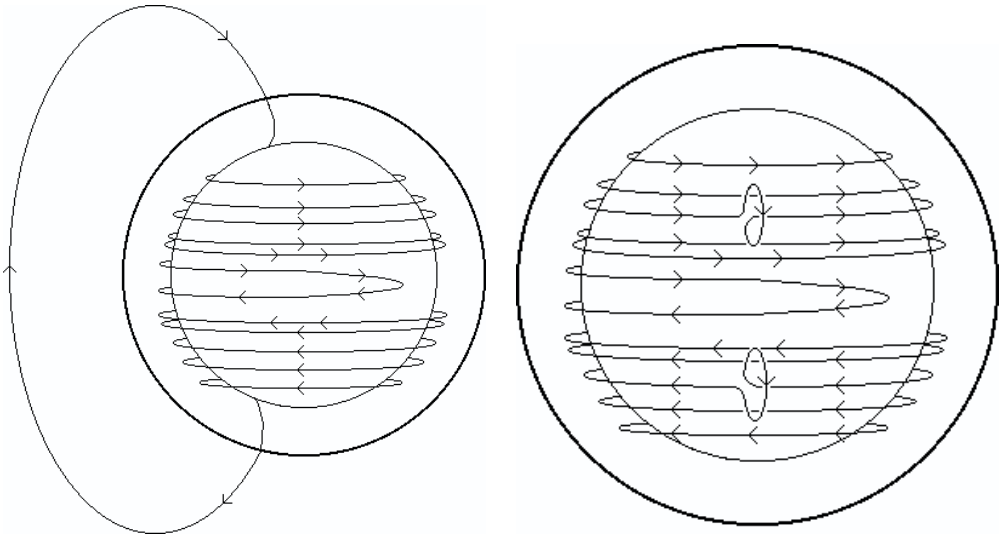

Figure 4.10: Illustration of the ω-effect (left) which stretches poloidal field lines and generates toroidal ones due to the differential rotation of the Sun, in which the equatorial regions rotate faster than the polar regions and the α-effect (right), in which rising flux tubes in the turbulent medium are twisted by coriolis effects.

4.7.5 Astrophysical Dynamos

Solar Dynamo

We have already explored many aspects of the solar dynamo. The 11-year reversals pose a major challenge to dynamo theory. Additionally, within that cycle, concentrations of strong magnetic field, such as sunspots, appear at mid-latitudes during the early phases of the cycle, but the zones of activity appear increasingly at lower latitudes as the cycle progresses. This gives rise to a "butterfly" pattern shown in Figure 4.11.

Another feature of solar magnetic fields is the polarity of emerging flux regions. This polarity follows a regular pattern, with the leading polarity opposite in the opposite hemispheres. The sense reverses with each solar cycle reversal, as shown in Figure 4.12. These facts, known as Hale's Law, are qualitatively consistent with the toroidal field generated due to differential rotation sketched in left portion of Figure 4.10, which then rises due to magnetic buoyancy.

Disk Dynamos

Astrophysical systems involving disks, such as accretion phenomena, are also sites of dynamo action. In these cases, kinematic instabilities give rise to turbulent fluid motions which, in turn, generate fields via dynamo action. These fields, however, are purely turbulent, with no large-scale mean field. Nonetheless, the turbulent diffusivity (for both matter and fields) plays a critical role in the evolution of these systems in terms of angular momentum transport and accretion rates.

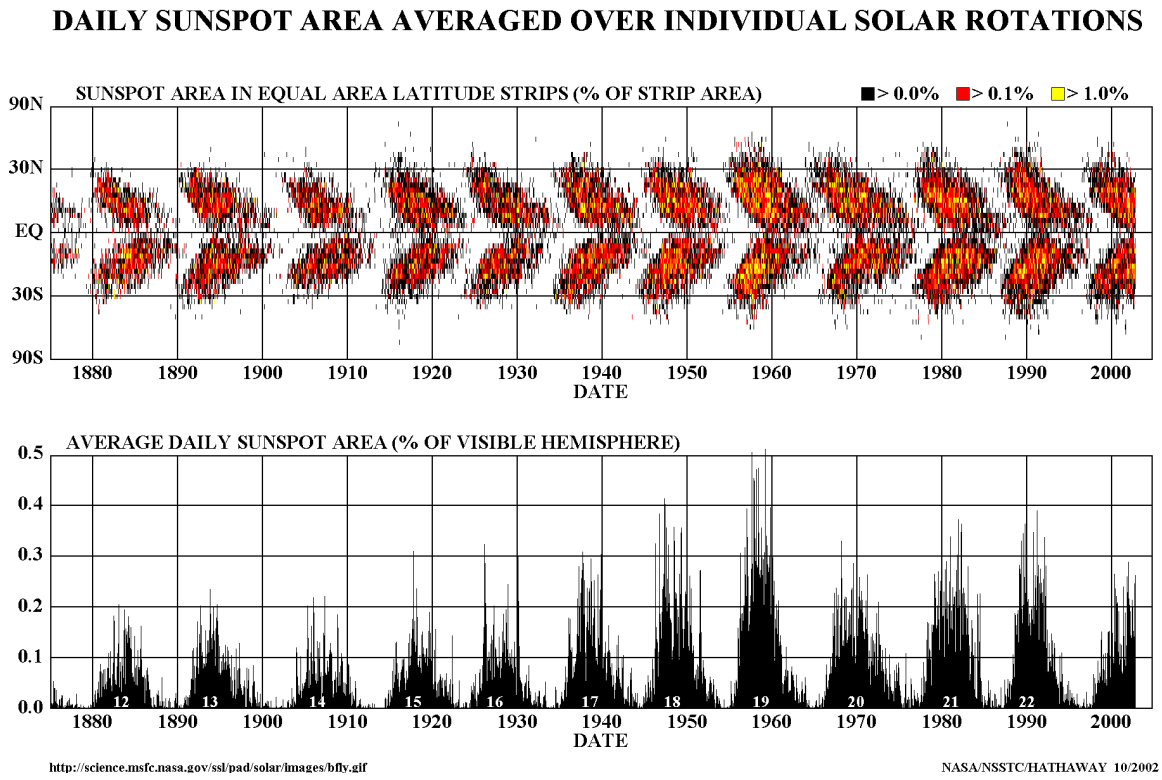

Figure 4.11: Appearance of strong flux regions at different solar latitudes (top) with time, which is related to solar activity as measured, e.g., by total sunspot numbers (bottom). The equatorward drift of emerging flux gives rise to a characteristic "butterfly" diagram.

4.8 Exercises

1. A perfectly conducting plasma has a velocity $-V_0\hat{x}$ and is threaded by a magnetic field $B_0\hat{y}$. An obstacle stands in the flow, and causes a deceleration of the plasma within the region R such that

$$\frac{dV}{dx} = +\left(1 - \left|\frac{y}{L}\right|\right) 0.9\frac{V_0}{L}$$

   Assume that the flow field is fixed once the plasma moves into the region $x < 0$, i.e., that $V(x < 0, y) = V(x = 0, y)$, and that the flow remains in the negative x-direction (i.e., there is no deflection of the flow by the obstacle). Take the $\hat{z}$ direction to be invariant. (see Figure 4.13)

   (a) By applying your knowledge of the frozen-in flux principle, sketch the magnetic field structure in the $x-y$ plane.

   (b) What is the magnetic field strength at $(0,0)$?

   (c) What has happened to the kinetic energy of the flow passing through the region R? (How does conservation of energy apply?)

   (d) What would really happen in the region $x < 0$ and why?

2. A uniform perfectly conducting spherical plasma cloud of mass density ρ_0, total mass M and radius R_0 is rotating at an angular frequency Ω_0. The cloud is permeated by a magnetic field

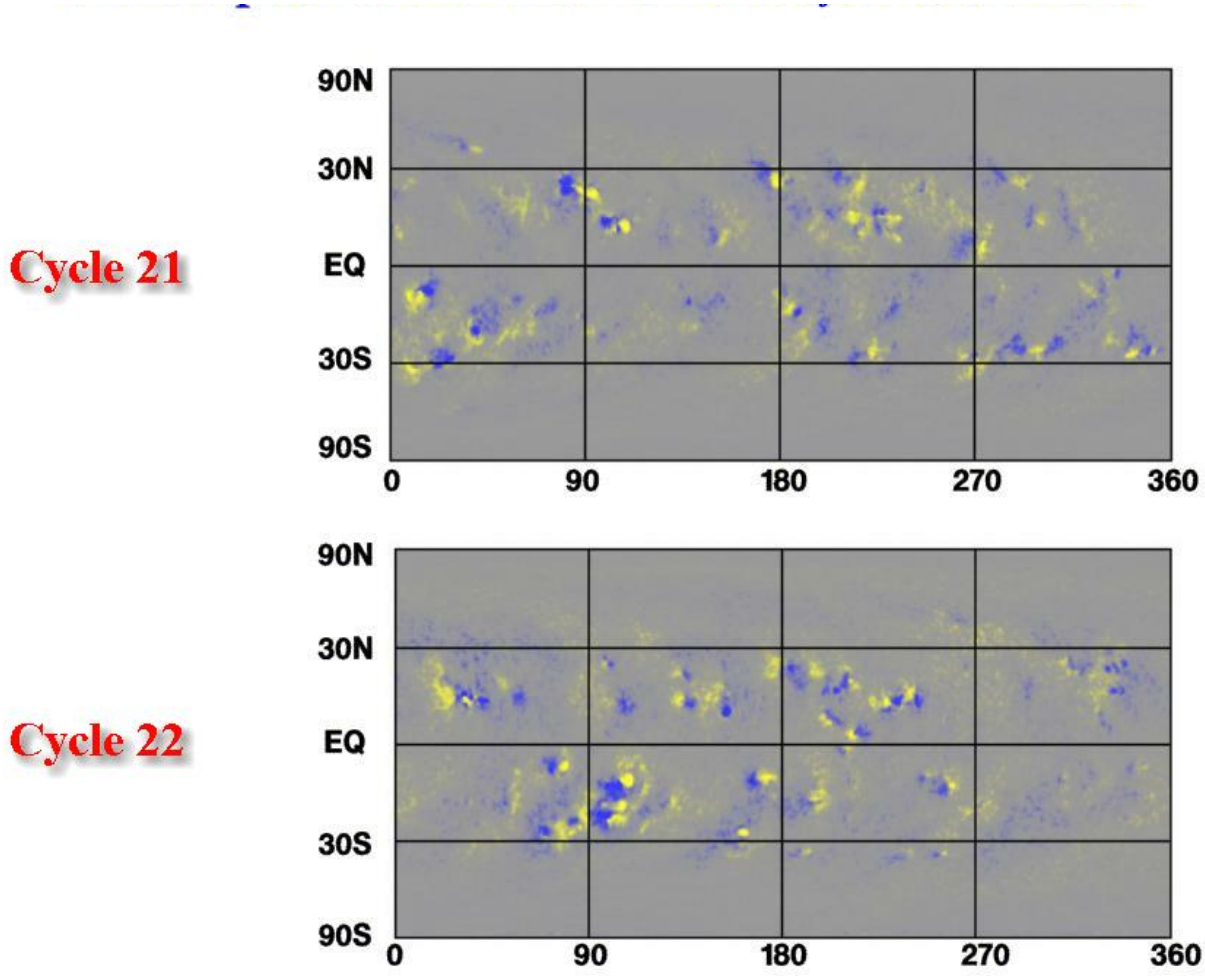

Figure 4.12: Magnetic polarity at various solar latitudes as a function of longitude during two solar cycles, illustrating Hale's Law. Note that within each cycle the leading polarity is opposite in opposite hemispheres, and that this polarity reverses from one cycle to the next.

which is everywhere aligned with the rotation axis, has a magnitude B_0 at the equatorial surface, and increases linearly to twice that value at the rotation axis.

(a) This cloud now suffers a collapse to a radius $R_1 < R_0$. The cloud remains uniform so that its total (conserved) angular momentum throughout the collapse phase is given by $\frac{2}{5}MR_0^2\Omega_0$. Find the resulting mass density, ρ_1, and angular velocity, Ω_1. Hence deduce that, at the equatorial surface the centrifugal force per unit volume, $\rho_1\Omega_1^2R_1$, has increased by a factor $(R_0/R_1)^6$ over its initial value.

(b) Use simple flux freezing arguments (without performing any explicit integrations) to estimate the factor by which the magnetic field, B_1, at the equatorial surface has increased. Hence, assuming that the magnetic profile remained roughly linear, *estimate*, e.g., to within a factor of order unity, the magnetic pressure force per unit volume at the equatorial surface and give an expression for this force in terms of its initial value.

(c) Finally, by comparing the centrifugal and magnetic forces found above, show that the magnetic forces increase relatively less, by a factor R_1/R_0, than the rotational ones, so that the

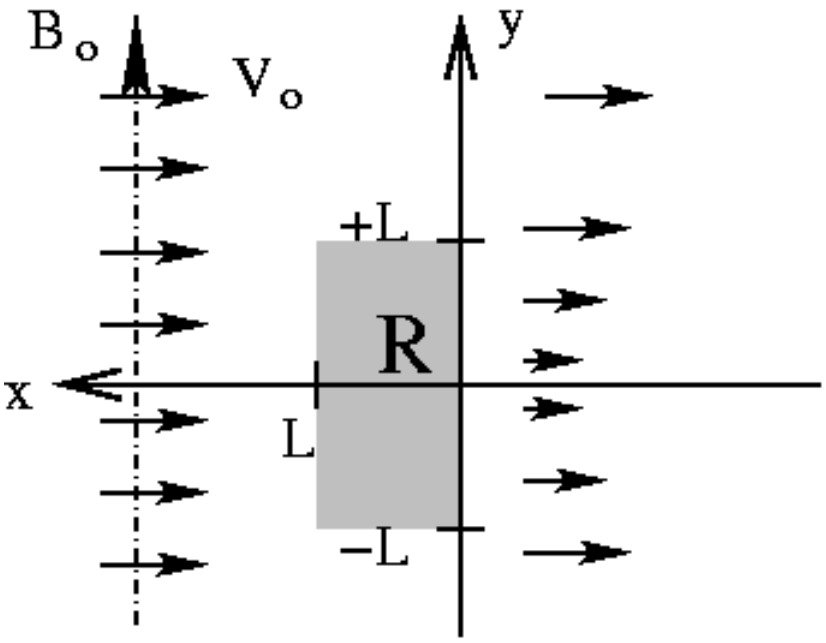

Figure 4.13: Flow hitting an obstacle.

conservation of angular momentum represents a more serious inhibitor of further collapse than the build up of magnetic pressure.

3. Consider a uniform plasma of density ρ threaded by a uniform magnetic field **B**. By making an analogy to the case of small perturbations on a string in which the mass per unit length is ρ and the tension T is equivalent to the magnetic field tension B^2/μ_0, show that the transverse waves on the string propagate with a phase velocity equivalent to the Alfvén speed.

4. Fill in the steps to derive the general MHD dispersion relations (4.59) and (4.60) from (4.49). [Hint: For (4.60) dot (4.49) with **k** and $\mathbf{B}_0$ and then work with the new variables $(\mathbf{k}\cdot\delta\mathbf{V})$ and $(\mathbf{B}_0\cdot\delta\mathbf{V})$.]

5. Evaluate the dispersion relation for fast and slow magnetosonic waves (4.60) in the regime $c_s^2 \ll v_A^2$ by expanding the radical $[\sqrt{1-x} \approx 1 - \frac{1}{2}x - \frac{1}{8}x^2 \ldots$ for $|x| \ll 1]$. Show that

   (a) the slow mode is guided in the sense that the group velocity $\partial\omega/\partial\mathbf{k}$ is directed along the background magnetic field.

   (b) that the pressure perturbations δp are out of phase with the perturbations in the magnetic field pressure $\delta|\mathbf{B}^2|/2\mu_0 \equiv \delta\mathbf{B}\cdot\mathbf{B}_0/\mu_0$. This is a bit challenging. Try dotting (4.49) with **k** and (4.46) with $\mathbf{B}_0$. Then identify the terms in the first dot product which are the same form as the second. The remaining terms are all proportional to $\mathbf{k}\cdot\delta\mathbf{V}$ and so you can derive a relationship between δp and $\delta\mathbf{B}\cdot\mathbf{B}_0$. Use your result for the dispersion relation to show that the proportionality constant is negative. [You can now easily also show that in the case of the fast magnetosonic wave the magnetic and thermal pressures are in phase.]

6. Consider the equilibrium of an isolated cylindrically symmetric flux tube of radius r_0 immersed in a uniform field $B_z\hat{z}$. Given that the plasma thermal pressure varies as $p(r) = p_0\left(1 - \frac{r}{r_0}\right)$ show

that the azimuthal magnetic field must vary according to

$$\frac{B_\phi^2}{2\mu_0} = \frac{r}{3r_0} p_0 \tag{4.79}$$

[You will need to solve Equation 4.68 or at least show that this is a valid solution in the region $r \leq r_0$. You will also need to assign appropriate boundary conditions at, say, $r = 0$.] Also, find the electric current density $\mathbf{j} = \nabla \times \mathbf{B}/\mu_0$ for this configuration.

7. More questions to follow (dynamos)

Chapter 5

The Solar Wind

5.1 Introduction

The solar wind is a flow of ionized solar plasma and an associated remnant of the solar magnetic field that pervades interplanetary space. It is a result of the huge difference in gas pressure between the solar corona and interstellar space. This pressure difference drives the plasma outward, despite the restraining influence of solar gravity. The existence of a solar wind was surmised in the 1950's on the basis of evidence that small variations in the Earth's magnetic field (geomagnetic activity) were produced by observable phenomena on the sun (solar activity), as well as from theoretical models for the equilibrium state of the solar corona. It was first observed directly and definitively by space probes in the mid-l960's.

Measurements taken by spacecraft-borne instruments since that time have yielded a detailed description of the solar wind across an area from inside the orbit of Mercury to well beyond the orbit of Neptune. Our interest in this distant and tenuous plasma stems from two important aspects of solar wind research.

The first of these concerns the role of the solar wind in the interdisciplinary subject known as solar-terrestrial relations. The solar wind is significantly influenced by solar activity (or, in physical terms, by changes in the solar magnetic field) and transmits that influence to planets, comets, dust particles, and cosmic rays that "stand" in the wind. The origin of the solar influence through interaction of the solar magnetic field with the expanding coronal plasma is a major topic in present-day solar-wind research.

The second important aspect of solar-wind research concerns the physical processes that occur in its formation and expansion from the hot solar corona to the cool and far more tenuous regions of the outer solar system. This expansion takes the magnetized plasma through huge variations in its properties; for example, collisions among ions or electrons in the expanding plasma are frequent in the corona, but extremely rare in interplanetary space. Thus the physics of this stellar plasma system can be examined under a wide variety of conditions, some of which are difficult or impossible to reproduce in terrestrial laboratories or in the immediate vicinity of the Earth. However, the solar wind is accessible to space probes, and its properties can be measured and its physical processes studied at a level of detail which is impossible for most astrophysical plasmas.

5.2 Description

Most of our observations of the solar wind have been made by spacecraft near the orbit of the Earth. Typical values for solar wind parameters at this distance (i.e., 1 AU) are given in Table 5.1. The solar wind exhibits considerable variations, with, for example, the flow speed often less than 300km/s or greater than 700km/s.

The embedded magnetic field (the interplanetary magnetic field or IMF) in the Earth's vicinity lies,

Table 5.1: Typical Solar Wind Parameters at 1AU

Parameter	**Value at 1AU**
Proton density	6.6 cm^{-3}
Electron density	7.1 cm^{-3}
He2+ density	0.25 cm^{-3}
Flow speed (radial)	450 km s^{-1}
Proton temperature	1.2×10^5 K
Electron temperature	1.4×10^5 K
Magnetic field	7 nT

on average, in the ecliptic plane, but at approximately 45° to the Earth-Sun line. We will consider simple models to account for these observed properties of the solar wind and the IMF.

5.3 Why is there a solar wind? - A simple model

The supersonic flow of the solar wind comes about from the conversion of thermal energy in the corona (at low velocities) to kinetic energy (high velocities) of radial outflow. We will investigate this conversion using a very simple model of the solar wind. This model makes a large number of assumptions, but nevertheless has most of the important features of more complicated models.

We use the MHD equations in the same notation as in Chapter 4 and look for steady state solutions with $\frac{\partial}{\partial t} = 0$. The equations for conservation of mass and momentum become

$$\nabla \cdot (\rho \mathbf{V}) = 0 \tag{5.1}$$

$$\rho (\mathbf{V} \cdot \nabla) \mathbf{V} = -\nabla p + \mathbf{j} \times \mathbf{B} + \rho \mathbf{F}_g \tag{5.2}$$

where $\mathbf{F}_g$ is the gravitational force per unit mass

$$\mathbf{F}_g = -\frac{GM_\odot}{r^2} \hat{r} \tag{5.3}$$

We now make three major assumptions

1. We assume radial symmetry, so that any flow is strictly radial, and all quantities depend only on the radial distance r.

2. We also neglect the magnetic force term in the momentum equation, so that we only examine the effect of the pressure gradient that drives the flow, and not any back-reaction from the magnetic field. (This might seem strange, given that the importance of magnetic fields has been stressed, but it makes the problem much more attractive!)

3. We treat the plasma as isothermal (i.e., $\gamma = 1$, constant temperature), with the pressure given by the ideal gas law $p = nk_b (T_e + T_i) = 2nk_b T$ and where the mass density is related to the particle number density by $\rho = nm$ ($m = m_e + m_i$). The assumption of constant temperature is equivalent to assuming infinite thermal conductivity.

The assumption of radial symmetry has the following consequences

$$\mathbf{V} = V(r) \hat{r} \tag{5.4}$$

$$\nabla p = \frac{dp}{dr}\hat{r} \tag{5.5}$$

$$\nabla \cdot (\rho \mathbf{V}) = \frac{1}{r^2}\frac{d}{dr}\left(\rho V r^2\right) \tag{5.6}$$

$$\rho\,(\mathbf{V}\cdot\nabla)\,\mathbf{V} = \rho V \frac{dV}{dr}\hat{r} \tag{5.7}$$

So, our simplified model reduces to

$$\frac{d}{dr}\left(\rho V r^2\right) = 0 \tag{5.8}$$

$$\rho V \frac{dV}{dr} = -\frac{dp}{dr} - \frac{\rho G M_\odot}{r^2} \tag{5.9}$$

$$p = \frac{\rho}{m} 2 k_b T \tag{5.10}$$

5.3.1 Static Atmosphere: $V(r) = 0$

Since we are trying to investigate the formation of the solar wind, it may seem perverse to start with the case of a static atmosphere. However, as well as being the historical starting point, it is revealing to find out why a static solar atmosphere is not possible.

Setting $V = 0$ automatically satisfies Equation 5.8 for mass conservation, and the momentum equation (5.9) becomes

$$0 = -\frac{dp}{dr} - \frac{\rho G M_\odot}{r^2} \tag{5.11}$$

Using (5.10) with T =constant we can find an equation for p only

$$\frac{1}{p}\frac{dp}{dr} = -\frac{G M_\odot m}{2 k_b T}\frac{1}{r^2} \tag{5.12}$$

which has the following solution

$$\ln p = \frac{G M_\odot m}{2 k_b T}\frac{1}{r} + K \tag{5.13}$$

where K is constant. Suppose that the pressure at the base of the corona, $r = R$, is $p = p_0$. Then we find the full expression for the pressure as a function of radial position

$$p(r) = p_0 \exp\left[\frac{G M_\odot m}{2 k_b T}\left(\frac{1}{r} - \frac{1}{R}\right)\right] \tag{5.14}$$

For $r > R$, $p < p_0$, i.e., the pressure decreases with radial position.

In the case of a "shallow" atmosphere such as the Earth's, where $r - R \ll R$, then the pressure decrease becomes exponential of the form $p = p_0 e^{-h/\lambda}$. But the problem we encounter for the Sun's corona is that the atmosphere is not shallow, so for large r

$$p \to p_0 \exp\left[-\frac{G M_\odot m}{2 k_b T}\frac{1}{R}\right] \tag{5.15}$$

Using typical values for the solar corona, with $T = 10^6$K, one finds that the exponential term is only a factor 3×10^{-4} below the coronal pressure, and this is much higher than the observed "interstellar" pressure. One is therefore led to the conclusion that a static solar atmosphere cannot be in equilibrium with the interstellar medium, and so we must look for solutions with an outflow velocity.

5.3.2 Solar Wind Solutions: $V(r) \neq 0$

The history of the prediction and eventual confirmation of the existence of the solar wind is an interesting one. In the late 1950's when Parker proposed a continual, supersonic flow from the corona, the result of the static atmosphere was known, while the possible incompatibility with the interstellar medium pressure was not really known for certain. However, it was acknowledged that there had to be a way for the sun to influence the Earth in a fairly rapid and powerful way, since large geomagnetic storms were often seen associated with, but a few days after, a solar flare. It was thought that the flare ejected a stream of protons in some collimated beam (the solar "corpuscular radiation theory"), but of course anybody with knowledge of plasmas would know that this single species beam would be very unstable. On the other hand Biermann had been making observations of the plasma tails of comets, and since the early 1950's had been emphasizing how these were permanent features, and that they always pointed away from the sun. Parker was aware of these observations, and decided that by proposing a steady, flowing solar wind he could explain both the orientation of the cometary plasma tails and also the way in which perturbations at the sun (e.g., flares) could be carried by the flow to the Earth, where they could perturb the magnetic field as measured at the surface of the Earth.

We now follow, in simplified form, the argument that Parker suggested.

Integrating the mass conservation equation (5.8) finds $\rho V r^2 = C$ where C is a constant, or equivalently

$$I = 4\pi r^2 \rho V \tag{5.16}$$

where I is the mass flux through a sun centred sphere of radius r, which is constant when the flow is independent of time.

Again assuming an isothermal expansion (5.10) for p the momentum equation (5.9) becomes

$$\rho V \frac{dV}{dr} = -2k_b T \frac{dn}{dr} - \frac{\rho G M_\odot}{r^2} \tag{5.17}$$

Dividing by $\rho \equiv nm$ gives

$$V \frac{dV}{dr} = -\frac{2k_b T}{m} \frac{1}{n} \frac{dn}{dr} - \frac{G M_\odot}{r^2} \tag{5.18}$$

Our aim is to reduce this to an equation for $V(r)$, so from the mass conservation equation

$$n = \frac{I}{4\pi m} \frac{1}{V r^2} \tag{5.19}$$

Differentiating

$$\frac{dn}{dr} = \frac{I}{4\pi m} \left(-\frac{1}{r^2 V^2} \frac{dV}{dr} - \frac{2}{V r^3} \right) \tag{5.20}$$

Simplifying, and substituting back into the momentum equation:

$$V \frac{dV}{dr} = \frac{4k_b T}{mr} + \frac{2k_b T}{m} \frac{1}{V} \frac{dV}{dr} - \frac{G M_\odot}{r^2} \tag{5.21}$$

And rearranging gives

$$\text{Parker's Solar Wind Equation} \qquad \left(V^2 - \frac{2k_bT}{m}\right)\frac{1}{V}\frac{dV}{dr} = \frac{4k_bT}{mr} - \frac{GM_\odot}{r^2} \tag{5.22}$$

This ends our search for a governing equation for the radial outflow. It is not too difficult to solve this ordinary differential equation. But it is interesting to look for the behaviour of solutions to this equation in a qualitative fashion, by asking how left hand side (LHS) and right hand side (RHS) can balance.

Considering the RHS: for the observed coronal temperatures one finds that the RHS is negative, i.e.

$$\frac{GM_\odot}{r^2} > \frac{4k_bT}{mr} \tag{5.23}$$

That is, the corona is gravitationally bound. For increasing r, gravitational term decreases faster than the thermal term. So the RHS for small r is negative, but becomes positive after passing through zero at the critical radius r_c at

$$\text{Critical Radius} \qquad r_c = \frac{GM_\odot m}{4k_bT} \tag{5.24}$$

Now consider the LHS. Observations show that at small r the flow velocities $V(r)$ are smaller than the thermal velocity, so

$$V^2 - \frac{2k_bT}{m} < 0 \tag{5.25}$$

But the RHS at this time is also negative, so in order to balance one must have $dV/dr > 0$, which implies that V increases with r. So at small r the flow is small but increases with radius. But as r increases beyond r_c there are two possible solutions which depend on what happens at r_c. At r_c the RHS is zero, so either $dV/dr = 0$ (and V has a maximum or minimum) or $V^2 - 2k_bT/m = 0$ (and dV/dr can remain positive). These possibilities are sketched in Figure 5.1

The solution which has dV/dr passing through zero at $r = r_c$ must have $dV/dr < 0$ for $r > r_c$, so that the flow becomes small at large radial distances. The problem with this case is that it resembles the static atmosphere, which does not balance with the known interstellar pressure. Thus we are led to reject this type of solution.

The solution with $V^2 - 2kT/m = 0$ at $r = r_c$, on the other hand, maintains $dV/dr > 0$ and has a flow speed which continues to increase with radial distance. If $V(r)$ increases with r, then the number density

$$n(r) = \frac{I}{4\pi m}\frac{1}{r^2V(r)} \tag{5.26}$$

decreases with r, and so the pressure $p = 2nk_bT$ becomes increasingly small at large radial distances, so that there is indeed the possibility of coming into balance with the interstellar pressure.

The critical radius is especially important in the following respect. The flow velocity at $r = r_c$ is $V = \sqrt{2k_bT/m}$. Recall that the speed of sound is given by

$$c_s^2 = \frac{\gamma p}{\rho} = \gamma\frac{2k_bT}{m} \tag{5.27}$$

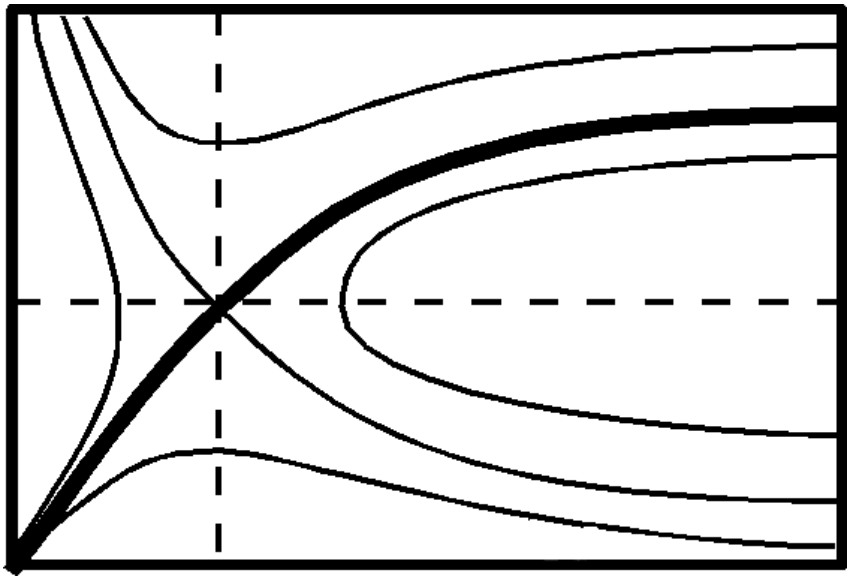

Figure 5.1: Possible solutions to Parker's solar wind equation (5.22). The breeze solution is close to the static atmosphere case and asymptotes to a finite pressure at large r. Only the solar wind solution, which passes through the sonic point at the critical radius r_c matches the solar and interstellar boundary conditions. Interestingly, Parker's equation only involves the square velocity, and so also includes accretion-type solutions, such as the solution which is sub-sonic at large r and increases through the sonic point to large velocities close to the star.

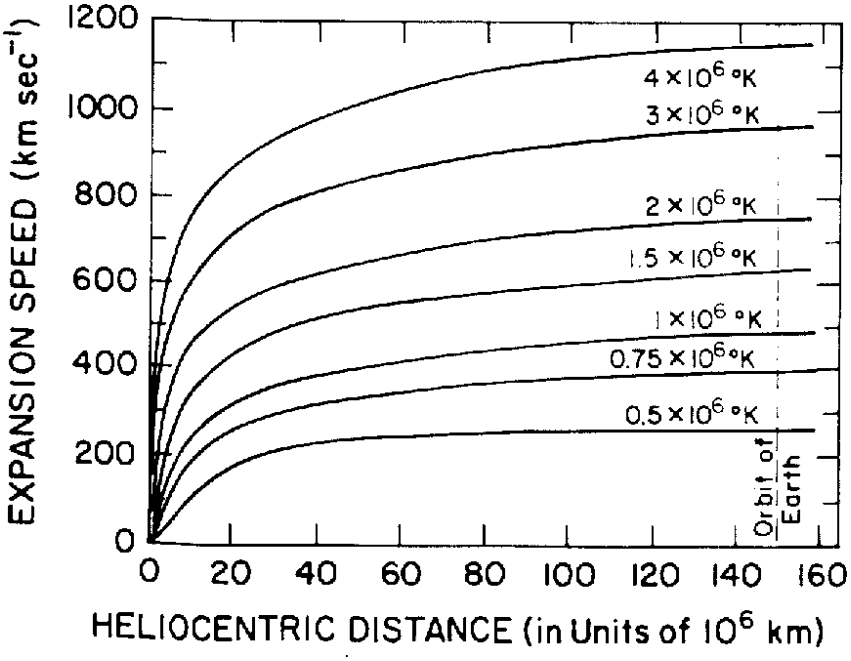

Figure 5.2: Isothermal radial expansion speed solutions $V(r)$ for different coronal temperatures.

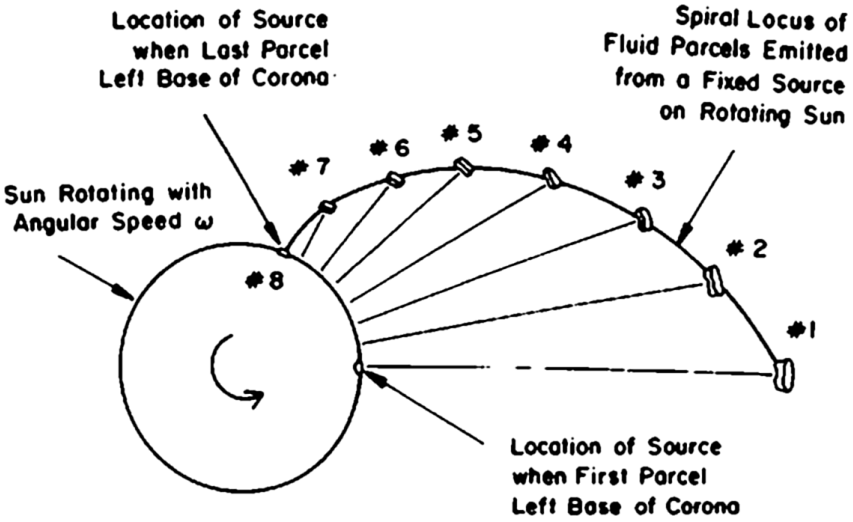

Figure 5.3: Loci of a succession of fluid parcels emitted at constant speed from a source rotating with the sun.

For an isothermal medium, $\gamma = 1$, and one can identify the critical radius at which the solar wind solution becomes supersonic. Observations do indeed reveal that the solar wind is supersonic at 1AU. Figure 5.2 shows solar wind solutions for various temperatures.

Much research effort has been spent making more sophisticated models of the solar wind, by including the effects of the magnetic field, thermal conductivity, the presence of alpha particles (ionized helium, which is an important minority species), and so on. Unfortunately, the increasing sophistication of the models has not resulted in any one model that can predict every feature of the solar wind at 1 AU (at the Earth's orbit). It seems necessary that additional heating must take place in the solar wind in the corona, so that the simple model above is not completely correct. But the nature of this additional heating process, although probably originally from the photospheric motions, has not yet been identified.

5.3.3 The Interplanetary Magnetic Field (IMF)

Since the Magnetic Reynold's (4.14) number in the solar wind is high, we expect that the Flux Freezing Theorem will be valid, and the magnetic field at the surface of the sun will be carried out into interplanetary space by the solar wind.

The situation is complicated by the fact that the sun (and hence the foot points of the magnetic field lines) rotates every 25.4 days. The apparent period of rotation at the Earth is about 27 days. This is an angular frequency of $\Omega \approx 2.7 \times 10^{-6}$rad/s. But once a plasma "parcel" has left the sun, it moves approximately radially, due to its high radial speed. However, the magnetic field line which passes through it is tied to the original coronal position which is rotating. The effect is to produce a spiral pattern, like the streams of water from a rotating water sprinkler.

Consider separate plasma parcels emitted from the same location at the corona. They move out radially, but they are joined by the same field line; plasma elements initially on the same field line, remain on that field line for all time (flux freezing). This is illustrated in Figure 5.3. Thus the IMF has spiral structure, which tends to wind tighter as one goes further from the sun (i.e., perpendicular to the axis of solar rotation), and which is less tightly wound as one passes from the ecliptic plane toward higher heliographic latitudes. The last point can be seen by considering plasma parcels emitted from a pole of the sun, in which case the footpoint stays aligned with the plasma parcel at all times.

What is the equation describing this spiral structure? We choose a corotating frame, angular fre-

quency Ω, so that the sun is stationary. The solar wind radial velocity $V_r = V(r)$ is the same as before, but in addition there is an azimuthal velocity $V_\phi = -\omega r$. (We are here just considering what happens in the ecliptic plane.)

In order for field lines to connect the same plasma parcels we must have

$$\frac{B_\phi}{B_r} = \frac{V_\phi}{V_r} = -\frac{\Omega r}{V_r} \tag{5.28}$$

which, since $V_r = dr/dt$ and $V_\phi = rd\phi/dt$, leads to

$$\frac{d\phi}{dr} = -\frac{\Omega}{V_r} \tag{5.29}$$

If V_r is constant (which is a pretty good approximation outside the critical radius r_c as can be seen, e.g., in Figure 5.2) we can solve this ordinary differential equation to find the equation of the field line

$$r = R - \frac{V_r}{\Omega}(\phi - \phi_0) \tag{5.30}$$

where $\phi = \phi_0$ at $r = R$. This spiral is known as an *Archimedean spiral* although, in the context of the solar wind, it is known as the *Parker spiral*.

What are the components of the IMF? We need to satisfy $\nabla \cdot \mathbf{B} = 0$, which in spherical polar geometry (and assuming spherical symmetry for the moment)

$$\nabla \cdot \mathbf{B} = \frac{1}{r^2}\frac{\partial}{\partial r}\left(r^2 B_r\right) \tag{5.31}$$

so that $B_r \propto r^{-2}$. Also the assumption of constant solar wind speed V is fairly good throughout the heliosphere, so that we can choose a reference point r_0, and writing

$$B_r = B_r(r_0)\left(\frac{r_0}{r}\right)^2 \tag{5.32}$$

then, from (5.28)

$$B_\phi = -\frac{\Omega}{V_r} B_r(r_0)\frac{r_0^2}{r} \tag{5.33}$$

So if the angle between the magnetic field and the sun-Earth line is ψ, then we have

$$\tan\psi = -\frac{B_\phi}{B_r} = \frac{\Omega r}{V_r} \tag{5.34}$$

At the Earth's orbit ψ is about 45°, and gets larger further away from the Sun.

Transforming back into the inertial (nonrotating) frame one can see that there is an induced electric field, because of the angle between the flow velocity and magnetic field

$$\mathbf{E} = -\mathbf{V} \times \mathbf{B} = +V B_\phi \hat{\theta} \tag{5.35}$$

In the above we have assumed that the flow is radial. The azimuthal velocity imparted directly by the solar rotation is negligible in the low coronal, but perhaps the magnetic field can influence this behaviour since the flow and field are frozen together. In a strong field, magnetic forces due to the field threading from the corona out to larger distances would force the wind to co-rotate with the Sun. This proceeds, if

at all, only until the flow energy density becomes dominant over that of the field (beyond which the field goes where the flow takes it!) So the field winds into the Parker sprial in regions where

$$\frac{B^2}{2\mu_0} \ll \frac{1}{2}\rho V^2 \tag{5.36}$$

that is, where $V \gg v_A$, where $v_A = B/\sqrt{\mu_0\rho}$ is the Alfvén speed. We can define the Alfvén radius R_A where $V = v_A$, which for typical values is at about $50R_\odot$, or 0.25AU. Inside the Alfvén radius the field is strong enough to control the flow, and cause the solar wind to corotate with the solar wind. Outside the Alfvén radius the field wraps up according to the Parker spiral.

While such co-rotation is not important for the present dynamics of the solar wind, this calculation does show that, for example, the angular momentum shed by stellar winds can be much larger than what might be expected due to the surface rotation, since escaping wind particles are rigidly rotating out to the Alfvén radius and thus carry away $(R_A/R_\star)^2$ more angular momentum.

5.4 The Real Solar Wind

So far we have considered only the most basic of solar wind models: one-fluid, spherically symmetric, and steady. The real solar wind is a much richer medium, providing numerous examples of important astrophysical phenomena on all scales.

5.4.1 Structure

Large Scale Structure

On the largest scales there are a variety of important structures found in the solar wind. These include:

Sectors The various regions of magnetic polarity at the Sun give rise to alternating regions of "toward" and "away" fields since the heliospheric current sheet which divides these is inclined relative the the ecliptic and highly warped. During periods of solar minimum the interplanetary field seen at the Earth is dominated by two recurring sectors (one toward, one away) per solar rotation. During periods of maximum activity, the IMF is much more complex, with four or more recognisable sectors and many more transient phenomena.

Fast/slow Streams Related to the magnetic structure are solar wind streams whose properties are dependent on the coronal conditions from which the originate. Open, coronal hole regions which predominate during solar minima give rise to high speed (600-800 km/s or more) streams. Solar wind emerging around closed loop regions ("streamers") is slower and more highly variable.

Co-rotating Interaction Regions CIRs are formed near and beyond 1AU due to the interaction of slow and fast solar wind streams. Due to the solar rotation, a slow solar wind parcel travelling radially outward will eventually get caught up by a fast parcel emitted from a different region on the Sun which has rotated into the same radial direction. This presents a classic stream-on-stream problem and results in a pair of forward/reverse shocks (see Chapter 7). In the outer heliosphere, these interactions merge and process the intervening solar wind.

Coronal Mass Ejections The Sun, especially during periods of high solar activity, releases large clouds of solar material which pass through the corona and accelerate to high speeds. These coronal mass ejections (CMEs) can fill an entire spherical quadrant with highly structured magnetic field and dense plasma. CMEs are the main drivers of geomagnetic activity.

Small Scale Structure

On plasma kinetic scales, the solar wind is a rich, collisionless medium with multiple plasma components (protons, electrons, alpha particles, ...) and magnetic field fluctuations. The study of these aspects sheds considerable light on the coronal heating and solar wind acceleration problems (which despite decades of research are far from understood) and also build expertise which can be applied to other astrophysical objects where winds and particle acceleration are believed to exist. Examples of these phenomena include

Waves The solar wind is a highly turbulent medium with a mixture of low frequency, MHD-like waves as well as high-frequency waves driven by accelerated particle beams and non-Maxwellian particle distributions.

Discontinuities The structure of discontinuities separating different plasma regimes (e.g., the fast and slow streams discussed above) is vital to understand how such regimes interact and under what circumstances the "cell model" (see Section 4.4) is appropriate.

Shocks Shocks abound in astrophysical environments, and the heliosphere offers an unrivalled laboratory for the study of collisionless shock formation, particle acceleration, and accompanying turbulence. Much of the material in Chapter 7 is based on observations at the Earth's bow shock and interplanetary shocks. Shocks are formed at stream interfaces and where the solar wind encounters obstacles with extended atmospheres/magnetic fields, such as planetary bow shocks and comets.

5.4.2 Other Physics

In our treatment of the solar wind, we have idealised the solar wind problem in order to expose its essential ingredients. Many important ingredients and problems have been neglected. Most were anticipated by Parker in his original papers written in the late 1950's. Research, both analytical and increasingly numerical, has sought to address many of these problems, with mixed success. Here is an incomplete list of topics

Coronal heating - beyond the obvious question of why the million degree corona exists at all above the few thousand degree solar surface given the solar energy source deep in the interior, it seems some extended heating is required.

Trans-collisional physics - the lower corona is collision-dominated; the outer corona/solar wind nearly collisionless. Treating the intervening regions is extremely difficult.

Thermal conduction - the solar wind is essentially the conversion of thermal energy to bulk flow, so the thermal transport processes are vital. Conduction in turbulent, collisionless media is not at all understood.

Multi-species - many species of ions are present in small amounts in the solar wind. Curiously, most species show temperatures which are roughly proportional to their masses (an observation with barely any conjectures as to its understanding save that it may be related to either cyclotron processes and/or shock processes). Minor ions also tend to flow somewhat faster than the main proton component, by an amount which is roughly the (decreasing with distance) Alfvén speed.

Electrons - although the solar wind is generally regarded as a super-sonic flow, which can be re-phrased as a flow faster than the thermal speeds $\sim \sqrt{k_b T/m}$, this is not the case for the lighter electrons. Electrons can travel freely out beyond the orbit of Jupiter and then return to the Sun. An interplanetary electric field is established to prevent the hot electrons running away.

3-D and transient phenomena - we have some observations of the solar wind over the Sun's poles from the Ulysses spacecraft, and many observations of transient phenomena in the ecliptic plane. While some 3-D time-dependent numerical models of the solar wind do exist, there remains much work to be done.

5.5 Exercises

1. (a) Verify that the expression

$$\frac{V^2}{2} - \frac{2k_bT}{m}\ln V = \frac{4k_bT}{m}\ln r + \frac{GM_\odot}{r} + K \tag{5.37}$$

is a solution to Equation 5.22 governing radial outflow of an isothermal solar wind.

(b) Use the conditions at the critical radius $r = r_c$ to determine K.

(c) Assume that the solution gives $V \sim constant$ for $r \geq (1/3)$AU and that the solar wind expansion remains isothermal. Calculate the solar wind proton density, the magnetic field strength, and the spiral angle at Mercury, Mars, Jupiter, and Neptune (at r =0.39AU, 1.5AU, 5.2AU, and 30AU respectively). Use the data given in Table 5.1 for the properties at Earth to determine any constants you may need.

2. Theoretical estimates of the radial distance of the subsolar magnetopause from a magnetized planet can be obtained by determining the distance at which the magnetic pressure $B^2/2\mu_0$ of the planetary dipole field balances the sum of the solar wind ram pressure (ρV^2) and interplanetary magnetic field pressure at the orbit of the planet. Using your data from the preceding question on the properties of the solar wind and IMF at the 4 planets, and the table below, estimate the stand-off distance of each magnetopause in units of planetary radius. Comment on the results. [You will see that the interplanetary field has a negligible influence essentially because the solar wind is super-Alfvénic.]

	Planetary Radius (km)	Magnetic Moment M (Tm^3)
Mercury	2490	4.6×10^{12}
Earth	6371	7.9×10^{15}
Mars	3400	1.0×10^{12}
Jupiter	71,400	1.5×10^{20}
Neptune	24,800	2.0×10^{17}

Note: $B_{\text{subsolar}}(r) \equiv \dfrac{M}{r^3}$

3. (a) Redo the derivation of Parker's solar wind equation (5.22) but replacing the isothermal equation of state (5.10) by an adiabatic one

$$p\rho^{-\gamma} = C$$

(b) Find the adiabatic equivalent to the solution given in (5.37). *Hint*: Show that the equivalent to the equation of motion (5.17) in this case can be written

$$\frac{d}{dr}\left(\frac{1}{2}V^2\right) = -\frac{\gamma}{\gamma-1}C\frac{d}{dr}\left(\rho^{\gamma-1}\right) + \frac{d}{dr}\left(\frac{GM_\odot}{r}\right) \tag{5.38}$$

Chapter 6

Magnetic Reconnection

6.1 Introduction

The convection approximation (in the case of high magnetic Reynold's number) introduced in Section 4.3 leads to the picture of astrophysical plasmas as separate cells partitioned by thin current sheets (see Figure 4.4), where, exactly because of their thinness, diffusion may be important. The local, small scale breakdown of the Flux Freezing theorem will result in diffusion of field lines so that a field line might now connect plasma elements from different sources. Thus the details of the very small scale physics of magnetic diffusion, i.e., the physics of conductivity in a plasma with strong gradients, will affect the global topology of the field line configuration.

If there is a strong field gradient such that the field on either side of the gradient is anti-parallel, then diffusion of the field at the gradient can lead to a loss of total magnetic flux, and this is termed magnetic annihilation. If on the other hand, there is an inflow into a limited diffusion region, then field lines are continually being convected into the diffusion region and meeting field lines with an opposite orientation. In this case the field lines can slip with respect to the plasma in the diffusion region, and merge with field lines from the opposite side of the gradient. The "reconnected" field lines can then be carried away from the diffusion region by the plasma outflow which balances the inflow. This situation is known as magnetic reconnection. Magnetic reconnection is important because it allows the two sides of the field gradient to be linked by a field line, and also because magnetic energy is continually liberated in the process, causing accelerated and heated plasma flows.

Although everybody understands the importance of reconnection, it is fair to say that the microphysics of the diffusion process (i.e., the finite conductivity) is *not* well understood!

6.2 Magnetic Annihilation

6.2.1 Static Annihilation

Assume a non-flowing plasma boundary, and initially (at $t = 0$) a complete, discontinuous reversal of the magnetic field direction, keeping constant field strength, so that there is a step function in $B_x = \pm Bo$ for $z \gtrless 0$. The current sheet, i.e., where the field changes direction is the $x-y$ plane. This configuration is sketched in Figure 6.1.

The evolution of this problem is governed by the Induction Equation (4.13), with zero flow velocity:

$$\frac{\partial \mathbf{B}}{\partial t} = \frac{1}{\mu_0 \sigma} \nabla^2 \mathbf{B} \tag{6.1}$$

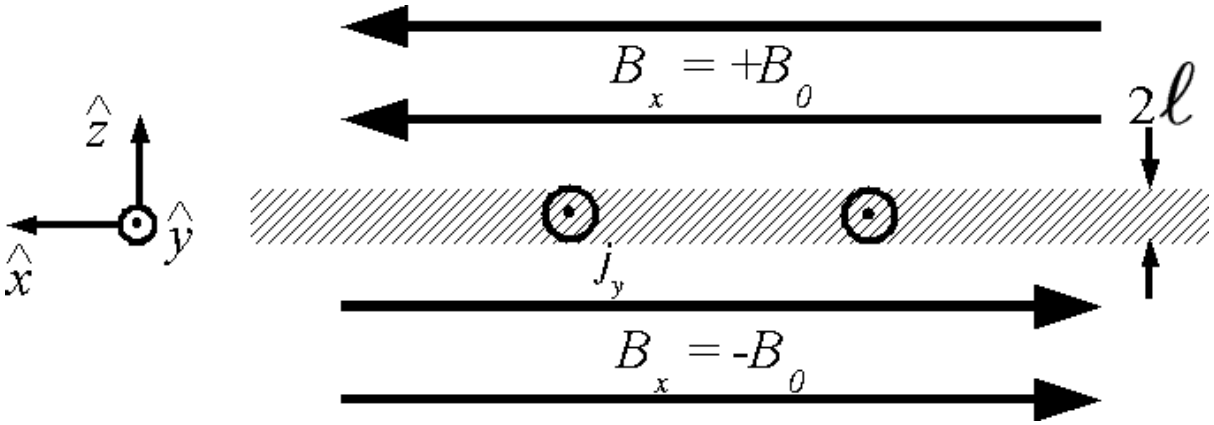

Figure 6.1: Geometry of a thin current sheet across which the magnetic field reverses over a scale 2ℓ

This reduces, for our problem to the case of one spatial dimension:

$$\frac{\partial B_x}{\partial t} = \frac{1}{\mu_0 \sigma} \frac{\partial^2 B_x}{\partial z^2} \tag{6.2}$$

The solution of this partial differential equation, a diffusion equation, is

$$B_x = B_0 \frac{2}{\sqrt{\pi}} \int_0^{\xi} e^{-u^2} du = B_0 \mathrm{erf}(\xi) \tag{6.3}$$

where

$$\xi = \left(\frac{\mu_0 \sigma}{t} \right)^{1/2} \frac{z}{2} \tag{6.4}$$

The current distribution corresponding to the magnetic field given by (6.3) is Gaussian, and has a width that increases in time as $\sqrt{t}$ (see Figure 6.2). Initially there is a rapid thickening of the current sheet and a conversion of field energy to plasma energy (i.e., thermal energy), but this process becomes slower and slower as the gradients weaken. Since the total flux in the system declines by the field lines from either side diffusing towards the centre of the current sheet and disappearing at the magnetic null, this is termed magnetic annihilation.

6.2.2 Dynamic Annihilation

In terms of converting magnetic energy to other forms (thermal, flow, etc.) static magnetic annihilation is not particularly useful, because it switches itself off by dissipating the field gradients. Rapid flux annihilation can be maintained if the plasmas on either side flow together so that the current sheet is always squeezed, and the gradients maintained. In this case inward convection matches the expansion from diffusion. A faster inflow leads to steeper gradients, which in turn leads to greater liberation of magnetic energy.

We can estimate the thickness of the current sheet using two methods. In the first method we balance the flux carried into the current sheet by the flow against the rate of flux annihilation.

Suppose the current sheet half width is ℓ, and the speed of inflow (on both sides) is V. Then the flux carried into the current sheet per unit time, per unit length (in y direction) is VB_0. On the other hand the

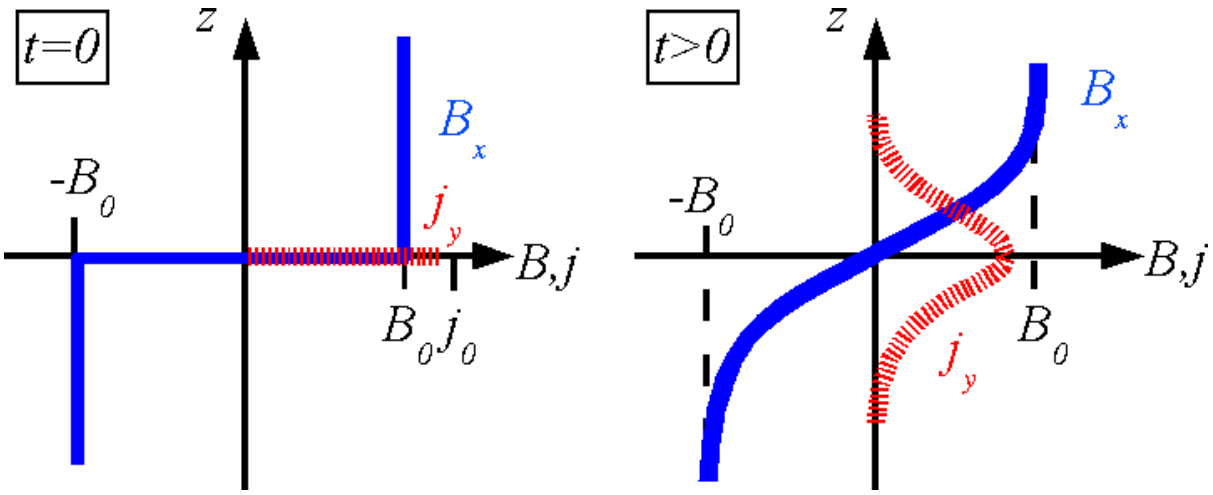

Figure 6.2: Evolution of an initially thin current sheet (left) due to magnetic diffusion. Note the broadening of the current-carrying region and the accompanying reduction of magnetic field strength (and hence energy).

rate of flux annihilation within the current layer can be estimated from the diffusion part of the induction equation (e.g., (6.2) as

$$\ell \frac{1}{\mu_0 \sigma} \frac{B_0}{\ell^2} \tag{6.5}$$

Therefore, equating flux arrival and annihilation rates gives

$$\ell \sim \frac{1}{\mu_0 \sigma V} \tag{6.6}$$

The other method to estimate the current sheet width is to note that both the inflow region (where convection dominates) and the current sheet (where diffusion dominates) are associated with an electric field, E_y in the y direction. For a steady state system which is independent of y (i.e., all quantities only depend on (x,z)), one notes that Faraday's Law reduces to $\nabla \times \mathbf{E} = \mathbf{0}$, so that E_y is spatially uniform, i.e., the same in both inflow region and current sheet. So, in the inflow region E_y is just given by the expression for the motional electric field: $E_y = VB_0$. In the diffusion region the electric field is approximately given by the conductivity term in Ohm's law, since the flow must be zero at the centre of the current sheet: $E_y \approx j_y/\sigma$. The current j_y in the y direction can be estimated from Ampere's Law (2.2)

$$j_y \approx \frac{B_0}{\mu_0 \ell} \tag{6.7}$$

So that, by equating these two expressions for E_y, one again finds:

$$\ell \sim \frac{1}{\mu_0 \sigma V} \tag{6.8}$$

We can now see that the magnetic Reynold's number for the current layer is simply:

$$R_m = \mu_0 \sigma V \ell \sim 1 \tag{6.9}$$

As expected from the balance of magnetic diffusion and convection that we have assumed for the steady current layer, the magnetic Reynold's number for the layer itself is unity, rather than the much higher value one would find for the overall system which sets up the current sheet.

In fact, we can find an analytic solution to the steady state induction equation, assuming equal and oppositely directed flow $V_z = \pm V_i$ for $z \lessgtr 0$, and assuming an undisturbed field of $B_x = \pm B_0$ far away from the current sheet. Making the further, rather unsatisfactory, assumption that the flow continues to be perpendicular to the current sheet and $\partial/\partial t = 0$ the x-component of (4.13) becomes

$$0 = -\frac{d}{dz}(V_z B_x) + \frac{1}{\mu_0 \sigma}\frac{d^2 B_x}{dz^2} \tag{6.10}$$

We shall solve this in the region $z > 0$ and then find the full solution using the symmetry of the problem. If we further assume that the inflow is constant, i.e., $V_z = -V_i$ we can then integrate once and re-arrange to find

$$\frac{dB_x}{dz} + (\mu_0 \sigma V_i) B_x = C \tag{6.11}$$

This is a first order linear ordinary differential equation with constant coefficients and can be solved by the standard technique of a complementary function (satisfies RHS=0) and particular integral. The general solution is

$$B_x = Ae^{-\mu_0 \sigma V_i z} + D \tag{6.12}$$

The constants A and D are determined by the boundary conditions that $B_x \to B_0$ as $z \to \infty$ (which gives $D = B_0$) and $B_x \to 0$ as $z \to 0$ to provide continuity at $z = 0$. Hence

$$B_x = B_0\left(1 - e^{-\mu_0 \sigma V_i z}\right) \qquad z > 0 \tag{6.13}$$

The solution for $z < 0$ is found by noting from the symmetry of the problem that $z \to -z$ requires $B_x \to -B_x$, whence the full solution may be written

$$B_x = \pm Bo\left(1 - e^{\mp \mu_0 \sigma V_i z}\right) \quad z \gtrless 0 \tag{6.14}$$

Of course, the one dimensional "annihilation" geometries which we have discussed are completely unrealistic since there is plasma inflow, but no exiting outflows, and we have assumed infinitely long current sheets.

6.3 Models of Magnetic Reconnection

A more realistic picture is where the diffusion-dominated region is limited in space. The flows into these "diffusion regions" are balanced by flows out along the current sheet.

A simple sketch of the main concepts is shown in Figure 6.3. In such a two-dimensional geometry this would give a magnetic neutral line (where $\mathbf{B} = \mathbf{0}$), and the field lines would have a so-called X-type configuration. The place where the field lines "reconnect", i.e., change their topology so that they link the two sides of the current sheet is called the X-point. The reconnected field lines form stretched out loops connecting the two sides. Magnetic tension in these loops accelerates the inflowing plasma away from the neutral line. As the loops shorten they liberate energy which goes into heating the plasma. Thus the outflow region is characterized by heated, accelerated plasma, and the convection term dominates in this region. One expects the diffusion region to be very small. Nevertheless, this small region can affect the global configuration of the magnetic field.

Note: we will be showing models of exactly anti-parallel reconnection, but reconnection can occur in more general geometries, in which case one can consider the reconnection of just the anti-parallel components of the field.

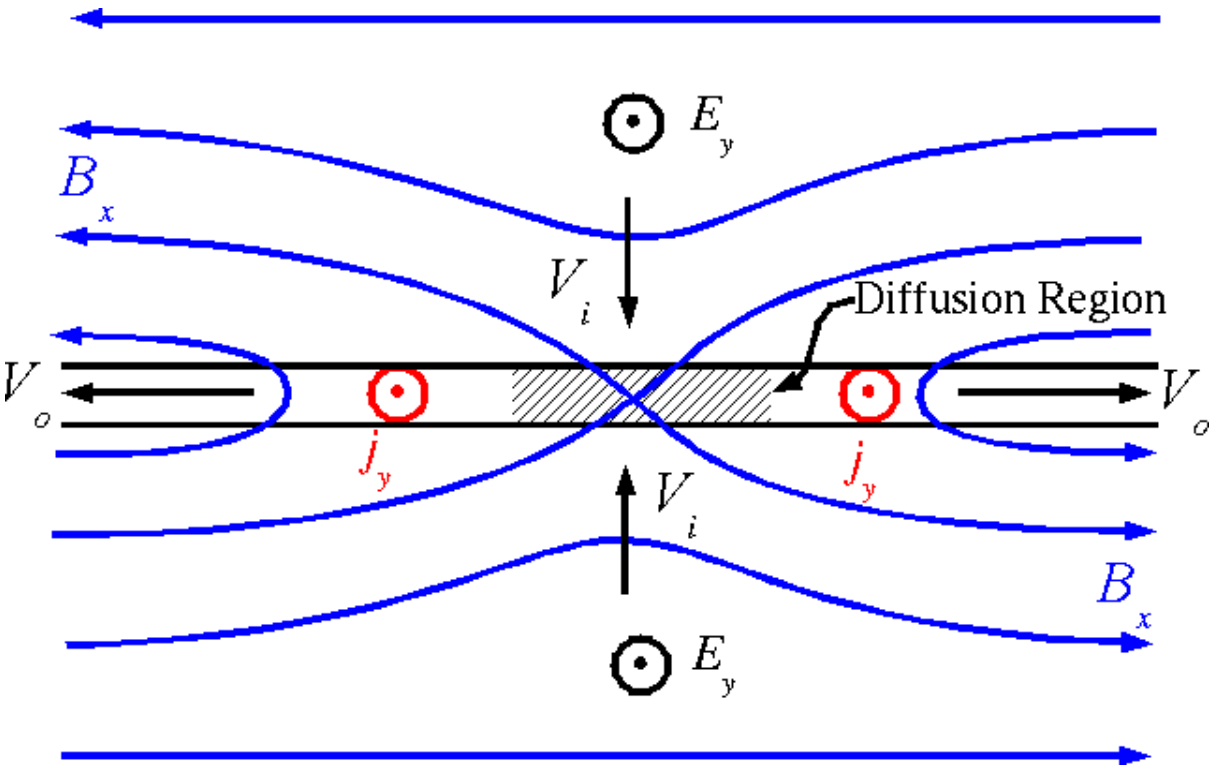

Figure 6.3: Sketch of reconnection in two dimensions. Magnetic diffusion in a small region results in a global reconfiguration of the magnetic topology, together with outflows along the current sheet.

6.3.1 Examples of Reconnection

Before we proceed to the more theoretical considerations, let's have a look at some astrophysical phenomena which are strongly linked with reconnection, and which have influenced greatly the development of this subject.

Solar Flares

A model of rapid energy release in a solar flare is illustrated in Figure 6.4. A magnetic arcade or flux rope can exist for an extended period in a MHD equilbrium in which the magnetic, plasma pressure, and gravitational forces balance. This may include "line-tying", in which the flux rope is held down by the effects of magnetic tension of field lines overlying it, both ends of which map back to the surface of the Sun, as illustrated in the top panel of Figure 6.4. In the pre-flare stage (middle panel) the injection of hot plasma onto the flux rope from each end provides increased buoyancy and a slow rise of the structure ensues. The overlying fields become more stressed, and energy is thus stored in this field. Finally, the bottom panel indicates the rapid rise and release of this stored energy as a result of reconnection of the stressed, closely anti-parallel field lines beneath the arcade. A second model in which reconnection releases a "plasmoid" is shown in Figure 6.5.

Open and Closed Planetary Magnetospheres

Coupling between the solar wind and the Earth's magnetosphere, both in terms of energy and plasma particles, occurs as a result of reconnection between the interplanetary magnetic field and the terrestrial magnetic field. When the IMF has a southward directed component of the field, reconnection occurs in

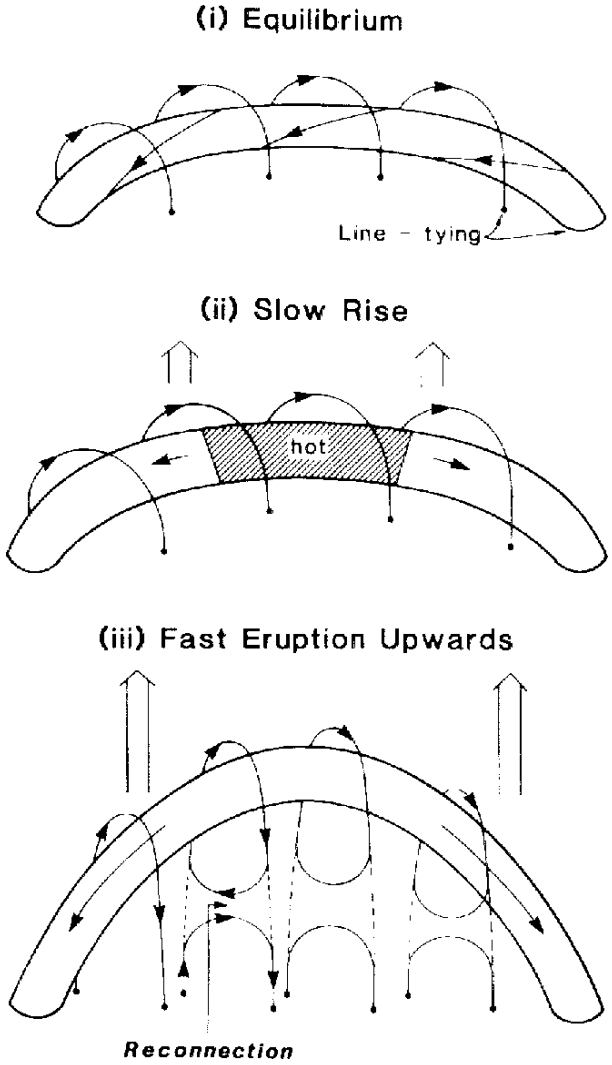

Figure 6.4: Illustration of a solar flare beginning (top to middle) with a slow rise of a line-tied flux rope followed by a rapid release due to magnetic reconnection (see text).

the vicinity of the subsolar dayside magnetopause (between the field lines marked 1'-1' and 1 in Figure 6.6). The magnetosphere becomes "open" and solar wind plasma is free to enter the magnetosphere by travelling along the newly reconnected field lines. In addition, the magnetic tension of the newly reconnected field lines (e.g. those labelled 2 and 2' in the figure, which are sharply bent) accelerates this plasma away from the reconnection site and over the poles of the Earth. These field lines eventually straighten (3,3'), but the external portion remains frozen into the solar wind flow, and therefore continues to convect tailwards (4,4'). This results in highly stretched field lines (5,5') being added to the magnetic tail, which then slowly convect towards the tail centre plane due to the $\mathbf{E} \times \mathbf{B}$ drift related to motional electric field $\mathbf{E}$ ($\mathbf{E}$ is everywhere out of the page in this 2-D representation, since it must be the same everywhere from Faraday's law and is directed out of the page in the solar wind region where it can be readily evaluated). The magnetotail is therefore a reservoir in which energy extracted from the solar wind flow is stored as magnetic energy. This also creates a central current sheet separating the anti-parallel field in the northern and southern halves of the tail (the lobes). Reconnection also occurs at this point (between the field lines marked 6,6') creating both closed field lines (marked 7) and inter-

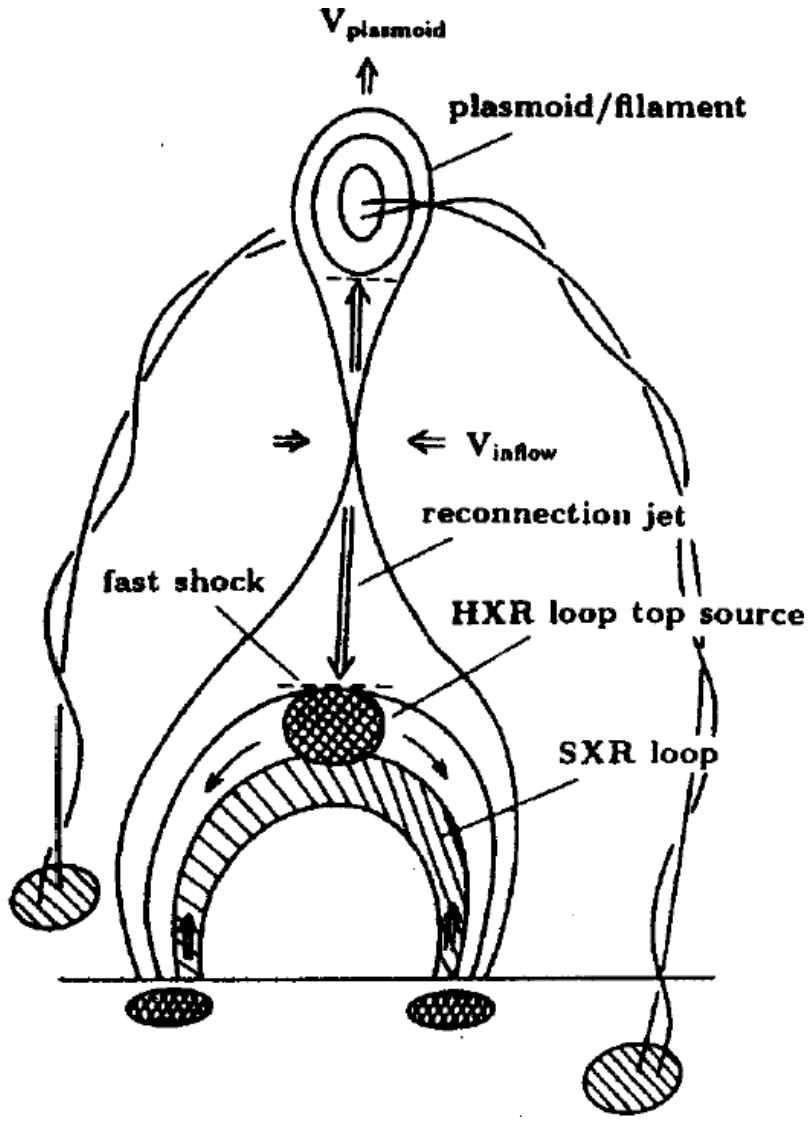

Figure 6.5: Illustration of a solar flare model in which magnetic reconnection releases an upward-moving plasmoid while the downward flux of particles gives rise to the X-rays and other flare-associated phenomena. (figure from Shibata et al., 1995) Note the similarity with the magnetospheric tail reconnection phenomena illustrated in Figure 6.6.

planetary field lines (marked 7'). The tension on these field lines accelerates plasma both earthward and tailward of the tail reconnection site, thus releasing the stored magnetic energy back to the plasma. The Earthward convection of plasma and magnetic flux eventually returns the closed field lines (8) back to the dayside (9), thus completing the magnetospheric convection cycle. Note that this flow of plasma within the magnetosphere (jets over the poles, drifts towards the tail centre plane, accelerated jets away from the tail reconnection site and then flows around the Earth at lower latitudes to return flux to the dayside) are the result of a highly localized break-down of the frozen-in flux condition at 2 points - the dayside magnetopause and the tail current sheet. Despite their limited extent (we have yet to directly encounter one with spacecraft), they dramatically affect the global system - this convection pattern is not possible without reconnection.

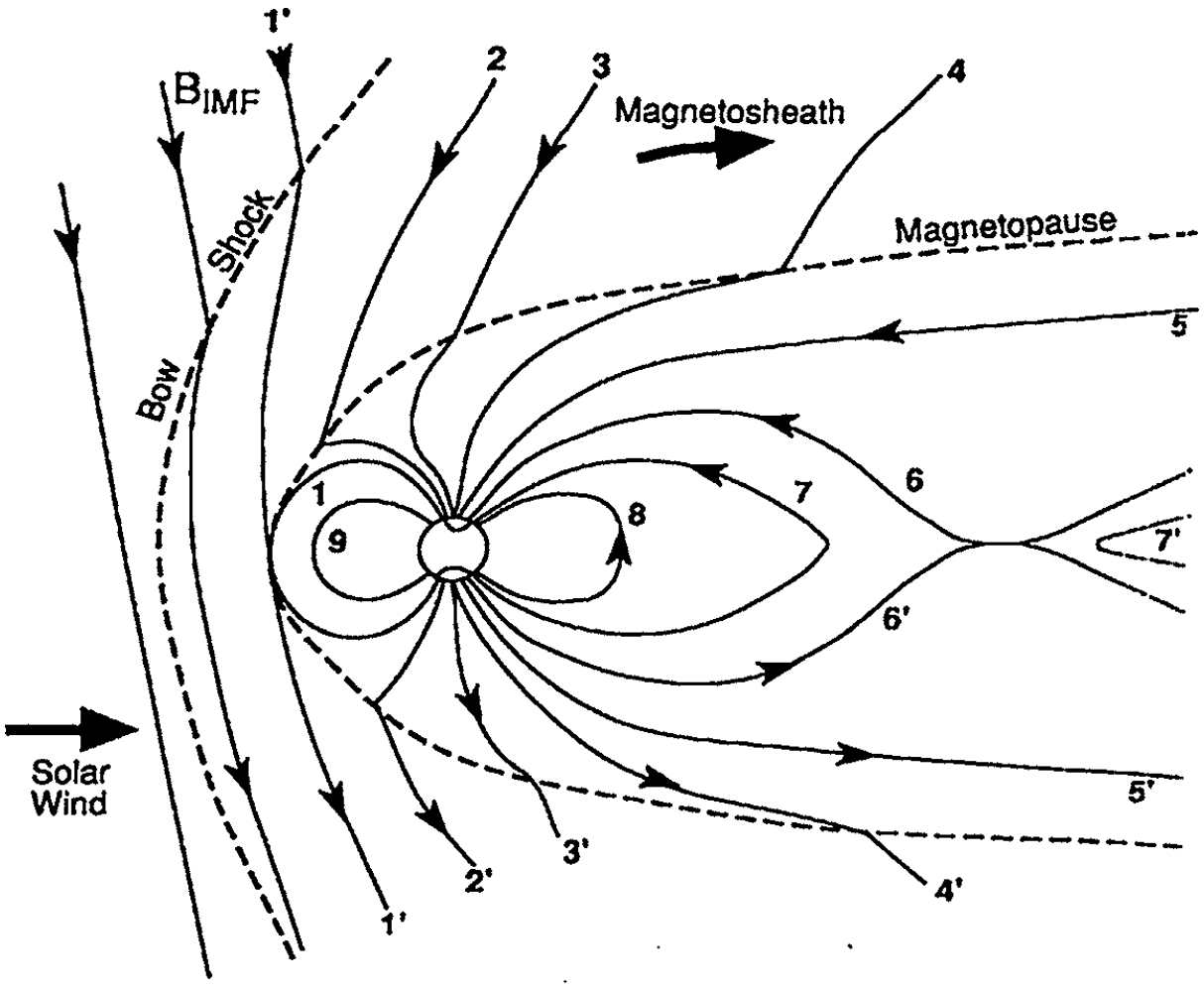

Figure 6.6: An open planetary magnetosphere. Plasma convection (and magnetic topology) is controlled and driven by reconnection at the magnetopause and in the tail. The text provides a description of the sequence of events numbered on the various field lines.

6.3.2 Sweet-Parker Model of Reconnection

Consider a time steady ($\partial/\partial t \equiv 0$), and two dimensional geometry ($\partial/\partial y \equiv 0$). Further assume that the plasma is incompressible so that mass density ρ is constant. The current sheet has symmetric flow in from both sides at speed V_i, and the plasma flows out along the current sheet at speed V_o, as sketched in Figure 6.7. Using the same arguments as before, we expect the thickness of the current sheet (diffusion region) to be

$$\ell \approx \frac{1}{\mu_0 \sigma V_i} \tag{6.15}$$

Suppose that ℓ stays constant for the system size L, where L is known. (That L is known and constant turns out to be a crucial assumption.)

From conservation of mass we know that the mass entering the diffusion region per unit time (and unit y-distance) is equal to that leaving out the ends, i.e.,

$$V_i L = V_o \ell \tag{6.16}$$

We will show that the outflow speed is approximately the Alfvén speed v_{Ai} of the inflow region.

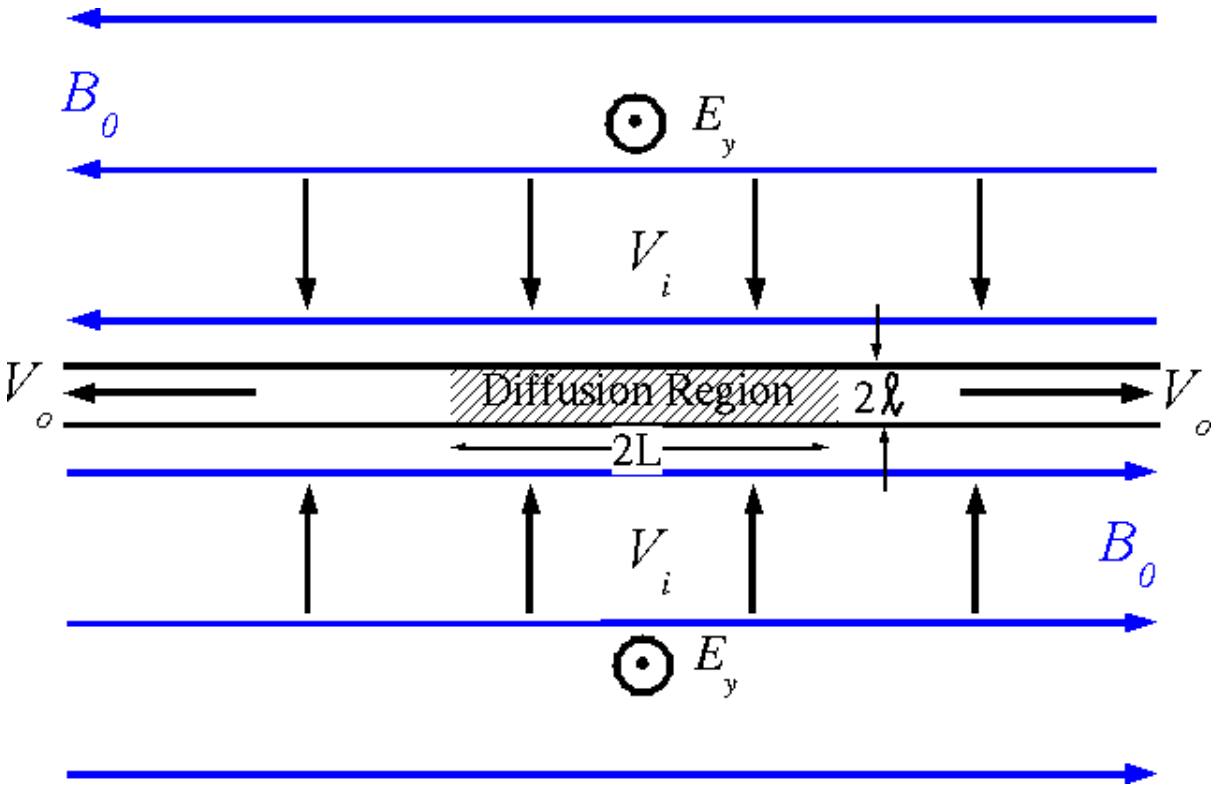

Figure 6.7: Geometry for the Sweet-Parker model of reconnection.

We can estimate the outflow velocity based on conservation of energy. The Poynting flux is the flux of electromagnetic energy, $\mathbf{S} = \mathbf{E} \times \mathbf{B}/\mu_0$, and this is converted almost entirely into plasma energy. In situations in which magnetic field energy is being converted to plasma kinetic and/or thermal energy we find that $\mathbf{j} \cdot \mathbf{E} > 0$, reflecting the dissipation of electromagnetic energy. In steady state one can express energy conservation as

$$\nabla \cdot \mathbf{S} + \mathbf{j} \cdot \mathbf{E} = 0 \tag{6.17}$$

i.e., the electromagnetic energy flux diverges if there are net sinks or sources. But rather than work with this equation we will simply balance the electromagnetic energy flux into the current sheet against the kinetic energy of the outflowing plasma.

The electromagnetic energy into the current sheet per unit area per second is

$$W_E = \frac{E_i B_i}{\mu_0} = \frac{V_i B_i^2}{\mu_0} \tag{6.18}$$

where we have used the convection electric field in the inflow region, $E_i = V_i B_i$. The mass of plasma entering the current sheet, per unit area per second is

$$F_m = \rho V_i \tag{6.19}$$

and this is accelerated to speed V_o. If we ignore the initial kinetic energy and any heating, the work done on this plasma is

$$W_P = \frac{\rho V_i V_o^2}{2} \tag{6.20}$$

By balancing W_E and W_P we find

$$V_o \approx \sqrt{2}\frac{B_i}{\sqrt{\mu_0 \rho}} = \sqrt{2} v_{Ai} \tag{6.21}$$

That is, as above, the outflow speed is approximately the Alfvén speed in the inflow region. This is generally true independent of the reconnection rate (there are several measures of the "rate" of reconnection, but typically either the inflow velocity V_i suitably normalised or equivalently the electric field E_y is used). The reconnection rate in this case determines how much plasma is accelerated, rather than how fast.

Given the magnetic Reynold's number for the inflow region: $R_m = \mu_0 \sigma v_{Ai} L$, the conservation of mass using our result (6.16) for V_o, and the width of the diffusion region ℓ from (6.15), we find

Sweet-Parker Reconnection Rate

$$V_i \approx \sqrt{\frac{v_{Ai}}{\mu_0 \sigma L}} = v_{Ai}\frac{1}{\sqrt{R_m}} \tag{6.22}$$

[Using V_i instead of v_{Ai} in R_m actually makes the situation worse, as then the same calculation results in $V_i \sim v_{Ai}/R_m$. Additionally, since v_{Ai} is a characteristic speed of the medium, its use in R_m is model independent.] And this poses a very serious problem, because the speed of inflow, which controls the rate at which flux is brought into the diffusion region will be small if the magnetic Reynold's number of the inflow region is large, which will generally be true.

For example, in a solar flare, which we think is rapid energy release associated with magnetic reconnection, $R_m \sim 10^8 \rightarrow 10^{10}$, which with an Alfvén speed of 100 kms^{-1} and $L \sim 10^4$, would give a time scale of tens of days! But we know that a solar flare releases its energy over the time scale of minutes and hours.

6.3.3 Petschek Reconnection Model

The difficulty in the Sweet-Parker model is that the amount of material processed, and hence energy liberated, is controlled by the width of the exit channel, which is controlled by the thickness 2ℓ of the diffusion region. The Petschek model circumvents this problem by widening the exit channel and having standing shock waves (actually MHD slow-mode shocks) on the edges of the exit channel which perform most of the conversion of magnetic energy to flow energy. (see Figure 6.8)

At the slow shocks the field and flow change abruptly in direction and strength: the field decreases in the outflow region, and the magnetic energy change is balanced by an increase in the flow speed. In the frame of the figure the shocks are stationary (standing shocks), but in the frame of the plasma in the inflow region they travel along the magnetic field at the inflow Alfvén speed $v_{Ai} = \sqrt{B_i/(\mu_0 \rho_i)}$. Thus, to ensure standing shocks we require:

$$V_i \cos\xi = v_{Ai} \sin(\chi - \xi) \tag{6.23}$$

where ξ is angle of shock to x-axis, and χ is angle of inflow magnetic field to x-axis. Here we have equated the plasma inflow speed normal to the shock with the component normal to the shock front of the shock propagation vector along the field (at an angle χ).

Next we note, by Faraday's Law, that E_y is the same in the inflow and outflow regions:

$$E_{iy} = V_i B_i \cos\chi = V_o B_o = E_{oy} \tag{6.24}$$

Then, from $\nabla \cdot \mathbf{B} = 0$ the normal component of the magnetic field on the two sides of the shock is the same:

$$B_i \sin(\chi - \xi) = B_o \cos\xi \tag{6.25}$$

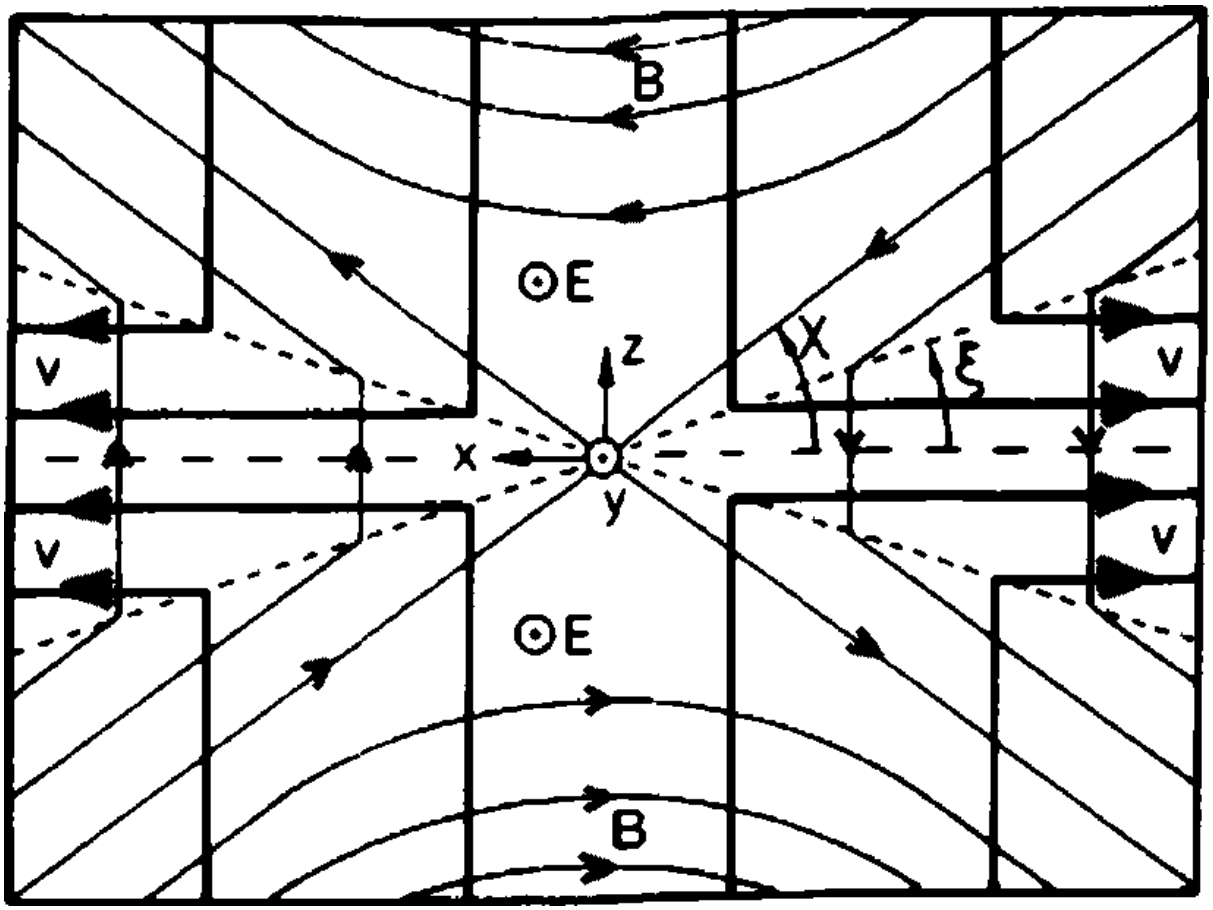

Figure 6.8: Geometry of the Petschek model for reconnection. Note the wide exit channels by comparison to the fixed-width ones in the Sweet-Parker model shown in Figure 6.7. These exit channels are bounded by slow shocks (dashed lines) which compress and heat the plasma while decompressing the magnetic field.

Therefore

$$V_o = V_i \cos\chi \frac{B_i}{B_o} = V_i \cos\chi \frac{\cos\xi}{\sin(\chi - \xi)} \tag{6.26}$$

But $\sin(\chi - \xi) = V_i \cos\xi / v_{Ai}$ so

$$V_o = v_{Ai} \cos\chi \tag{6.27}$$

In other words the outflow is roughly the same as the inflow Alfvén speed, reminiscent of our earlier work in the Sweet-Parker model (see Equation 6.21).

Next, we conserve mass across the shock boundary:

$$\rho_i V_i \cos\xi = \rho_o V_o \sin\xi \tag{6.28}$$

where $\rho_o > \rho_i$, i.e., there is compression at the shock (and since the magnetic field weakens this shock is related to the slow magnetosonic mode - see Exercise 5 on p.57 - in that the magnetic and thermal pressures are in opposition). Therefore one can find that:

$$V_o = \frac{\rho_i}{\rho_o} \frac{1}{\tan\xi} V_i \tag{6.29}$$

Eliminating V_o between (6.27) and (6.29) and then eliminating the angle ξ by expanding $\sin(\chi-\xi) = \sin\chi\cos\xi - \cos\chi\sin\xi$ in (6.23) we reach

$$\text{Petschek Reconnection Rate} \qquad V_i = v_{Ai}\frac{\sin\chi}{\left(1+\frac{\rho_i}{\rho_o}\right)} \tag{6.30}$$

Since $0 < \rho_i/\rho_o < 1$ it follows that

$$\frac{1}{2} < \frac{V_i}{v_{Ai}} < 1 \tag{6.31}$$

In other words, the inflow speed, which determines the reconnection rate and the rate of energy liberation, is now a reasonable fraction of the inflow Alfvén speed. More precise calculations show that the fraction is about 0.1. The Petschek model provides the justification that magnetic reconnection is a viable mechanism for energy release and magnetic topology reconfiguration in astrophysical plasmas.

6.4 Evidence for Reconnection

As discussed above, we do not understand the microphysics of the diffusion region, and they are evidently small enough to have so far missed detection by spacecraft. However, observations of rapid energy release in solar flares and the global convection pattern within the magnetosphere are strongly suggestive that such a process must be occurring. In addition, models of reconnection suggest that as a result of this process, plasma flows at speeds of order the inflow region Alfvén speed should be produced. These flows are large scale, and thus should be more easily detected. This is indeed the case, as illustrated in Figure 6.9 which shows 2 hours of observational data from the ISEE-2 spacecraft, outbound across the dayside magnetopause on August 12th 1978. From top to bottom, the 5 panels show the ion number density, the ion temperature, the magnitude of the ion flow velocity, and the *y*-component of the same, and the north-south (B_z) component of the magnetic field, each as a function of time. At 1700 hours universal time (UT), the spacecraft is in the magnetosphere and observes field and plasma parameters typical of this region - a low ion density, but high temperature, a strong positive B_z component of the field, and very little plasma flow. This contrasts sharply with the data at 1900 UT, when the spacecraft has passed out into the magnetosheath (shocked solar wind) where the plasma is relatively denser and cooler, and the field strength is weaker (and in this case has a negative B_z component, antiparallel to the magnetospheric field). The current sheet separating these two distinct plasma regions was crossed just after 1830 UT, as designated by the two vertical lines, where there are strong gradients in the magnetic field. However, the important thing to note is that there are intervals prior to 1830 UT, when the spacecraft is still in the magnetosphere (the magnetic field is unchanged), but the observed plasma has densities and temperatures which are more characteristic of the external magnetosheath. This indicates that the magnetosheath plasma has access to the magnetosphere, which it can only do if the frozen-in flux condition has broken down globally (unlikely) or if the magnetospheric and magnetosheath fields have become connected and the sheath plasma can stream in along the field lines. This, of course, is possible if reconnection is occurring at a nearby diffusion region. Moreover, note that the plasma flow speeds in these regions are higher than those in both the magnetosphere and magnetosheath. In other words, this magnetosheath-like plasma has undergone acceleration as it crossed the magnetopause current layer. Although the exact calculation needs to be done in the rest frame of the plasma transverse to the magnetopause, it is possible to show that these flows are in fact of order the upstream Alfvén speed, as predicted by all the reconnection models. This is strong evidence for the reconnection process being of fundamental importance in astrophysical and space plasmas.

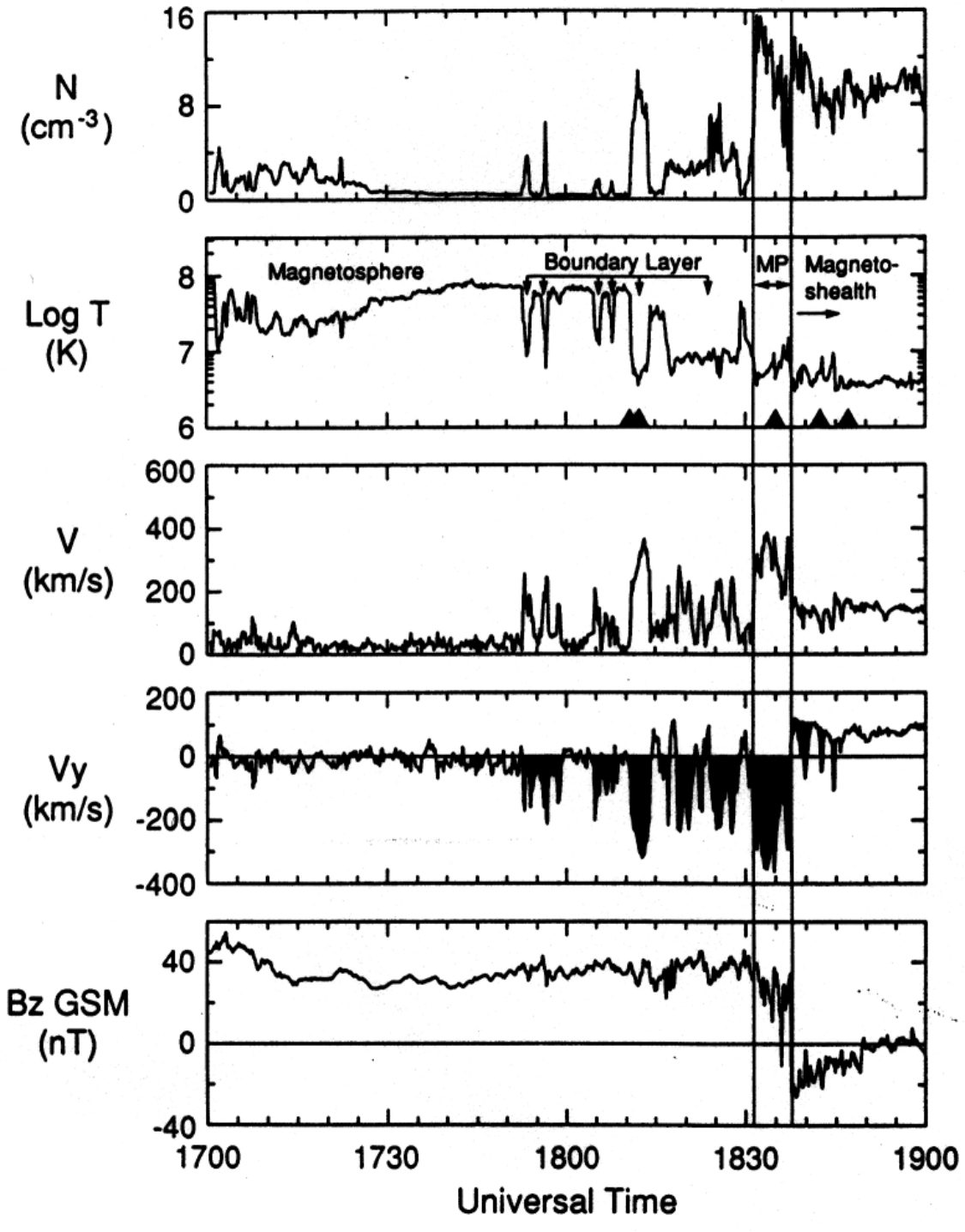

Figure 6.9: Data from the ISEE-2 satellite showing the ion and magnetic field variations in the vicinity of the Earth's magnetopause (see Figure 6.6). The text describes the evidence for accelerated flows and plasma access consistent with magnetic reconnection occuring between the Earth's magnetic field and that of the solar wind in the magnetosheath region behind the Earth's bow shock.

6.5 Exercises

1. For the magnetic annihilation solution given in Equation 6.14, find the electric field $\mathbf{E}$ (you should remind/convince yourself that this electric field is everywhere constant). Hence calculate the Poynting flux $\mathbf{S} = \mathbf{E} \times \mathbf{B}/\mu_0$ and show that it is directed toward $z = 0$. Show further that $|\mathbf{S}(z \to +\infty)|$ is equal to $\int_0^\infty \mathbf{E} \cdot \mathbf{j} dz$ and interpret this result.

2. Consider a region downstream from a reconnection neutral line in which the hairpin-like field lines are given by $\mathbf{B} = (B_x(z), 0, B_z)$ where B_x reverses across a current sheet at $z = 0$, B_z is constant, and $B_z \ll B_x$ (i.e., the angle χ between the field and the current sheet is small such that $\cos\chi \approx 1$). A spatially uniform electric field $\mathbf{E} = (0, E_y, 0)$ exists across the system. Assume the plasma in the system is cold, of number density n, and subject only to $\mathbf{E} \times \mathbf{B}$ drifts in the observer's frame of reference.

   (a) In the frame in which the electric field is transformed away, the hairpin-like field lines are stationary, there is no $\mathbf{E} \times \mathbf{B}$ drift, and particles move along the field line but cannot change their speed. By balancing the magnetic tension outside of the current sheet with the change of momentum of particles as they move through the current sheet and change direction, find the speed of the particles in this frame.

   (b) Hence show that in the rest frame of the observer the field lines move along the current sheet away from the neutral line at a speed $v_A/\sqrt{2}$ and that the outflow plasma speed is $\sqrt{2}v_A$.

   (c) Consider a line of unit length in the y-direction. In steady state, the magnetic reconnection rate can be considered as equivalent to the amount of magnetic flux crossing this line per unit time. Show that the reconnection rate is thus equivalent to E_y and that the reconnection rate determines B_z in the system.

   (d) An alternative way of visualising the acceleration of particles is as follows: In the field line rest frame, particles move into the current sheet along the x-direction at the speed determined in (2a). In the current sheet, their direction of motion is reversed by performing a half gyration in the B_z field (as $B_x = 0$ at $z = 0$). What distance is the particle displaced in the y-direction?

   (e) In the observer's rest frame, a displacement in the y-direction means that the particle has moved along the electric field E_y, and will thus have gained energy. Using the results above, relate the final kinetic energy to that gained by moving along the electric field and hence again show that the outflow plasma speed is $\sqrt{2}v_A$.

Chapter 7

Shocks and Discontinuities

7.1 Shocks: Introduction

Note: most of the following was written for another purpose, and some time ago (!), so there is a discontinuity in style.

The universe is woven through by plasmas in motion. Between the planets, between the stars, between the galaxies there are flows of plasma and field energy, and wherever these flows exceed the speed of sound and/or the Alfvén speed there will also be shock waves. In the solar system there are shocks in front of all the planets, in their magnetotails, and formed in the solar corona and solar wind. Shocks are the most studied nonlinear waves of plasmas, they are places where the plasma and field go through dramatic changes: changes in density, temperature, field strength, flow speed. These changes, combined with the collisionless nature of space plasmas and the wide variety of wave modes, produce a rich collection of different shock types. In addition, shocks in collisionless plasmas are not just interesting in their own right, but also because they are involved in a massive range of plasma phenomena, which stretches and expands our knowledge of basic plasma processes.

Most of the everyday notions of what a shock wave is come from supersonic aircraft or explosive blasts. The study of shocks began with ordinary gas dynamics in the late nineteenth century, and reached its maturity during the 1940s, at the time of the development of high performance aircraft. The study of plasma shocks surfaced during the 1950s, with interest in fusion plasmas and shocks caused by explosions in the upper atmosphere. But also, it was realized, shocks would exist in collisionless plasmas, such as found in interplanetary space (the solar wind) and in other more exotic astrophysical objects.

Collisions in an ordinary gas serve to transfer momentum and energy among the molecules, and they provide the coupling which allows the basic wave, the sound wave, to exist. In a *collisionless* plasma the collisional coupling is absent. This is expressed by saying that the mean free path between collisions is greater than the size of the system. For example, in the solar wind the collision mean free path, as calculated from gas kinetic theory, is about 1AU (1AU=distance from Earth to sun = 1.5×10^8 km). But, from observations, the thickness of the Earth's bow shock, which forms in front of the magnetosphere, is only 100–1000 km. This means that, whatever is happening at the shock, collisions cannot be important, and instead there are processes in operation which are unique to collisionless plasmas. Since the start of spaceflight we have collected many observations of shocks, to such an extent that laboratory collisionless shock studies have been eclipsed. The ability to make detailed observations of the particle distributions as well as the fields means that we have the opportunity to study in close up a phenomena which we know exists in similar forms throughout the universe.

7.2 Shocks Without Collisions

The plasmas that are found in the magnetosphere, in interplanetary space and elsewhere in the universe are very different from an ordinary gas. As we have seen in Chapters 4 and8 plasma can support several different types of wave, involving fields and particles, rather than the single sound wave of a gas. But the greatest difference is that most space plasmas are *collisionless*. This means that the media are either so rarefied (i.e., under-dense) or hot, that Coulomb collisions between the constituent particles happen so infrequently that they do not play an important role. In a normal gas collisions between molecules ensure that they all have the same temperature, irrespective of type; collisions provide the mechanism to propagate pressure and temperature changes; dissipation in the form of viscosity is also an outcome of collisions. Collisions also ensure that in equilibrium the distribution of molecular speeds is Maxwellian.

Knowing what collisions do in an ordinary gas it is fairly easy to list what the lack of collisions produces in a plasma. Different types of particles, e.g., protons and electrons, can have different temperatures. The particle distribution functions can be very different from Maxwellian, so that the concept of temperature has to be broadened to that of "kinetic temperature," i.e., a velocity moment of the particles' distribution function. The important role of the magnetic and electric fields in a plasma also means that the distribution functions may no longer be isotropic in velocity space. All these effects, and more, lead to a superabundance of phenomena involving particles and fields.

Examples of collisionless shocks are spread throughout the universe. The most studied is the Earth's bow shock, which is a standing shock in the solar wind ahead of the Earth's magnetosphere. The magnetic field of the Earth forms an obstacle to the supersonically flowing solar wind. The bow shock makes the solar wind transition to subsonic speeds, so that it can flow around the magnetosphere. It has a curved shape, symmetrical about the Sun-Earth line, close to a paraboloid of revolution. The position of the nose of the bow shock (the most sunward part) is at about $15R_E$ from the Earth's center (an Earth radius $= 1R_E = 6371$km). The shock is a few R_E ahead of the magnetosphere, and this distance is called the stand-off distance. The exact position of the bow shock relative to the Earth depends on the solar wind ram pressure, because the magnetosphere is slightly "spongy." The stand-off distance is a function of the shape of the obstacle; blunt obstacles have larger stand-off distances. The region of subsonic solar wind behind the bow shock is called the magnetosheath. Typically the interplanetary magnetic field (i.e., the solar magnetic field as carried by the solar wind) is at an angle of 45° to the Sun-Earth line. Thus, the magnetic field intersects the shock at different angles around its curved surface, with corresponding changes in the character of the shock. All of the planets with magnetospheres or ionospheres have bow shocks in front of them, and most have been seen at least once or twice by interplanetary probes such as Voyager, Pioneer, etc.

Shocks occur in the solar atmosphere (the corona) during solar flares and other manifestations of solar activity. Flares and coronal mass ejections can inject energy and material into the solar wind driving travelling interplanetary shocks which propagate out through the solar system. The solar wind has high speed and low speed streams, coming from different source regions on the sun. Shocks can form at the interface between a slow stream being overtaken by a fast stream. In more exotic astrophysical bodies one finds jets of material from active galactic nuclei (AGN), and there are probably shocks formed at the interface between the jet material and the interstellar medium. In supernovae massive amounts of energy are deposited in a very short time, and shocks are formed as the supernova remnant (SNR) piles up material as it expands away from the newly formed pulsar.

It would seem that lack of collisions could make our problem impossibly complex. However, to an extent we are saved by the fact that the action of the magnetic field tends to replace the role of collisions in "binding" the particles of the plasma together. So we will base our analysis on an MHD description of the plasma. Since MHD does not include, except by trickery, effects due to individual particles ("kinetic" effects), it cannot tell us anything about how a shock provides dissipation, or what the structure of the shock will be. But MHD will be suitable to describe the plasma far upstream and downstream of the

shock itself.

7.3 Shock Conservation Relations

However bizarre a shock may be we know that mass, energy and momentum will be conserved. We can use MHD to relate the plasma states upstream and downstream of the shock using these conservation relationships. Note that in this description the shock is very much a "black box," which changes the state of the plasma (field, density, etc.), while we can't tell anything about what is actually happening within the shock. Most importantly we don't know anything about how "big" (i.e., thick) the shock is, since MHD has no fundamental length scale, and the scales which should be important (e.g., particle gyroradius) have been left out of MHD. In the case of an ordinary gas or fluid the relations between the upstream and states were first derived by Rankine and Hugoniot towards the end of the nineteenth century. In the case of a collisional gas these "Rankine-Hugoniot" relations determine *uniquely* the downstream state in terms of the upstream state. This has the important result that in an ordinary gas there is a unique transition between a given supersonic flow and a subsonic state. The shock structure is determined by the dissipation mechanism, which is usually just viscosity. This result produces a shock which has a thickness of just a few collisional mean free paths. Actually, even an ordinary gas can have a more complicated shock structure, especially when the shock conditions produce chemical reactions (e.g., disassociation of molecules), or partial ionization.

For a collisionless plasma, except for the single fluid case, the conservation relations (also known as the shock jump or Rankine-Hugoniot relations) do not provide a unique prescription for the downstream state, mainly because energy conservation only gives information about the total pressure (and hence temperature), and not about how it is divided amongst the different types of particles in the plasma. In other words, we need to know about the shock structure, about how the shock works, in order to know how much the ions and electrons heat in passing through the shock.

In deriving the MHD Rankine-Hugoniot relations we make certain assumptions, such as that the shock is, on average, stationary in the shock frame; that the energy in waves is not important; that the particle distributions can be described by Maxwellians (or at least by low order moments such as the density, bulk velocity, etc.) and the plasma pressure is isotropic. One of the basic observational tests for a shock is a comparison with the Rankine-Hugoniot relations. This is often a basis for a discussion about whether the observed "thing" is actually a shock. Often, what are really being tested are the assumptions which go into our derivation of the jump conditions. In this case it is best to return to our basic definitions of a shock which we discussed earlier. The Rankine-Hugoniot relations are only one possible expression of the conservation of energy and momentum.

Let us consider the simple case of a one-dimensional, steady shock. We will work in a frame where the shock is stationary. The x axis will be aligned with the shock normal, so that the plane of the shock is parallel to the y-z plane. We will also assume uniform upstream and downstream media (flow, field, density, and pressure) away from the shock transition itself. We can think of the shock as a discontinuity, but in reality it will have some thickness given by the kinetic processes at the shock. The basic geometry is shown in Figure 7.1. We shall see later that the reference frame and axes can be chosen in such a way that the flow and field are confined to the $x-z$ plane.

The shock separates two regions of steady flow. Plasma flows into the shock on one side (upstream) and out the other side (downstream), and we label these two regions u and d, respectively. The shock causes a change in the plasma description from mass density ρ_u, velocity $\mathbf{V}_u$, magnetic field $\mathbf{B}_u$, pressure p_u, etc., to the downstream values ρ_d, $\mathbf{V}_d$, $\mathbf{B}_d$, p_d. The jump across the shock in any quantity X can be expressed using the following notation:

$$[X] = X_u - X_d \tag{7.1}$$

The MHD description gives us a set of conservation equations for the mass, energy, and momentum. For

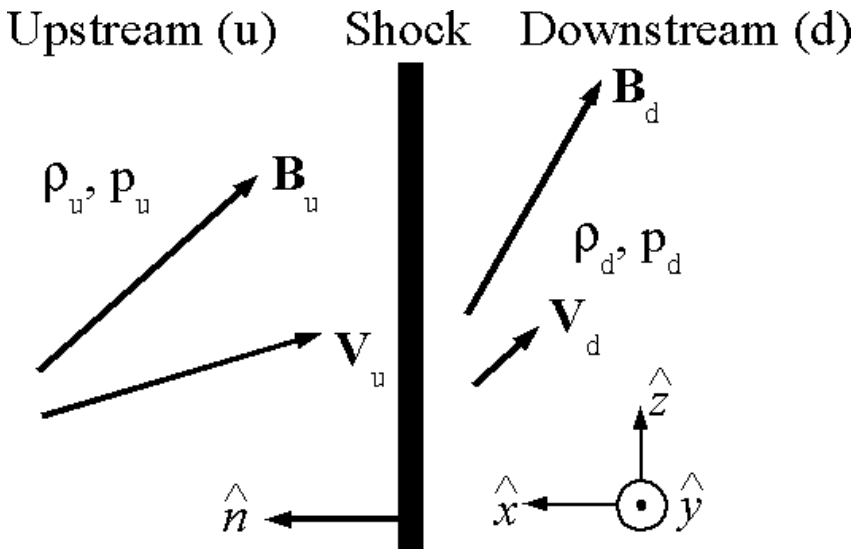

Figure 7.1: Geometry and notation for the derivation of the 1D Rankine-Hugoniot relations for a shock transition between the super-"sonic" upstream flow and sub-"sonic" downstream state. The velocity and field vectors are not, ab initio, confined to the $y-z$ plane both upstream and downstream.

any quantity a conservation equation has the form:

$$\frac{\partial Q}{\partial t} + \nabla \cdot \mathbf{F} = 0 \tag{7.2}$$

where Q and $\mathbf{F}$ are the density and flux, respectively, of that conserved quantity. If the shock is steady ($\partial/\partial t \equiv 0$) and one dimensional (ie., there are variations only along the x axis, so that $\partial/\partial y \equiv \partial/\partial z \equiv 0$), then (7.2) implies that

$$\frac{d}{dx}(F_x) = 0 \tag{7.3}$$

which in turn implies that $(\mathbf{F}_u - \mathbf{F}_d) \cdot \hat{n} = 0$, where we denote the unit vector normal to the shock surface by $\hat{n}$. Therefore, the component of the conserved flux normal to the shock remains constant, and this can be written:

$$[F_n] = 0 \tag{7.4}$$

The subscript n indicates the normal component, which, for the geometry we are considering, is the same as the x component.

For MHD we have the equation for the conservation of mass, or continuity equation (4.1), which is already in the form (7.2). In 1-D we thus have

$$\frac{d}{dx}(\rho V_x) = 0 \tag{7.5}$$

which leads to the jump condition for the shock:

$$[\rho V_x] = 0 \tag{7.6}$$

This tells us, as we would expect, that if the shock slows the plasma, then the plasma density increases.

The MHD momentum equation (4.2) and equation of state (4.3) are not in conservation form. The momentum equation can be re-cast, using both the continuity equation and $\nabla \cdot \mathbf{B} = 0$, into the following conservation form

$$\frac{\partial(\rho \mathbf{V})}{\partial t} + \nabla \cdot \left[\rho \mathbf{V}\mathbf{V} + \left(p + \frac{B^2}{2\mu_0} \right) \boldsymbol{I} - \frac{\mathbf{B}\mathbf{B}}{\mu_0} \right] = \mathbf{0} \tag{7.7}$$

Dotting this equation with $\mathbf{V}$ and making use of all the other MHD equations leads, somewhat tediously, to a total energy conservation equation

$$\frac{\partial}{\partial t} \left(\frac{1}{2}\rho V^2 + \frac{p}{\gamma - 1} + \frac{B^2}{2\mu_0} \right) + \nabla \cdot \left(\mathbf{V} \frac{1}{2}\rho V^2 + \frac{\gamma}{\gamma - 1} p\mathbf{V} + \frac{\mathbf{E} \times \mathbf{B}}{\mu_0} \right) = 0 \tag{7.8}$$

These allow us to write down the corresponding jump conditions. Firstly, the conservation of momentum normal to the shock surface is

$$\left[\rho V_x^2 + p + \frac{B^2}{2\mu_0} \right] = 0 \tag{7.9}$$

This reflects the momentum changes due to the pressure and magnetic forces, although in this form it is clear that the pressure and magnetic field can be thought of as carrying momentum fluxes in their own rights.

The transverse momentum also has to balance, and this gives:

$$\left[\rho V_x \mathbf{V}_t - \frac{B_x}{\mu_0} \mathbf{B}_t \right] = 0 \tag{7.10}$$

The t subscript indicates the components transverse to the shock, i.e., parallel to the shock surface. This equation reflects the tangential stresses related to any bend or kink in the magnetic field (since ρV_x is constant from (7.6) and we shall see below that B_x is also constant).

The final conservation equation from MHD is for the energy. We have assumed that the plasma has an adiabatic equation of state so that $p\rho^{-\gamma} =$ constant. For a normal monatomic gas $\gamma = 5/3$. Actually, the real equation of state will probably not be adiabatic, but the results we obtain will still be qualitatively correct. The shock jump condition from the energy conservation Equation 7.8 is:

$$\left[\rho V_x \left(\frac{1}{2} V^2 + \frac{\gamma}{\gamma - 1} \frac{p}{\rho} \right) + V_x \frac{B^2}{\mu_0} - \mathbf{V} \cdot \mathbf{B} \frac{B_n}{\mu_0} \right] = 0 \tag{7.11}$$

The first two terms are the flux of kinetic energy flow energy and internal energy. The last two terms come from the electromagnetic energy flux $\mathbf{E} \times \mathbf{B}/\mu_0$ where we have used the ideal MHD result that $\mathbf{E} = -\mathbf{V} \times \mathbf{B}$.

Equations 7.6, 7.9, 7.10, and 7.11 are the jump conditions for the gas, but there are also purely electromagnetic boundary conditions. From Maxwell's equation $\nabla \cdot \mathbf{B} = 0$ the normal component of the magnetic field is continuous ($B_x =$ constant):

$$[B_x] = 0 \tag{7.12}$$

From Faraday's Law $\nabla \times \mathbf{E} = -\dfrac{\partial \mathbf{B}}{\partial t}$, with the assumption that $\dfrac{\partial}{\partial t} = 0$, the tangential component of the electric field must also be continuous. Using $\mathbf{E} = -\mathbf{V} \times \mathbf{B}$, this becomes:

$$[V_x \mathbf{B}_t - B_x \mathbf{V}_t] = 0 \tag{7.13}$$

The set of conservation relations have been found with the intention of using them to calculate shock jump conditions, but in fact we have not explicitly forced the solutions of Equations 7.6, 7.9, 7.10,

Table 7.1: Possible types of discontinuity/shock in ideal MHD

Discontinuities

Contact Discontinuity	$\mathbf{V}_u = \mathbf{0}$, $B_n \neq 0$	Density jump arbitrary, but pressure and all other quantities are continuous.
Tangential Discontinuity	$V_x = 0$, $B_n = 0$	Plasma pressure and field change maintaining static pressure balance.
Rotational Discontinuity	$V_n = B_n/\sqrt{\mu_0 \rho}$	Form of intermediate shock in isotropic plasma, field and flow change direction but not magnitude.

Shock Waves: $\mathbf{V}_u \neq \mathbf{0}$

Parallel Shock	$B_t = 0$	Magnetic field unchanged by shock.
Perpendicular Shock	$B_n = 0$	Plasma pressure and field strength increases at shock.
Oblique Shocks	$B_t \neq 0$, $B_n \neq 0$	
Fast Shock		Plasma pressure and field strength increase at shock, magnetic field bends away from normal.
Slow Shock		Plasma pressure increases, magnetic field strength decreases, magnetic field bends towards normal.
Intermediate Shock		Only shocklike in anisotropic plasma.

7.11, 7.12, and 7.13 to be shock-like. The solutions of these equations describe a number of different types of MHD discontinuity, including shocks. For a discontinuity to be a shock there must be a flow of plasma through the shock surface ($V_n \neq 0$), and there must be some dissipation and compression across the shock. A further distinction can be made between discontinuities which are threaded by a magnetic field (i.e., $B_n \neq 0$), and those which are not. Shocks with a normal magnetic field component are called oblique, which refers to the angle between the shock normal and the upstream magnetic field (see below). Table 7.1 summarizes the usual classification of MHD discontinuities. We shall give some specific examples of the use of the conservation relations below, but there are a few general points to be made first.

The conservation relations are a set of six equations. If we wish to find the downstream state in terms of the upstream state, then there are six unknowns: ρ, V_n, V_t, p, B_n and B_t. This means that the downstream state is specified uniquely by the conservation equations, as in ordinary fluid theory. However, we only have to introduce either an anisotropic pressure (e.g., pressures parallel and perpendicular to the magnetic field are often used), or another fluid (e.g., electrons or heavy ions), and then there will be more unknowns that equations. In such cases we are forced to use additional relations, from theory or observation, to provide the missing information.

As seen in Table 7.1 the oblique shocks are divided into three categories, the fast, slow and intermediate (sometimes known as Alfvén), which corresponds to the three modes of small amplitude waves in MHD. The intermediate shock is really a special case, since it is only shock-like under special circum-

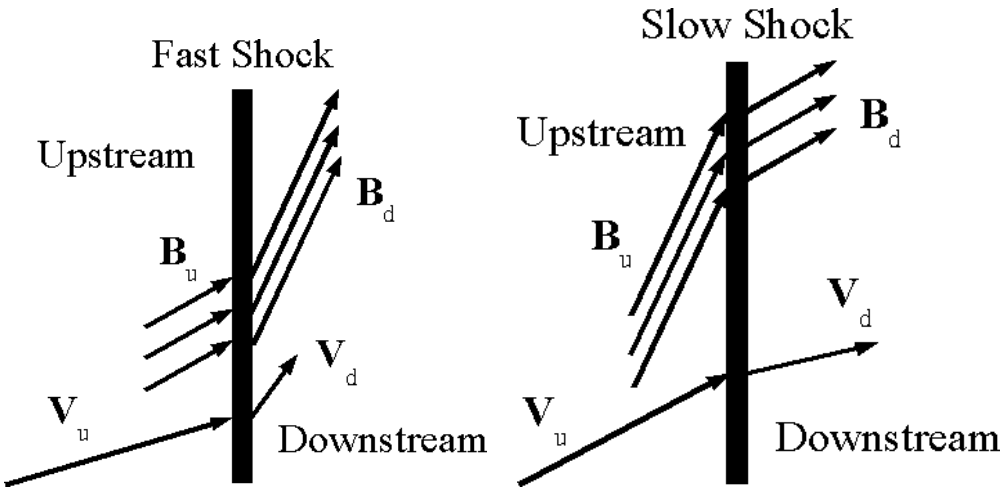

Figure 7.2: Refraction of magnetic field and flow away from (left) or toward (right) in the case of a fast shock (left) and slow shock (right).

stances. In an isotropic plasma (as we have been dealing with) it is not a shock, and is rightfully called a rotational discontinuity; it will not be discussed further.

The fast and slow shocks have the same behavior of plasma pressure and magnetic field strength as at the corresponding MHD linear waves derived in Section 4.6.1, but the shock jump conditions are fully nonlinear. This can be explained by observing that the shock jump conditions are valid for shocks of any strength. In particular, they must be true for very weak shocks. For consistency then, in the weak shock limit the shock jump relations must correspond to the modes of small amplitude MHD waves. Thus even in the fully nonlinear (large amplitude limit) the shock relations have the heritage of the linear modes. Another explanation is that the formation of a shock can be produced by the steepening of a large amplitude wave. Such a wave could steepen because the speed of waves with shorter wavelength could be changed by the wave itself. This would produce a distortion of the wave, with some parts of the wave moving relative to others. This could eventually lead to sharp gradients, and hence shock formation. Such shocks would again be expected to retain characteristics of the original mode of the wave.

Across a fast mode shock the field strength increases, but the normal component is constant, so that the increase is all in the transverse component. Therefore, at a fast shock the downstream field turns *away* from the shock normal. Conversely, at a slow shock the downstream field bends *towards* the shock normal. These characteristics are illustrated in Figure 7.2. It seems from observations that fast shocks are by far the most frequent type of shock observed in solar system plasmas. Planetary bow shocks are fast mode shocks, as are most interplanetary shocks in the solar wind. Most of our discussion later will concentrate on fast shocks. Slow shocks are rarer, although they have been observed, and they play an important part in Petschek's model of magnetic reconnection (see Figure 6.8).

7.3.1 The Exactly Parallel Shock

The parallel shock has the upstream magnetic field parallel to the shock normal, i.e., $\mathbf{B}_u = B_x\hat{n}$, $\mathbf{B}_{ut} = \mathbf{0}$. We will use the conservation relations in the frame where the upstream flow is also parallel to the shock normal, so that $\mathbf{V}_u = V_x\hat{n}$, $\mathbf{V}_{ut} = \mathbf{0}$.

An important result can be obtained by eliminating $\mathbf{V}_t$ from Equations 7.10 and 7.13 (and assuming

$V_n \neq 0$, $B_n \neq 0$).

$$\left[\left(1-\frac{B_n^2}{\mu_0 \rho V_n^2}\right) V_n \mathbf{B}_t\right] = \mathbf{0} \tag{7.14}$$

In the case of a parallel shock the quantity in parantheses is in general non-zero. If $\mathbf{B}_{ut} = \mathbf{0}$, then to satisfy (7.14) $\mathbf{B}_{dt}$ is also zero. Thus the direction of the field is unchanged by the shock. But since B_x is the only non-zero component of the field, and since it does not change, it follows that the total magnetic field is also left unchanged by the shock. There is a compression in the plasma, but not in the field. Feeding this result back into the conservation relations removes all mention of the magnetic field. From the MHD perspective this means that the shock is like an ordinary fluid shock, and the magnetic field does not play a role. However, in the context of a collisionless plasma the only way for dissipation to occur is via field-particle processes, so it is certain that here the fields somehow play a crucial role, e.g., in some wave/turbulent manner.

7.3.2 The Exactly Perpendicular Shock

At the *exactly perpendicular* shock the upstream field is perpendicular to the shock normal. In this case, $B_x = 0$ and $\mathbf{B}_u = \mathbf{B}_{ut}$. Again we examine the case where the upstream flow is parallel to the shock normal: $\mathbf{V}_u = V_{ux}\hat{x}$. To ensure shocklike solutions there will be a nonzero mass flux through the shock:

$$\rho_u V_{ux} = \rho_d V_{dx} \neq 0 \tag{7.15}$$

We define a density *compression ratio* $r = \rho_d/\rho_u$. Using the above equation we can write $V_{dx} = (1/r)V_{ux}$. We can now begin to apply the jump conditions. Equation 7.10 becomes

$$\rho_u V_{ux} \mathbf{V}_{ut} - \rho_d V_{dx} \mathbf{V}_{dt} = 0 \tag{7.16}$$

which implies that $\mathbf{V}_{dt} = \mathbf{0}$, because $\mathbf{V}_{ut} = \mathbf{0}$ and $\rho V_x \neq 0$.

From Equation 7.13, using $B_x = 0$, the jump condition becomes:

$$V_{ux}\mathbf{B}_{ut} = V_{dx}\mathbf{B}_{dt} \tag{7.17}$$

This tells us that the upstream and downstream fields are parallel. Because there is no normal magnetic field or transverse flow velocity, throughout the system, from now on we will simply use B_u, B_d, and V_u, V_d. Using the compression ratio r, we see that $B_d = rB_u$. In other words, the field compresses as much as the flow.

In the perpendicular case Equation 7.9 reduces to:

$$\rho_u V_u^2 + p_u + \frac{B_u^2}{2\mu_0} = \rho_d V_d^2 + p_d + \frac{B_d^2}{2\mu_0} \tag{7.18}$$

which can be rewritten as

$$\rho_u V_u^2 \left(1-\frac{1}{r}\right) + (p_u - p_d) + \frac{B_u^2}{2\mu_0}\left(1-r^2\right) = 0 \tag{7.19}$$

After substituting for V_d and B_d, the energy jump condition equation (7.11) in the perpendicular case, becomes:

$$\frac{1}{2}\rho_u V_u^2 \left(1-\frac{1}{r^2}\right) + \frac{\gamma}{\gamma-1}\left(p_u - \frac{1}{r}p_d\right) + \frac{B_u^2}{\mu_0}(1-r) = 0 \tag{7.20}$$

Equations 7.19 and 7.20 can be used to eliminate p_d, and we are left with an equation for r, the compression ratio, in terms of the upstream parameters.

$$(r-1)\left\{r^2\frac{(2-\gamma)}{M_A^2} + r\left(\frac{\gamma}{M_A^2} + \frac{2}{M_{cs}^2} + \gamma - 1\right) - (\gamma+1)\right\} = 0 \tag{7.21}$$

In this equation we have introduced the Alfvénic Mach number M_A, which is the ratio of the upstream flow speed (along the shock normal) to the upstream Alfvén speed; similarly we define the sonic Mach number M_{cs} as the ratio of the upstream flow speed to the upstream sound speed.

$$\text{Alfvén Mach Number} \qquad M_A = \frac{V_u}{B_u/\sqrt{\mu_0 \rho_u}} \tag{7.22}$$

and

$$\text{Sonic Mach Number} \qquad M_{cs} = \frac{V_u}{\sqrt{\gamma p_u/\rho_u}} \tag{7.23}$$

One of the solutions of equation 7.21 is clearly $r = 1$, which represents a downstream field, velocity, and density unchanged from the upstream values. Obviously, this doesn't correspond to a compressive shock (although it is a good check on the algebra!). The quadratic term in (7.21) leaves two other solutions, one of which is negative if $\gamma < 2$. This negative r solution is unphysical, and so we are left with one solution for the compression ratio. An interesting limit is the high Mach number limit, when $M_A \gg 1$ and $M_{cs} \gg 1$. In this case Equation 7.21 becomes $r(\gamma-1)-(\gamma+1) = 0$, or:

$$r = \frac{\gamma+1}{\gamma-1} \tag{7.24}$$

Therefore there is a finite limit to the compression which depends only on γ. Remember that γ is just an indication of how the plasma heats, and is not dependent on the upstream parameters. In particular, for a monatomic gas $\gamma = 5/3$, and this gives a limiting compression of four. So at a high Mach shock the maximum jump that can be expected in the field, density and velocity is by a factor four. But don't forget that this factor four, which is much quoted, depends on the details of how the plasma heats at the shock, and a polytropic equation of state hides all these details in an effective (assumed constant) γ.

Another consequence of the high Mach number limit (i.e., large upstream flow energy) can be obtained from equation 7.20 where the terms dependent on B_u and p_u can be neglected. Remembering that r is independent of the upstream parameters, there is thus a direct proportionality between the ram energy of the flow $\frac{1}{2}\rho V_u^2$ and the downstream thermal pressure p_d. This is just an illustration of the operation of the high Mach number shock: it takes the flow energy upstream, and converts it to thermal energy downstream. Finally, at the perpendicular shock both the field strength and the density increase. From the discussion above it follows that the shock is a fast mode shock. Indeed, it is possible to show from (7.21), after noting that $r > 1$, that the upstream flow V_u must be faster than the fast magnetosonic speed at perpendicular propagation (i.e., (4.58) in the upstream medium. Similar logic leads to the conclusion that the downstream flow is slower than the downstream fast magnetosonic speed, so that the shock does indeed bring about a transition from super-magnetosonic to sub-magnetosonic (see Exercise 7.5.2). There is no slow mode perpendicular shock solution to (7.21). This is unsurprising given the result that slow mode waves do not propagate perpendicular to the magnetic field.

7.3.3 Oblique Shocks

The general case of oblique shocks, i.e., those for which the upstream field is neither exactly parallel nor perpendicular to the shock normal, is conceptually the same as those we have been looking at, although the algebra is a bit more tedious. We shall see later that the angle θ_{Bn} which the upstream field makes with the shock normal $\hat{n}$ plays a crucial controlling role in the processes occuring at such shocks. While

we will not perform the full Rankine-Hugoniot analysis in the general case, we note here that, as depicted in Figure 7.2 and discussed in Table 7.1 both slow mode and fast mode transitions are possible.

One important feature of oblique MHD shocks emerges from Equation 7.14. Let us begin by noting that it is always possible to move to a frame of reference in which the shock is at rest and the upstream velocity is directed into the shock along the shock normal. This is called the "Normal Incidence Frame," or NIF. [Imagine the 3D version of Figure 7.1 in which the shock is at rest. Now translate along the shock surface; the normal component of velocity doesn't change, but you can make the tangential one take on any value, including zero.] So in the NIF, there are only two directions of relevance to the upstream region: the shock normal $\hat{n}$ and the magnetic field $\mathbf{B}_u$. These two vectors define a plane. Now (7.14) tells us that the downstream tangential magnetic field $\mathbf{B}_{dt}$ is parallel to the upstream one, and hence the total downstream magnetic field $\mathbf{B}_d$ lies in this same plane. Finally, the transverse momentum equation (7.10) shows that any downstream tangential flow $\mathbf{V}_{dt}$ must be parallel to the tangential magnetic field, so the downstream flow also lies in this same frame. If we started from a frame other than the NIF, we would have concluded that the *jump* in tangential velocity $[\mathbf{V}_t]$ would be confined to this plane, as is a jump in the normal velocity component. This simply reflects the fact that the tangential velocity is related to the field tension, which acts in the same direction as the "kink" in the field; there are no forces directed out of this plane. Thus we reach

> **Coplanarity Theorem**: At oblique MHD shocks, the shock normal $\hat{n}$, upstream and downstream magnetic fields $\mathbf{B}_u$ and $\mathbf{B}_d$, and jump in velocity $\mathbf{V}_u - \mathbf{V}_d$ are all coplanar.

The Coplanarity Theorem simplifies the analysis. It also makes it possible to estimate the direction of shock propagation from real data since, for example, $\mathbf{B}_u \times \mathbf{B}_d$ and $\mathbf{B}_u - \mathbf{B}_d$ are both perpendicular to the normal, whence

$$\hat{n} = \frac{(\mathbf{B}_u \times \mathbf{B}_d) \times (\mathbf{B}_u - \mathbf{B}_d)}{|(\mathbf{B}_u \times \mathbf{B}_d) \times (\mathbf{B}_u - \mathbf{B}_d)|} \tag{7.25}$$

is the "magnetic coplanarity normal."

There is one important exception to the coplanarity theorem, and that arises from inspection of (7.14) when the expression in parentheses is zero, i.e.,

$$V_n = \frac{B_n}{\sqrt{\mu_0 \rho}} \equiv v_{An} \tag{7.26}$$

or the normal flow is Alfvénic. In this case $\mathbf{B}_t$ can rotate out of the coplanarity plane. This special case corresponds to a rotational discontinuity, and the other Rankine Hugoniot relations can be used to demonstrate, in MHD, that there is no compression of the plasma, no deceleration, no heating, and no change in the field magnitude. Thus rotational discontinuities are not shocks.

For completeness, there are also special cases when the tangential field is present on only one side or the other. These are known as "switch-on" or "switch-off" shocks. These cases obey the coplanarity theorem (on the side with no tangential field, there is only one defining direction, namely $\hat{n}$).

7.4 Shock Structure

7.4.1 Real Shocks

So far we have described some fundamental concepts about shocks, and mentioned some examples of where shocks will be formed. But in the case of shocks in space we are in an almost unique position,

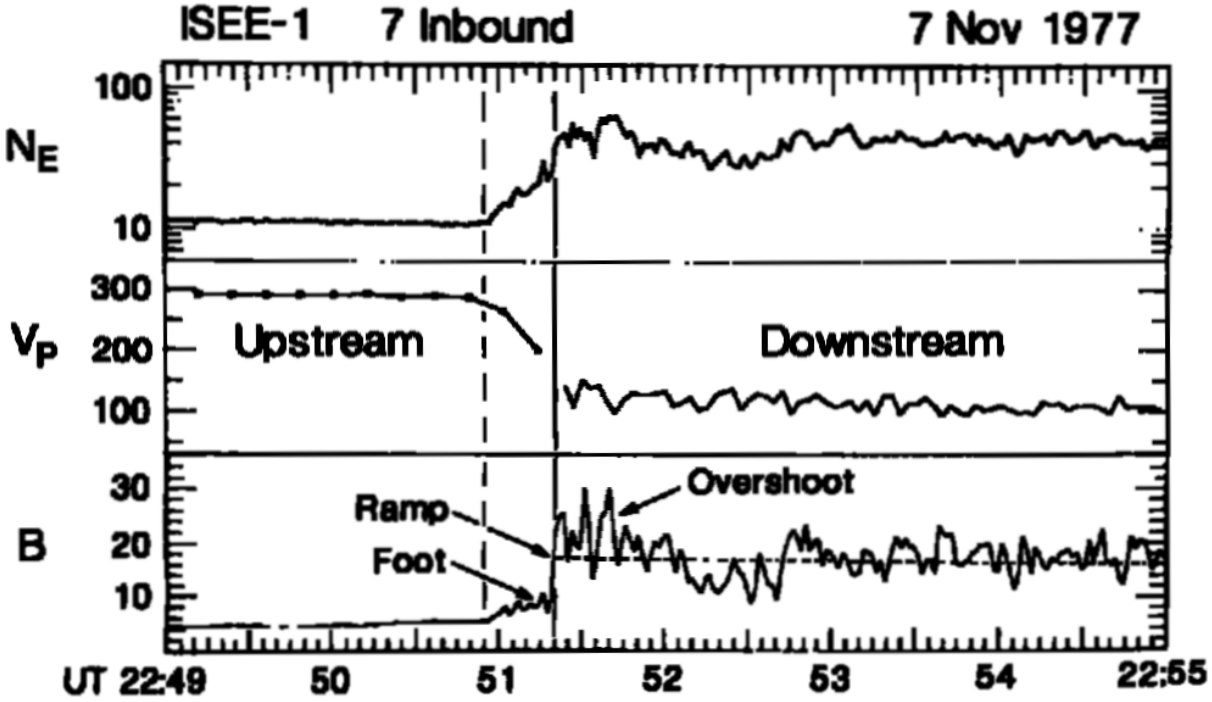

Figure 7.3: Observations of a supercricital quasi-perpendicular shock in space

since we have direct observations of naturally occurring shocks. It is possible to generate collisionless shocks in the laboratory, and shock heating was one of the hopes for controlled nuclear fusion. But laboratory experiments cannot approach the scale or global nature of the naturally occurring space shocks. Space observations are also unique in that the smallest plasma scale (the Debye length) is usually larger than the spacecraft. This means that we can truly make a point measurement, since our measurement devices do not affect the plasma (at least if we are careful). With increasing space technology we are making higher and higher resolution measurements of the space shocks. Not only are we measuring the upstream and downstream states, but we can also measure how the plasma changes as it passes through the shock. In other words, we can study the collisionless dissipation mechanisms in action.

Figure 7.3 shows the measurements made as a spacecraft passed through the Earth's bow shock. Instruments onboard measure the magnetic field. By counting particles arriving at the satellite, the electron and proton distribution functions can be measured, and from these the density and the flow speed of the solar wind as it passes through the shock can be calculated. The satellite has a very small speed, and usually observations of the bow shock happen when the shock moves across the satellite. This can happen because of slight changes in the solar wind speed or density. The observations consist of time series for the different quantities, and if the speed of the shock relative to the satellite is constant, then the profiles we observe in *time* will be the same as the shock's profile in *space*. In the figure the satellite is initially in the solar wind, and then the shock moves outwards and the observations are taken as the shock moves over the satellite.

In passing from upstream to downstream it is obvious that the velocity decreases, and the density increases. That is, there is compression at the shock. Also the magnetic field is shown, and this increases like the density, so it is a fast mode shock. The next thing to notice is that although, the shock is thin, it is not just a smooth transition. Instead, there is structure within the transition: There is a "foot," a "ramp," and an "overshoot," and we will see later that these are controlled by the way in which the solar wind protons heat at the shock. For example, the thickness of the foot equals the distance to which protons

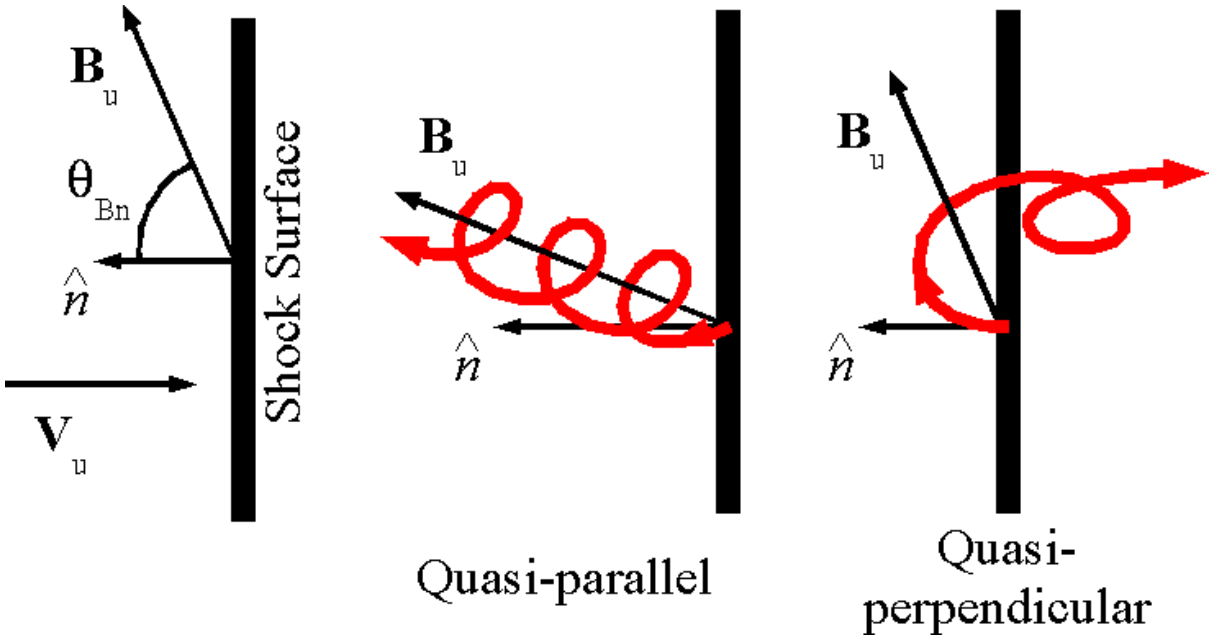

Figure 7.4: Shock geometry θ_{Bn} (left) and the motion of reflected ions in the case of quasi-parallel geometries (middle) and quasi-perpendicular ones (right).

are reflected by the shock before drifting through it.

7.4.2 Different Parameters Make Different Shocks

The most important result from space observations of shocks is that there are many different types of shock depending on the shock parameters. We have already seen that the Rankine-Hugoniot relations lead to different modes of shocks, but even restricting ourselves to fast mode shocks, like planetary bow shocks, we find different types of shock structure. Early on there were quite serious debates about whether the Earth's bow shock was actually stable; perhaps all the different profiles seen in observations were just fleeting glimpses of an ever changing entity. A major contribution was to show that there was a definite pattern to the observations, and that the type of shock was determined by the complete set of shock parameters describing the upstream conditions. The most important factors in controlling the type of shock are the direction of the upstream magnetic field (relative to the shock surface) and the strength of the shock.

We will first look at the influence of the direction of the upstream field, sometimes called the shock geometry. Figure 7.4 shows a one-dimensional shock, and marked on it is the unit vector $\hat{n}$ normal to the shock surface. A convenient way to describe the direction of the upstream field is the angle θ_{Bn} between it and the shock normal. Depending on θ_{Bn} the shock has dramatically different behaviors. When $\theta_{Bn} = 0$ the shock is called parallel, and when $\theta_{Bn} = 90^\circ$ it is called perpendicular. The terms quasi-parallel and quasi-perpendicular are used to divide the range of possible θ_{Bn} values, with the actual dividing line usually chosen as 45°. Another term, oblique, refers to a shock which is neither exactly perpendicular or parallel, but it is also sometimes used to refer to the no man's land between quasi-parallel and quasi-perpendicular.

The importance of the parallel/perpendicular distinction is clear when we consider the motion of a particle which is initially headed away from the shock. Such particles arise either by escaping upstream from the downstream side or by being reflected at the shock itself. The motion of these particles is particularly simple if we transform away the motional electric field by moving along the shock surface

(towards the top of Figure 7.4) so that the upstream velocity $\mathbf{V}_u$ is aligned with the magnetic field $\mathbf{B}_u$. In this frame, the "de Hoffmann-Teller frame," the shock is still at rest and now the particle motion is pure gyromotion plus field-aligned guiding centre motion, since $\mathbf{E}' = -\mathbf{V}' \times \mathbf{B}' \equiv \mathbf{0}$. It suffices, therefore, to decompose the initial velocity of the particle into these components in order to follow these particles.

In the case of a quasi-parallel shock the field lines pass through the shock and a particle's motion along the field will carry the particle through (and away from) the shock relatively easily. On the other hand, at quasi-perpendicular shocks the field lines are almost parallel to the shock surface, so particle motion along the magnetic field would need to be very rapid (more technically, the pitch angle would need to be quite small) if the particle is to escape from the shock. For most pitch angles, the particle gyration at a quasi-perpendicular shock brings the particle back to the shock. There is a further simple conclusion to be drawn from the parallel/perpendicular distinction: Because particle motion in the normal direction is "easier" at the parallel shock, compared to the perpendicular shock, then we can expect that the scale of the parallel shock will be larger than for the perpendicular shock. Of course, this can only be said with certainty once we know the exact dissipation mechanisms. Also our arguments about particle motion are really only true for the ions, which have much larger gyroradii than the electrons, but that is not so bad because they determine most of the structure of collisionless shocks. (Because of their much greater mass the ions carry most of the mass and energy flow in a plasma.)

The shock angle θ_{Bn} is the most important factor in controlling the shock type, but almost every plasma parameter can have an effect: temperature, composition (i.e, what types of ions are present), and shock Mach number M. The Mach number indicates the strength of the shock, and is a measure of the amount of energy being processed by the shock. As might be expected, the higher the Mach number the more dramatic the behavior of the shock. In the solar system shocks can be found with Mach number between (almost) 1 and perhaps 20, but in more violent astrophysical objects, like the shocks produced by super-nova remnants, the Mach number could be of the order of a thousand. The processes operating at such shocks remain unclear, but for the solar system shocks we believe that we have a fair understanding. However, even for solar system shocks this statement is only true for *quasi-perpendicular* shocks. At the present time, quasi-parallel shocks are a topic of ongoing debate; the easy particle access results in an extended region of waves, turbulence, and shock-energised suprathermal particles.

In the quasi-perpendicular shock there is a clear distinction, at least theoretically, between a type of low Mach number shock, the subcritical shock, and a higher Mach number shock, the supercritical shock. For most of the time the Earth's bow shock is supercritical, and to find subcritical shocks we usually have to wait for a suitable interplanetary shock. As the name suggests there is a "critical" Mach number which separates the two types of shock. This critical Mach number is at $M_A \sim 2.7$ for $\theta_{Bn} = 90^\circ$, and decreases as θ_{Bn} decreases. The Earth's bow shock has values for M_A in the range $\sim 1.5 - 10$.

Observationally the difference between these two types of shock is clear. Our original example (Figure 7.3) was of a supercritical shock. We have already mentioned the *structure* visible within the shock: The field has a single sharp jump (called the *ramp*), but it is preceded by a gradual rise called the *foot* which is related directly to the gyrating orbits of ions reflected by the shock and returned to the shock surface as sketched in the right panel of Figure 7.4. Also, the field right at and behind the ramp is higher than its eventual downstream value, and this is called the *overshoot*. Like good biologists we have arrived at this separation into component parts only after seeing many examples. And we have ignored what we don't think is important, which in this case is all the small wiggles in the field. We label this as small amplitude turbulence, which may play a role, but which doesn't control or overwhelm the basic shock structure.

In contrast with the structure of the supercritical shock, the subcritical shock resembles much more the profile of a shock in an ordinary gas. Figure 7.5 shows several examples of low Mach number shocks ranging from subcritical to slightly supercritical. The top two have relatively simple ramps from the upstream to the downstream value, with little or no foot or overshoot. There is wave which appears

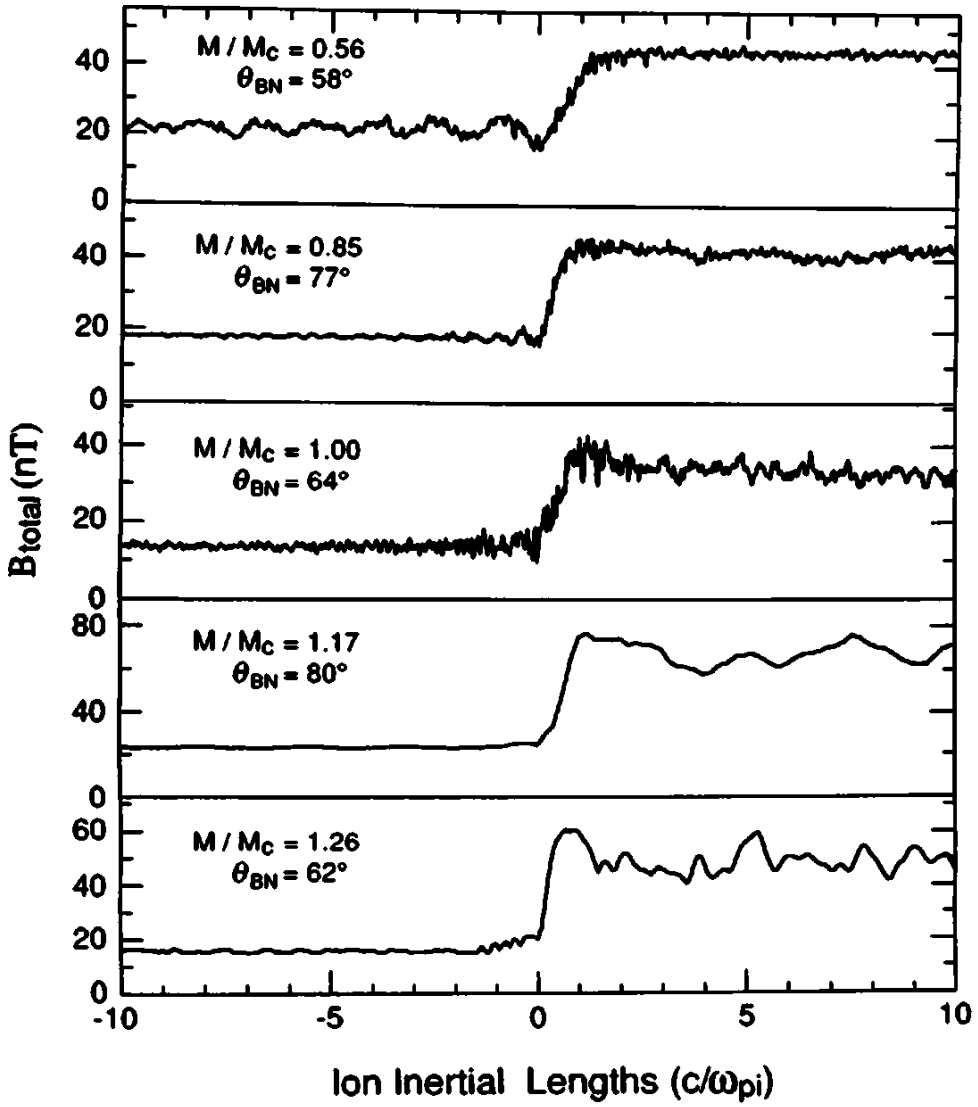

Figure 7.5: Observed profiles of the magnetic field magnitude at several quasi-perpendicular shocks ranging from sub-critical (top) through to super-critical (bottom).

in the upstream region. This wave, the *precursor*, has a single, well-defined wavelength. The presence of this precursor depends on both the θ_{Bn} and the Mach number; it corresponds to non-MHD aspects of shorter wavelength waves which travel faster than the fast magnetosonic wave and hence can escape upstream. Notice that the wavelength is smaller in the second, more perpendicular, of these examples.

As supercriticality is reach and surpassed, the foot and overshoot become apparent. Here, too, the size, shape, and extent of these features depend on the shock geometry and Mach number.

7.5 Exercises

1. Fill in the steps in Section 7.3.2 leading to Equation 7.21.

2. Shocks must be compressive, so the density ratio $\rho_d/\rho_u \equiv r > 1$. Re-arrange Equation 7.21 to form an inequality making use of $r > 1$ and hence show that in this case of perpendicular shocks,

provided $1 \leq \gamma \leq 2$, the upstream flow speed must be super-fast-magnetosonic, i.e., faster than $v_f = \sqrt{c_s^2 + v_A^2}$ given in (4.58). For bonus marks, given this result construct a two-line (maximum) argument to show that the *downstream flow* must be sub-fast-magnetosonic. [Hint: think about the Rankine-Hugoniot relations in reverse.]

3. A planar slow mode shock is propagating through a plasma which, away from the shock itself, obeys the ideal MHD equations. In the rest frame of the shock, the shock lies in the $y-z$ plane, and upstream of the shock the inflow velocity is $\mathbf{V}_u = -V_u\hat{x}$ where $\hat{x}$ is the shock normal which points into the upstream region. The upstream medium is uniform with mass density ρ_u, pressure p_u, and magnetic field $\mathbf{B}_u = B_u(cos\theta_u, 0, \sin\theta_u)$. If the shock "switches off" the transverse magnetic field component, so that in the downstream region $\mathbf{B}_d = (B_d, 0, 0)$, combine the continuity (mass conservation) and z momentum jump conditions to show that the downstream region has a z-flow component (the "jet" in Petschek reconnection) given by

$$\frac{V_{dz}}{V_u} = \frac{\cos\theta_u \sin\theta_u}{M_A^2}$$

where

$$M_A \equiv \frac{V_u}{B_u/\sqrt{\mu_0\rho_u}}$$

is the upstream Alfvénic Mach number.

4. Referring to Figure 6.8 for the geometry of the slow mode shocks in Petschek reconnection, express the upstream shock conditions (ρ, $\mathbf{V}$, $\mathbf{B}$) in terms of the field geometry χ, shock geometry ξ, electric field $\mathbf{E}$ and distant field strength B in a standard shock coordinate system. Assume that the incoming plasma is cold, i.e., $p_u = 0$. Use the Rankine Hugoniot relations to find the downstream state B_d, V_d, ρ_d, and p_d. Assume that the downstream field and flow directions are as shown in the figure. [This question requires careful thinking and working.]

5. Sudden changes are detected in the solar wind and interplanetary magnetic field. The radial velocity of the solar wind remains constant, but the density jumps from 5 to 10 cm^{-3}. The proton temperature jumps from 5eV before the discontinuity to 13.8eV afterward, but the electron temperature remains constant at 15eV. The magnetic field of $(0, -8, 6)$nT before the discontinuity rotates and drops in strength to $(0, 3, 4)$nT. What type of discontinuity might this be, and why?

6. An interplanetary shock crosses the spacecraft *Space Physics Explorer* and its magnetometer detects an upstream magnetic field of $(6.36, -4.72, 0.83)$nT and a downstream magnetic field of $(10.25, -9.38, 1.74)$nT. Using the magnetic coplanarity theorem (and if needed $[B_n] = 0$) determine the orientation of the normal. The plasma analyzer detects an upstream velocity of $(-378, 33.1, 19.9)$km/s and a downstream velocity of $(-416.8, 7.3, 51.2)$km/s. If the upstream density was 7.5 protons/cm^3 and the downstream density was 11 protons/cm^3, calculate the velocity of the shock. [Hint: In the rest frame of the shock, $\mathbf{V}_u^* = \mathbf{V}_u - V_{sh}\hat{n}$, $\mathbf{V}_d^* = \mathbf{V}_d - V_{sh}\hat{n}$, and you will need to use the Rankine-Hugoniot relations. Assume that the solar wind is purely protons, together with an equal number of electrons.]

Chapter 8

Multi-Fluid Models

8.1 Formulation

We have seen that the one-fluid MHD model of astrophysical plasmas, developed in Chapter 4 and explored further in subsequent chapters, embraces many fundamental aspects. These include a complete mathematical representation of mass conservation, fluid forces including electromagnetic effects, an equation of state (with an ad hoc polytropic index), and the consequences of Maxwell's equations, especially magnetic induction, flux freezing, and diffusion. We left out, or glossed over, the implications of plasmas necessarily being comprised of more than one species (i.e., they must have at least an ion species and electrons), phenomena on particle timescales (cyclotron and/or plasma frequencies), transport processes such as conduction and viscosity, and interactions leading to instabilities.

Here we begin to address many of these deficiences by considering a plasma to be made up of more than one species. To keep the problem manageable, we continue to work with fluid concepts as opposed to the richer kinetic descriptions. Thus we assume that the plasma can be well-represented by its fluid parameters, e.g., density, bulk velocity, temperature, etc., although we now each species can have different values of these quantities.

Specifically, we denote the different species by the subscript "j." Then we introduce the following notation:

$$m_j \quad \text{mass of a particle} \tag{8.1}$$

$$q_j \quad \text{charge on a particle} \tag{8.2}$$

$$n_j \quad \text{number density} \tag{8.3}$$

$$\mathbf{V}_j \quad \text{bulk velocity} \tag{8.4}$$

$$p_j \quad \text{pressure in species rest frame} \tag{8.5}$$

Note in particular that we have *not* defined a single, common centre of mass frame and measured all the pressures in that frame. We treat each species on its own. While this has the advantage that it allows us to describe each species better, it complicates some problems because the pressures are all measured in different frames. In the centre of mass frame there are then contributions to the pressure which arise from the relative bulk motions.

Now let us build the mathematical description of such a multi-fluid plasma. Most of this relies, as we did in Chapter 4, on concepts of conservation equations and fluid elements. For example, conservation of the number of particles of each species requires

$$\frac{\partial n_j}{\partial t} + \nabla \cdot (\mathbf{V}_j n_j) = 0 \tag{8.6}$$

by comparison with (4.1). This is usually referred to as the continuity equation.

The equation of motion for a fluid element of species "j" is (cf., (4.2)

$$n_j m_j \left(\frac{\partial}{\partial t} + \mathbf{V}_j \cdot \nabla \right) \mathbf{V}_j = -\nabla p_j + n_j q_j \left(\mathbf{E} + \mathbf{V}_j \times \mathbf{B} \right) + \mathbf{K}_j \tag{8.7}$$

where we have now retained the separate electric and magnetic forces, and introduced an interaction force $\mathbf{K}_j$ which represents momentum added to species "j" from the other species in the system. This momentum transfer mimics collisions and other kinetic effects not included directly in the multi-fluid description. Since the total momentum of the plasma must be conserved, one species' gain must be another's loss, so that $\sum_j \mathbf{K}_j = \mathbf{0}$.

We could also adopt an ad hoc polytropic approximation here, as we did in Chapter 4. However, we might need to incorporate energy transfers amongst the different species, and so we instead derive an energy equation based on the thermodynamics of a fluid element. The first law of thermodynamics tells us

$$dU = dW + dQ \tag{8.8}$$

where U is the internal (i.e., thermal) energy, dW is the external work done on the element (by the pressure forces on it), and dQ is the heat added to the element. For an element of volume $\mathcal{V}$, there is $\frac{1}{2}k_b T_j$ of thermal energy in each degree of freedom. If we assume that the species is monatomic then there are only the 3 translational degrees of freedom, and so $U = \frac{3}{2}p\mathcal{V}$. Now the net work (force times distance) done by the external pressure is simply $dW = -p\,d\mathcal{V}$. Thus the first law becomes

$$d\left(\frac{3}{2}p\mathcal{V}\right) \equiv \mathcal{V}d\left(\frac{3}{2}p\right) + \frac{3}{2}p\,d\mathcal{V} = -p\,d\mathcal{V} + dQ \tag{8.9}$$

Here d denotes a change in a quantity following the fluid element, and so should be associated with the convective derivative $\partial/\partial t + \mathbf{V}_j \cdot \nabla$ similar to (4.5). [This is not strictly true for the dQ term since, thermodynamically, dQ is not a real differential, but that will not concern us here.] Noting that the continuity equation (8.6) can be written $d(n_j\mathcal{V}) = 0$, (following an element, the number of particles it contains doesn't change) dividing by $\mathcal{V}$, collecting terms, and using (8.6) leads to

$$\left(\frac{\partial}{\partial t} + \mathbf{V}_j \cdot \nabla \right) \left(\frac{3}{2} p_j \right) = -\frac{5}{2} p_j \nabla \cdot \mathbf{V}_j + H_j \tag{8.10}$$

where H_j represents the heat added per unit volume to the j^{th} species from all the others. It is straightforward to show that, in the absence of heat addition, Equation 8.10 reduces to (4.3) with $\gamma = 5/3$.

We need only add Maxwell's equations to complete the system. In particular, we need the induction equation

$$\frac{\partial \mathbf{B}}{\partial t} = -\nabla \times \mathbf{E} \tag{8.11}$$

together with Poisson's equation

$$\nabla \cdot \mathbf{E} = \frac{\rho_q}{\varepsilon_0} = \frac{1}{\varepsilon_0} \sum_j n_j q_j \tag{8.12}$$

and Ampere's Law including the displacement current

$$\begin{aligned} \nabla \times \mathbf{B} &= \mu_0 \mathbf{j} + \frac{1}{c^2} \frac{\partial \mathbf{E}}{\partial t} \\ &= \mu_0 \sum_j n_j q_j \mathbf{V}_j + \frac{1}{c^2} \frac{\partial \mathbf{E}}{\partial t} \end{aligned} \tag{8.13}$$

Notice that while each species has its own set of equations, they are coupled through Maxwell's equations which require the total charge and current densities.

8.2 Generalised Ohm's Law

The multi-fluid description allows us to re-examine the conducting properties of a plasma since we can now follow the charge carriers separately. This improves on Equation 4.9 which we wrote down as a generic Ohm's Law for a conductor.

We consider a two-fluid system with electrons ("e") and ions ("i"). For simplicity we assume the ions are singly ionized. Then we multiply the equation of motion (8.7) of each species by q_j/m_j to reach

$$n_i e\left(\frac{\partial}{\partial t}+\mathbf{V}_i\cdot\nabla\right)\mathbf{V}_i = -\frac{e}{m_i}\nabla p_i+\frac{n_i e^2}{m_i}(\mathbf{E}+\mathbf{V}_\mathrm{i}\times\mathbf{B})+\frac{e}{m_i}\mathbf{K}_i \tag{8.14}$$

$$-n_e e\left(\frac{\partial}{\partial t}+\mathbf{V}_e\cdot\nabla\right)\mathbf{V}_e = +\frac{e}{m_e}\nabla p_e+\frac{n_e e^2}{m_e}(\mathbf{E}+\mathbf{V}_\mathrm{e}\times\mathbf{B})-\frac{e}{m_e}\mathbf{K}_e \tag{8.15}$$

We now add these two equations, noting that $\mathbf{K}_e=-\mathbf{K}_i\equiv-\mathbf{K}$, that $n_e\approx n_i=n$ on scales larger than a Debye length, and that the electric current $\mathbf{j}\equiv n_i e\mathbf{V}_i-n_e e\mathbf{V}_e$. This results in

$$\begin{aligned} ne\frac{\partial}{\partial t}\left(\frac{\mathbf{j}}{ne}\right)+ne(\mathbf{V}_i\cdot\nabla\mathbf{V}_i-\mathbf{V}_e\cdot\nabla\mathbf{V}_e) &= -e\nabla\left(\frac{p_i}{m_i}-\frac{p_e}{m_e}\right)+ne^2\left(\frac{1}{m_i}+\frac{1}{m_e}\right)[\mathbf{E}+\mathbf{V}_e\times\mathbf{B}]+ \\ &\quad +\frac{e}{m_i}\mathbf{j}\times\mathbf{B}+e\mathbf{K}\left(\frac{1}{m_i}+\frac{1}{m_e}\right) \end{aligned} \tag{8.16}$$

The quantity $\mathbf{K}$ is the momentum transferred to the ions from the electrons. If this transfer is due to collisions (or any process which tends to equilibrate the species' motion), then we expect such a frictional force to be proportional to the relative motion. That is, we expect $\mathbf{K}\propto\mathbf{V}_e-\mathbf{V}_i\propto-\mathbf{j}$ so that we may write, say, $\mathbf{K}=-ne\mathbf{j}/\sigma$ where σ will turn out to be the conductivity of the plasma. Multiplying (8.16) by μ/ne^2 where $\mu\equiv m_i m_e/(m_i+m_e)\approx m_e$ and re-arranging leads to

Generalised Ohm's Law

$$\begin{aligned} \mathbf{E}+\mathbf{V}_\mathrm{e}\times\mathbf{B} = {} & \frac{\mathbf{j}}{\sigma}- \\ & -\frac{1}{ne}\nabla\left(\frac{\mu}{m_e}p_e-\frac{\mu}{m_i}p_i\right)- \\ & -\frac{\mu}{nem_i}\mathbf{j}\times\mathbf{B}+ \\ & +\mu\frac{\partial}{\partial t}\left(\frac{\mathbf{j}}{ne^2}\right)+\frac{\mu}{e}(\mathbf{V}_i\cdot\nabla\mathbf{V}_i-\mathbf{V}_e\cdot\nabla\mathbf{V}_e) \end{aligned} \tag{8.17}$$

The top line is just the MHD Ohm's Law (4.9) apart from the explicit dependence on the electron velocity. This dependence reveals that it is the electrons which are more mobile; the electron frame is the rest frame of the "conductor." The next line corresponds to "thermo-electric" fields. Since $\mu\approx m_e\ll m_i$ we can see that only the electron contribution is likely to be significant. Such electric fields arise because pressure gradients drive the lighter electrons, leading to a charge separation electric field which prevents them from running away from the ions.

The $\mathbf{j}\times\mathbf{B}$ term is known as the Hall term due to the presence of the magnetic field. The associated electric field is perpendicular both to the magnetic field and the electric current. The final set of terms in (8.17) come from the inertial portions of the equations of motion. They are typically small unless there are rapid temporal variations or large currents. Hall and inertial effects can be extremely important on the microscopic scale, however. For example, the initiation and structure of reconnecting plasmas is controlled by these terms.

8.3 Waves in Cold Two-fluid Plasmas

The multi-fluid formulation is an excellent starting point for exploring the rich wave properties of multi-species plasmas. In particular, we can relax the MHD assumption of large length scales ($L \gg r_L, \lambda_D$) and long timescales ($\tau \gg 1/\Omega_c, 1/\omega_{pe}$) although we still cannot include all the kinetic effects.

We proceed in identical fashion to that in Section 4.6.1 by linearising and Fourier analysing the governing equations. In this case these equations are (8.6), (8.7), (8.10), together with Maxwell's Equations (8.11), (8.12),and (8.13). Here, we allow for the species to have relative drifts, so that $\mathbf{V}_j = \mathbf{V}_{j0} + \mathbf{V}_{j1}$ but we assume that all species are cold, i.e., $p_j \equiv 0$.

This leads to the following set:

$$
\begin{aligned}
(-\omega + \mathbf{k}\cdot\mathbf{V}_{j0})\delta n_j + (\mathbf{k}\cdot\delta\mathbf{V}_j)\, n_{j0} &= 0 && (8.18)\\
i m_j n_{j0}\,(-\omega + \mathbf{k}\cdot\mathbf{V}_{j0})\,\delta\mathbf{V}_j &= n_{j0} q_j\,(\delta\mathbf{E} + \delta\mathbf{V}_j\times\mathbf{B}_0 + \mathbf{V}_{j0}\times\delta\mathbf{B}) + \\
&\quad + \delta n_j q_j\,(\mathbf{V}_{j0}\times\mathbf{B}_0) && (8.19)\\
\mathbf{k}\times\delta\mathbf{E} &= \omega\delta\mathbf{B} && (8.20)\\
i\mathbf{k}\cdot\delta\mathbf{E} &= \sum_j \frac{\delta n_j q_j}{\varepsilon_0} && (8.21)\\
i\mathbf{k}\times\delta\mathbf{B} &= \mu_0 \sum_j q_j\,(\delta n_j \mathbf{V}_{j0} + n_{j0}\delta\mathbf{V}_j) - \frac{i\omega\delta\mathbf{E}}{c^2} && (8.22)
\end{aligned}
$$

Note that $\nabla\cdot\delta\mathbf{B} = 0$ is preserved by (8.20) if it is satisfied initially, so we have not included that equation. Indeed, dotting (8.22) with $\mathbf{k}$ and using the continuity result (8.18) reveals that Poisson's equation is also redundant (in effect, continuity of mass implies continuity of charge). Nonetheless, for some applications Poisson's equation is more convenient, so we shall keep both here.

Plasma texts (e.g., that by Boyd and Sanderson) systematically explore the variety of waves which can exist in even a relatively simple, two-fluid (ions and electrons) plasma. We shall content ourselves here with a couple of examples which are not accessible to MHD treatment.

8.3.1 Two-stream Instability

Let us start with a plasma composed of two equal, counterstreaming (electron) beams in the absence of a magnetic field. Consider for simplicity a 1-D problem in which $\mathbf{k}$, the velocities (both background and fluctuations), and the fluctuating electric field are all co-linear. Thus $\mathbf{V}_{j0} = \pm\mathbf{V}_0 \equiv \pm V_0\hat{k}$ and $n_{j0} = n_0$. There will be a background of a third species (ions, to provide overall charge neutrality) which we will assume is dynamically unimportant. The governing equations reduce in this case to:

$$
\begin{aligned}
-(\omega \mp kV_0)\delta n_j + k\delta V_j n_0 &= 0 && (8.23)\\
-im(\omega \mp kV_0)\delta V_j &= q\delta E && (8.24)\\
ik\delta E &= \frac{q}{\varepsilon_0}\sum_{j=1,2}\delta n_j && (8.25)
\end{aligned}
$$

where the upper sign corresponds to $j = 1$ and the lower to $j = 2$. Solving for δn_j yields

$$\begin{aligned} \delta n_j &= \frac{n_0 k \delta V_j}{\omega \mp k V_0} = \frac{n_0 k}{\omega \mp k V_0} \left[\frac{-q\delta E}{im(\omega \mp k V_0)} \right] \\ &= \frac{i n_0 q}{m} \frac{k}{(\omega \mp k V_0)^2} \delta E \end{aligned} \tag{8.26}$$

Substituting this result into (8.25) yields an equation in δE:

$$ik\delta E = \frac{q}{\varepsilon_0} \frac{i n_0 q}{m} k \delta E \left[\frac{1}{(\omega - k V_0)^2} + \frac{1}{(\omega + k V_0)^2} \right] \tag{8.27}$$

or

$$\delta E = \omega_p^2 \left[\frac{1}{(\omega - k V_0)^2} + \frac{1}{(\omega + k V_0)^2} \right] \delta E \tag{8.28}$$

where $\omega_p^2 \equiv n_0 q^2 / m\varepsilon_0$ is the square of the plasma frequency of each beam. Non-trivial δE thus requires

$$1 = \omega_p^2 \left[\frac{1}{(\omega - k V_0)^2} + \frac{1}{(\omega + k V_0)^2} \right] \tag{8.29}$$

which is the desired dispersion relation. A couple of lines of algebra yields

$$\omega^4 - 2\omega^2 \left(k^2 V_0^2 \right) + k^2 V_0^2 \left(k^2 V_0^2 - 2\omega_p^2 \right) = 0 \tag{8.30}$$

which is a quadratic equation in ω^2. Expanding the solution for small k (i.e., $k^2 V_0^2 / \omega_p^2 \ll 1$ yields two approximate roots

$$\omega^2 \approx 2\omega_p^2 + 3(k V_0)^2 \tag{8.31}$$

which is just the dispersion relation for plasma oscillations modified slightly by the beam relative drifts and

Two Stream Instability	$\omega^2 \approx -(k V_0)^2$

(8.32)

This represents two modes, $\omega = +ikV_0$ and $\omega = -ikV_0$. Recalling that the fluctations vary as $e^{i(\mathbf{k}\cdot\mathbf{x} - \omega t)}$ we see that one of these modes decays as $e^{-(kV_0 t)}$ while the other grows as $e^{+(kV_0 t)}$. Thus the initial configuration is unstable, the (presumed small) fluctuations grow until a nonlinear regime is reached. Typically, the nonlinear stage of an instability tends to destroy or disrupt the "free energy" which drives the instability in the first place. In the present case this would be through a deceleration of the relative beam motion, turning that energy into electric energy and ultimately heat.

In general, plasmas don't like beams, currents, etc., and are usually unstable to waves of some kind for any significant beam or current features. The nonlinear aspects of such instabilities scatters plasma particles, reducing the beam/current, and thus subsuming the role of collisions. The consequences of such scattering on the current carried by the plasma is termed "anomolous resistivity."

8.3.2 Electron Whistler Waves

Let us now explore one of the "natural" plasma modes, known as a whistler wave. Whistlers were important in the history of understanding the Earth's magnetic field and atmosphere. We shall see that they are dispersive; higher frequency waves travel faster and thus arrive first, giving the characteristic

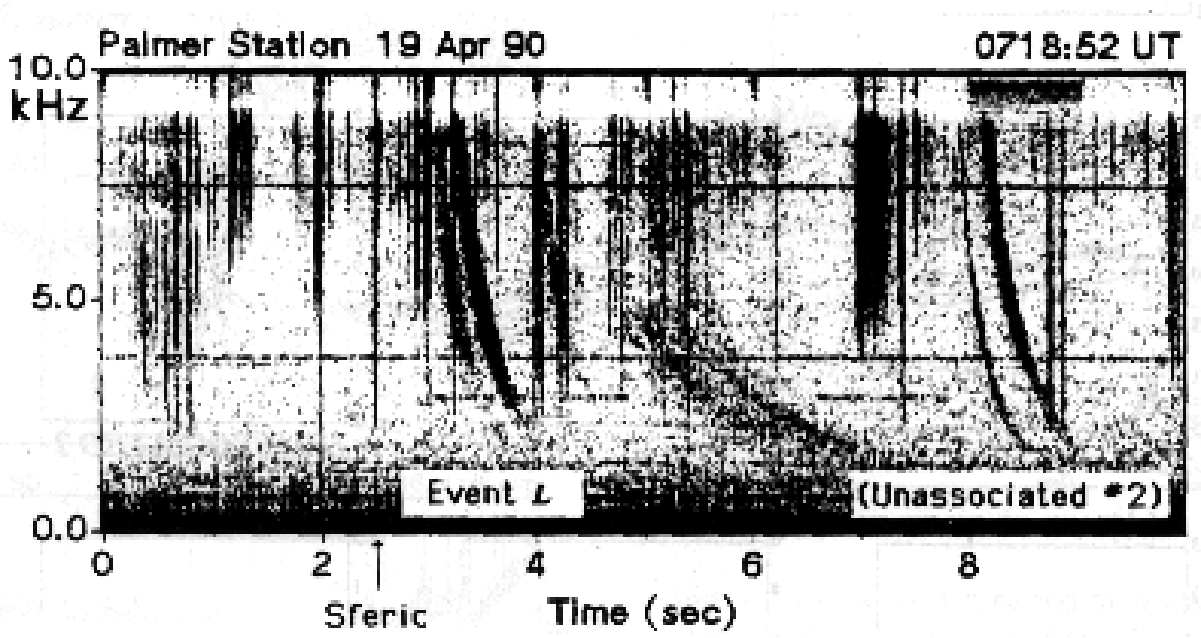

Figure 8.1: Dynamic spectrum of frequency vs. time showing several sweeping arcs characteristic of whistler waves in the Earth's atmosphere. [From Burgess and Inan, 1993]

falling tone (which you can hear on a shortwave radio) from which they are named. These features can be seen in the observations shown in Figure 8.1. Moreover, whistlers can travel from one hemisphere along the Earth's dipole field to the other, and thus travel through the "magnetosphere." Knowing their dispersion properties allowed ionospheric physicists to determine the density and other parameters from the waves received on the ground.

We return to the basic cold multi-fluid wave equations (8.18)-(8.22). In this case, we consider only one species, electrons, and again assume that there is a background of ions which, due to their larger mass, are dynamically unimportant. We assume that there is no drift, i.e., $\mathbf{V}_{j0} = \mathbf{0}$ and that the wave-vector $\mathbf{k}$ is aligned with the equilibrium magnetic field $\mathbf{B}_0$. Whistlers turn out to be transverse, so we shall save some algebra by assuming that there is no longitudinal fluctuation, i.e., $\mathbf{k}\cdot\delta\mathbf{V} = 0$. Then we see immediately that there are no density fluctuations, and hence there is no longitudinal electric field, so that we can dispense with both the continuity and Poisson's equations. Eliminating $\delta\mathbf{B}$ using (8.20) leaves:

$$-im\omega\delta\mathbf{V} = q\delta\mathbf{E} + q\delta\mathbf{V}\times\mathbf{B}_0 \tag{8.33}$$

$$\frac{i}{\omega}\mathbf{k}\times(\mathbf{k}\times\delta\mathbf{E}) = \mu_0 q n_0 \delta\mathbf{V} - \frac{i\omega}{c^2}\delta\mathbf{E} \tag{8.34}$$

Note that $\mathbf{k}\times(\mathbf{k}\times\delta\mathbf{E}) = \mathbf{k}(\mathbf{k}\cdot\delta\mathbf{E}) - k^2\delta\mathbf{E} = -k^2\delta\mathbf{E}$. We shall now solve (8.33) for $\delta\mathbf{V}$ and substitute the result into (8.34). To do this, we introduce a coordinate system with $\mathbf{B}_0 = B_0\hat{z}$. The x and y components of (8.33) can be written

$$\begin{pmatrix} -i\omega & -\Omega \\ \Omega & -i\omega \end{pmatrix}\begin{pmatrix} \delta V_x \\ \delta V_y \end{pmatrix} = \frac{q}{m}\begin{pmatrix} \delta E_x \\ \delta E_y \end{pmatrix} \tag{8.35}$$

where $\Omega \equiv qB_0/m$ is the cyclotron frequency. Inverting the matrix of coefficients leads to

$$\begin{pmatrix} \delta V_x \\ \delta V_y \end{pmatrix} = \frac{-q/m}{\omega^2-\Omega^2}\begin{pmatrix} -i\omega & \Omega \\ -\Omega & -i\omega \end{pmatrix}\begin{pmatrix} \delta E_x \\ \delta E_y \end{pmatrix} \tag{8.36}$$

Substituting this into (8.34) and a bit of tidying results in

$$\left(k^2c^2-\omega^2\right)\begin{pmatrix}\delta E_x\\ \delta E_y\end{pmatrix}=\frac{\omega_p^2\omega}{\omega^2-\Omega^2}\begin{pmatrix}-\omega & -i\Omega\\ i\Omega & -\omega\end{pmatrix}\begin{pmatrix}\delta E_x\\ \delta E_y\end{pmatrix} \tag{8.37}$$

which can be cast into a homogeneous linear system of the form

$$\boldsymbol{\mathcal{A}}\cdot\delta\mathbf{E}\equiv\begin{pmatrix}k^2c^2-\omega^2+\dfrac{\omega_p^2\omega^2}{\omega^2-\Omega^2} & \dfrac{+i\omega_p^2\omega\Omega}{\omega^2-\Omega^2}\\ \dfrac{-i\omega_p^2\omega\Omega}{\omega^2-\Omega^2} & k^2c^2-\omega^2+\dfrac{\omega_p^2\omega^2}{\omega^2-\Omega^2}\end{pmatrix}\begin{pmatrix}\delta E_x\\ \delta E_y\end{pmatrix}=\begin{pmatrix}0\\ 0\end{pmatrix} \tag{8.38}$$

where $\boldsymbol{\mathcal{A}}$ is related to the dieletric tensor of the medium. Non-trivial solutions require $\det\boldsymbol{\mathcal{A}}\equiv 0$ from which the dispersion relation can be found. Indeed, the first step can be seen practically by inspection to yield

$$\frac{k^2c^2}{\omega_p^2}-\frac{\omega^2}{\omega_p^2}+\frac{\omega^2}{\omega^2-\Omega^2}=\pm\frac{\omega\Omega}{\omega^2-\Omega^2} \tag{8.39}$$

We now evaluate this in the limit that $\omega^2\ll\omega_p^2$. Ignoring then the second term and multiplying by $(\omega^2-\Omega^2)$ gives a simple quadratic

$$\omega^2\left(1+\frac{k^2c^2}{\omega_p^2}\right)\mp\omega\Omega-\frac{k^2c^2}{\omega_p^2}\Omega^2=0 \tag{8.40}$$

Applying the quadratic formula (note that the $\mp$ sign in the above is independent of that in the quadratic formula), and expanding the result in the long wavelength regime ($k^2c^2/\omega_p^2\ll 1$) yields two different modes (each of which can propagate in either directions so that there are four roots altogether). One is a cylcotron resonance ($\omega=\pm\Omega$) while the other is

Cold Whistler Mode	$\omega=\pm\Omega\dfrac{k^2c^2}{\omega_p^2}\equiv\dfrac{k^2v_A^2}{\Omega}\dfrac{m_i}{m_e}$	(8.41)

Notice that these whistler waves have $\omega\propto k^2$, and so the phase speed ω/k increases with k; shorter wavelength, higher frequency whistler waves travel faster. Moreover, the group velocity $\partial\omega/\partial k$ is faster than this phase velocity (by a factor of 2) and also increases with k. Thus the energy/information carried by a whistler likewise doesn't travel at a single speed. Typically, ionospheric whistlers are excited by lightning and other transient phenomena. This single spike, which is comprised of a range of frequencies, then "disperses" as it travels along the magnetic field.

8.3.3 Other Waves

The derivation of the whistler dispersion relation reveals some of the complexity and richness of waves in plasmas. The more general case, in terms of real multi-fluids (i.e., including ions which participate in the wave motion), is a fascinating subject which is complicated but still manageable. The results can be collected, in the case of cold plasmas at least (i.e., those for which all the thermal pressures are ignorable), into a single diagram, known as the Clemmow-Mullaly-Allis or CMA diagram. This is shown in Figure 8.2. It represents the phase speeds of the various modes under various frequency and plasma regimes in the same way that the Friedrich's Diagram of Figure 4.8 shows the phase fronts of the

MHD waves in an MHD "pond." Indeed, the fast and Alfvén portions of the MHD Friedrichs Diagram can be recognised in the top right portion of Figure 8.2.

Further progress on waves and instabilities involving plasma populations requires abandoning the fluid treatments and commencing with kinetic, Vlasov theory. This is a fascinating subject, with interesting mathematics and physics at each junction, but is beyond the scope of the present course.

8.4 Exercises

1. Starting from the first law of thermodynamics, fill in the derivation of the internal energy equation (8.10) and verify the claim that it reduces to a polytrope with $\gamma = 5/3$ in the absence of heat addition.

2. If the momentum transfer between ions and electrons can be represented by a simple streaming friction, so that $\mathbf{K}_i = \nu_c m_e n(\mathbf{V}_e - \mathbf{V}_i)$, follow the derivation of (8.16) and (8.17) to find an expression for the conductivity σ in terms of the collision frequency ν_c and other constants or parameters.

3. Show that in the general cold multi-stream problem the dispersion relation for purely electric waves in the absence of a magnetic field is

$$\sum_j \frac{\omega_{pj}^2}{(\omega - \mathbf{k}\cdot\mathbf{V}_{j0})^2} = 1 \tag{8.42}$$

4. Fill in the steps from (8.33) leading to the whistler dispersion relation (8.41).

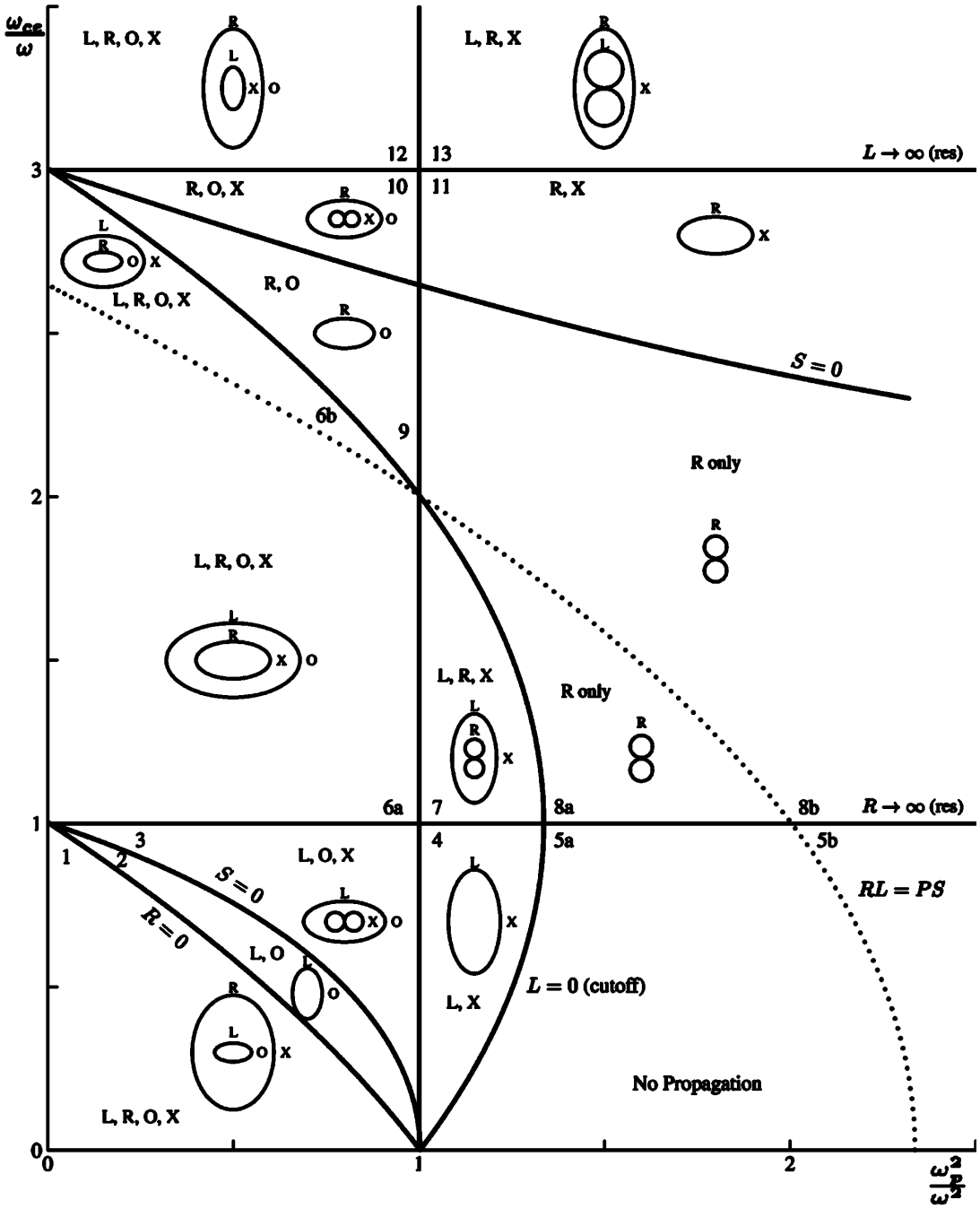

Figure 8.2: Clemmow-Mullaly-Allis (CMA) diagram for waves in a two-fluid, cold plasma. The vertical axis is Ω_e/ω which reveals the magnetic field dependence of the modes, while the horizontal axis is ω_{pe}^2/ω^2, which shows the density dependence. For convenience, an unrealistically small mass ratio m_i/m_e has been chosen to compute this diagram. The space is divided into various regions within which the wave dispersion properties don't change. Within each region are shown figures of constant phase for the different modes propagating in different directions with respect to the background magnetic field. These can be thought of as the ripples made by dropping pebbles into a plasma pond, and extends the Friedrichs Diagram shown in Figure 4.8 to higher frequencies and other regimes. [From www.physics.auburn.edu/ swanson/chap2.pdf]

Appendix A

Useful Mathematical Results and Physical Constants

A.1 Physical Constants

Quantity	symbol	Value
Proton Mass	m_p	1.6726×10^{-27}kg
Electron Mass	m_e	9.1095×10^{-31}kg
Electron-to-proton mass ratio	m_p/m_e	1836.2
Speed of light in vacuum	c	2.9979×10^{8}m/s
Gravitational Constant	G	6.672×10^{-11} N m^2 kg^{-2}
Boltzmann constant	k_b	1.3807×10^{-23}J/K
Electronic charge	e	1.6022×10^{-19}C
Permittivity of free space	ε_0	8.8542×10^{-12}F/m
Permeability of free space	μ_0	$4\pi \times 10^{-7}$H/m
Mass of the Earth	M_E or $M_\oplus$	5.972×10^{24}kg
Radius of the Earth	R_e or R_E	6.3712×10^{6}m
Magnetic Dipole moment of Earth		8×10^{22}A m^2 $= 0.3 \times 10^{-4}$T R_E^3
Surface Magnetic Field of Earth		3×10^{-5}T
Mass of the Sun	$M_\odot$	1.99×10^{30} kg
Radius of the Sun	$R_\odot$	6.96×10^{8}m
Sun-Earth distance	AU	1.50×10^{11}m $= 215 R_\odot$

A.2 Vector Identities

$$\mathbf{A}\cdot\mathbf{B}\times\mathbf{C} = \mathbf{B}\cdot\mathbf{C}\times\mathbf{A} = \mathbf{C}\cdot\mathbf{A}\times\mathbf{B} \tag{A.1}$$

$$\mathbf{A}\times(\mathbf{B}\times\mathbf{C}) = (\mathbf{C}\times\mathbf{B})\times\mathbf{A} = \mathbf{B}(\mathbf{A}\cdot\mathbf{C}) - \mathbf{C}(\mathbf{A}\cdot\mathbf{B}) \tag{A.2}$$

$$\nabla(fg) = f\nabla g + g\nabla f \tag{A.3}$$

$$\nabla\cdot f\mathbf{A} = f\nabla\cdot\mathbf{A} + \mathbf{A}\cdot\nabla f \tag{A.4}$$

$$\nabla\times(f\mathbf{A}) = f\nabla\times\mathbf{A} + \nabla f\times\mathbf{A} \tag{A.5}$$

$$\nabla \cdot (\mathbf{A} \times \mathbf{B}) = \mathbf{B} \cdot \nabla \times \mathbf{A} - \mathbf{A} \cdot \nabla \times \mathbf{B} \tag{A.6}$$

$$\nabla \times (\mathbf{A} \times \mathbf{B}) = \mathbf{A}(\nabla \cdot \mathbf{B}) - \mathbf{B}(\nabla \cdot \mathbf{A}) + (\mathbf{B} \cdot \nabla)\mathbf{A} - (\mathbf{A} \cdot \nabla)\mathbf{B} \tag{A.7}$$

$$\mathbf{A} \times (\nabla \times \mathbf{B}) = (\nabla \mathbf{B}) \cdot \mathbf{A} - (\mathbf{A} \cdot \nabla)\mathbf{B} \tag{A.8}$$

In particular, slightly re-arranged and specialised

$$(\nabla \times \mathbf{B}) \times \mathbf{B} = \mathbf{B} \cdot \nabla \mathbf{B} - \nabla B^2/2 \tag{A.9}$$

$$\nabla (\mathbf{A} \cdot \mathbf{B}) = \mathbf{A} \times (\nabla \times \mathbf{B}) + \mathbf{B} \times (\nabla \times \mathbf{A}) + (\mathbf{A} \cdot \nabla)\mathbf{B} + (\mathbf{B} \cdot \nabla)\mathbf{A} \tag{A.10}$$

$$\nabla \times \nabla f = 0 \tag{A.11}$$

$$\nabla \cdot \nabla \times \mathbf{A} = 0 \tag{A.12}$$

$$\nabla \times (\nabla \times \mathbf{A}) = \nabla (\nabla \cdot \mathbf{A}) - \nabla^2 \mathbf{A} \tag{A.13}$$

A.3 Vector Operators in Various Coordinate Systems

A.3.1 Cartesian Coordinates

In a Cartesian System (x, y, z)

$$\nabla f = \left(\frac{\partial f}{\partial x}, \frac{\partial f}{\partial y}, \frac{\partial f}{\partial z} \right) \tag{A.14}$$

$$\nabla \cdot \mathbf{A} = \frac{\partial f}{\partial x} + \frac{\partial f}{\partial y} + \frac{\partial f}{\partial z} \tag{A.15}$$

$$\nabla \times \mathbf{A} = \left(\frac{\partial A_z}{\partial y} - \frac{\partial A_y}{\partial z}, \frac{\partial A_x}{\partial z} - \frac{\partial A_z}{\partial x}, \frac{\partial A_y}{\partial x} - \frac{\partial A_x}{\partial y} \right) \tag{A.16}$$

$$\nabla^2 f = \frac{\partial^2 f}{\partial x^2} + \frac{\partial^2 f}{\partial y^2} + \frac{\partial^2 f}{\partial z^2} \tag{A.17}$$

A.3.2 Cylindrical Coordinates

In a Cylindrical Polar Coordinate system (r, ϕ, z)

$$\nabla f = \left(\frac{\partial f}{\partial r}, \frac{1}{r}\frac{\partial f}{\partial \phi}, \frac{\partial f}{\partial z} \right) \tag{A.18}$$

$$\nabla \cdot \mathbf{A} = \frac{1}{r}\frac{\partial}{\partial r}(rA_r) + \frac{1}{r}\frac{\partial A_\phi}{\partial \phi} + \frac{\partial A_z}{\partial z} \tag{A.19}$$

$$\nabla \times \mathbf{A} = \left(\frac{1}{r}\frac{\partial A_z}{\partial \phi} - \frac{\partial A_\phi}{\partial z}, \frac{\partial A_r}{\partial z} - \frac{\partial A_z}{\partial r}, \frac{1}{r}\frac{\partial}{\partial r}\left(rA_\phi\right) - \frac{1}{r}\frac{\partial A_r}{\partial \phi} \right) \tag{A.20}$$

$$\nabla^2 f = \frac{1}{r}\frac{\partial}{\partial r}\left(r\frac{\partial f}{\partial r} \right) + \frac{1}{r^2}\frac{\partial^2 f}{\partial \phi^2} + \frac{\partial^2 f}{\partial z^2} \tag{A.21}$$

A.3.3 Spherical Polar Coordinates

In a spherical polar coordinate system (r, θ, ϕ)

$$\nabla f = \left(\frac{\partial f}{\partial r}, \frac{1}{r}\frac{\partial f}{\partial \theta}, \frac{1}{r\sin\theta}\frac{\partial f}{\partial \phi} \right) \tag{A.22}$$

$$\nabla \cdot \mathbf{A} = \frac{1}{r^2}\frac{\partial}{\partial r}\left(r^2 A_r\right) + \frac{1}{r\sin\theta}\frac{\partial}{\partial \theta}\left(A_\theta \sin\theta\right) + \frac{1}{r\sin\theta}\frac{\partial A_\phi}{\partial \phi} \tag{A.23}$$

$$\nabla \times \mathbf{A} = \left(\frac{1}{r\sin\theta}\frac{\partial}{\partial \theta}\left(A_\phi \sin\theta\right) - \frac{1}{r\sin\theta}\frac{\partial A_\theta}{\partial \phi}, \frac{1}{r\sin\theta}\frac{\partial A_r}{\partial \phi} - \frac{1}{r}\frac{\partial}{\partial r}\left(rA_\phi\right), \frac{1}{r}\frac{\partial}{\partial r}\left(rA_\theta\right) - \frac{1}{r}\frac{\partial A_r}{\partial \theta} \right) \tag{A.24}$$

$$\nabla^2 f = \frac{1}{r^2}\frac{\partial}{\partial r}\left(r^2\frac{\partial f}{\partial r} \right) + \frac{1}{r^2\sin\theta}\frac{\partial}{\partial \theta}\left(\sin\theta\frac{\partial f}{\partial \theta} \right) + \frac{1}{r^2\sin^2\theta}\frac{\partial^2 f}{\partial \phi^2} \tag{A.25}$$

$$\begin{aligned} (\mathbf{A}\cdot\nabla)\mathbf{B} = & \left[A_r\frac{\partial B_r}{\partial r} + \frac{A_\theta}{r}\frac{\partial B_r}{\partial \theta} + \frac{A_\phi}{r\sin\theta}\frac{\partial B_r}{\partial \phi} - \frac{A_\theta B_\theta + A_\phi B_\phi}{r} \right]\hat{r} \\ & + \left[\frac{A_\theta B_r}{r} + A_r\frac{\partial B_\theta}{\partial r} + \frac{A_\theta}{r}\frac{\partial B_\theta}{\partial \theta} + \frac{A_\phi}{r\sin\theta}\frac{\partial B_\theta}{\partial \phi} - \frac{A_\phi B_\phi}{r}\cot\theta \right]\hat{\theta} \\ & + \left[\frac{A_\phi B_r}{r} + \frac{A_\phi B_\theta}{r}\cot\theta + A_r\frac{\partial B_\phi}{\partial r} + \frac{A_\theta}{r}\frac{\partial B_\phi}{\partial \theta} + \frac{A_\phi}{r\sin\theta}\frac{\partial B_\phi}{\partial \phi} \right]\hat{\phi} \end{aligned} \tag{A.26}$$

Appendix B

The Mathematics of Waves

B.1 Fourier Analysis

Many branches of physics involve the study of wave properties of the media in question. These waves illustrate the way the various restoring forces in the medium manifest themselves in the dynamics. In the case of linearised equations of motion, the resulting perturbations can always be broken down into any convenient summation of linear modes. Particularly convenient and common is the use of Fourier techniques to represent the disturbance as a linear superposition of harmonic plane waves.

In the case of a simple function of time $g(t)$, Fourier's theorem enables us to re-write this in terms of a Fourier Series as:

$$g(t) = \frac{a_0}{2} + \sum_{n=1}^{\infty} a_n \cos 2n\pi t/\tau + b_n \sin 2n\pi t/\tau \tag{B.1}$$

where

$$\left\{ \begin{array}{c} a_n \\ b_n \end{array} \right\} = \frac{2}{\tau} \int_{-\tau/2}^{+\tau/2} g(t) \left\{ \begin{array}{c} \cos 2n\pi t/\tau \\ sin 2n\pi t/\tau \end{array} \right\} dt \tag{B.2}$$

where τ is time interval under consideration. The a_n's and b_n's give the amplitude of the nth harmonic of the fundamental period τ, i.e., at a frequency $f_n = n/\tau$.

If we let the time interval τ get larger and larger, the interval between successive modes gets smaller and smaller. In the limit as $\tau \to \infty$ the discrete sum in Equation (B.1) gets replaced by an integral which defines what is known as the Fourier transform

$$g(t) = \frac{1}{\sqrt{2\pi}} \int_{-\infty}^{+\infty} \tilde{g}(\omega) e^{-i\omega t} d\omega \tag{B.3}$$

where now the Fourier transform $\tilde{g}(\omega)$ is

$$\tilde{g}(\omega) = \frac{1}{\sqrt{2\pi}} \int_{-\infty}^{+\infty} g(t) e^{i\omega t} dt \tag{B.4}$$

Now $\tilde{g}(\omega)$ provides the (differential) amplitude of the disturbance at an angular frequency $\omega \equiv 2\pi f$. Note that in this continuous frequency approach for the decomposition of $g(t)$ there is a certain degree of arbitrariness in the normalisation of $\tilde{g}$ and other treatments may write the above with the factor 2π distributed differently between the transform and its inverse. Additionally, traditional mathematical treatments use the opposite sign convention for ω in the exponential functions. The above is used here to reinforce the physics convention that propagating waves have a time dependence $\propto e^{-i\omega t}$.

The power of Fourier analysis lies in the fact that it is complete, in the sense that any (integrable) function $g(t)$ can be decomposed into its Fourier components in a unique way, and the resulting Fourier series/transform converges to $g(t)$ everywhere except at places where $g(t)$ is discontinuous. Moreover,

differentiating $g(t)$ with respect to t merely multiplies the integrand in Equation (B.3) by $-i\omega$, so that time derivatives become algebraic multiplications in the frequency domain. Thus, for example, the equation

$$\frac{dg}{dt} = h(t) \tag{B.5}$$

can be Fourier transformed to give:

$$\int_{-\infty}^{+\infty} -i\omega\tilde{g}e^{-i\omega t}d\omega = \int_{-\infty}^{+\infty} \tilde{h}e^{-i\omega t}d\omega \tag{B.6}$$

But since the complex exponential functions are complete and orthogonal, this requires simply

$$-i\omega\tilde{g} = \tilde{h} \tag{B.7}$$

thereby enabling the original differential equation to be solved algebraically for each Fourier component.

B.2 Waves in Space and Time: 1D

B.2.1 Phase Speeds

Fourier techniques can be applied to good advantage in the study of waves which propagate in space as well as oscillating in time. In one dimension we have:

$$g(x,t) = \int_{-\infty}^{+\infty}\int_{-\infty}^{+\infty} \tilde{g}(k,\omega)e^{i(kx-\omega t)}d\omega\,dk \tag{B.8}$$

where $k = 2\pi/\lambda$ is the wavenumber of the wave, whose wavelength (distance between wave crests) is λ. It is customary to define the k-dependence with the opposite sign convention to that used for ω so that points of constant wave phase have

$$\text{phase} = kx - \omega t = \text{constant} \tag{B.9}$$

For example, points at phase = 0 satisfy $kx - \omega t = 0$, or

$$x - \frac{\omega}{k}t \equiv x - v_{ph}t = 0 \tag{B.10}$$

where obviously

$$\boxed{\text{Phase Speed} \qquad v_{ph} = \frac{\omega}{k}} \tag{B.11}$$

is the wave phase speed. In terms of the wavelength λ, period T, and frequency f we have

$$v_{ph} = \frac{\omega}{k} = \frac{2\pi f}{2\pi/\lambda} = \lambda f = \frac{\lambda}{T} \tag{B.12}$$

which simply says that a wave travels one wavelength in one period.

B.2.2 Group Speed

For simple waves, the phase speed also represents the speed at which information and/or energy are transported by the waves. This is the case for "non-dispersive" media, in which v_{ph} is a constant (independent of the wavelength or frequency). In dispersive media, however, the phase speed can be very different from the speed of information transport. Since we are considering cases where ω/k are not constant, there will be some relationship between the wave angular frequency and wavenumber which is known as the dispersion relation. For convenience we denote this as

$$\omega = \omega(k) \tag{B.13}$$

although there may be occasions where the dispersion in time is more relevant, and one might consider $k = k(\omega)$ as the dependent variable.

We now construct a wavepacket which is localised in space and seek to determine not only the propagation of the points of constant phase, but also the displacement of the bulk of the wave amplitude. Such a packet is constructed from a set of wavenumbers within an interval Δk of some central wavenumber k_0, so that

$$g(x,t) = \int_{-\infty}^{+\infty} A(k) e^{i(kx-\omega(k)t)} dk \tag{B.14}$$

where $A(k)$ is a function peaked at k_0, and we have used the dispersion relation to perform the integration over ω, which merely picks out the ω satisfying $\omega = \omega(k)$. Notice that at $t = 0$ the envelope of the wave packet can be found by re-writing the above as

$$g(x,t=0) = e^{ik_0 x} \int_{-\infty}^{+\infty} A(k) e^{i(k-k_0)x} dk \tag{B.15}$$

The pure exponential outside the integral is the "carrier" wave, while the integral gives the shape of the envelope which modulates these oscillations. We take advantage of the form of $A(k)$ by expanding $\omega(k)$ about k_0, so that

$$kx - \omega(k)t \approx (k-k_0)x + k_0 x - \omega(k_0)t - \left.\frac{d\omega}{dk}\right|_{k_0} (k-k_0)t \tag{B.16}$$

$$= (k_0 x - \omega_0 t) + (k-k_0)\left(x - \frac{d\omega}{dk} t\right) \tag{B.17}$$

where $\omega_0 \equiv \omega(k_0)$. We define the group speed by

$$\boxed{\text{Group Speed} \qquad v_g = \frac{d\omega}{dk}} \tag{B.18}$$

Thus our disturbance obeys

$$g(x,t) = e^{i(k_0 x - \omega_0 t)} \int_{-\infty}^{+\infty} A(k) e^{i(k-k_0)(x-v_g t)} dk \tag{B.19}$$

Comparing this with Equation (B.15) shows that the phase oscillations of the carrier propagate as expected at the phase speed ω_0/k_0 from the part in front of the integral. This is a totally *un*-localised wave. Inside the integral is the envelope of these oscillations. This envelope is just that found in (B.15) but evaluated at $x - v_g t$ instead of x; that is, the envelope moves at a speed v_g.

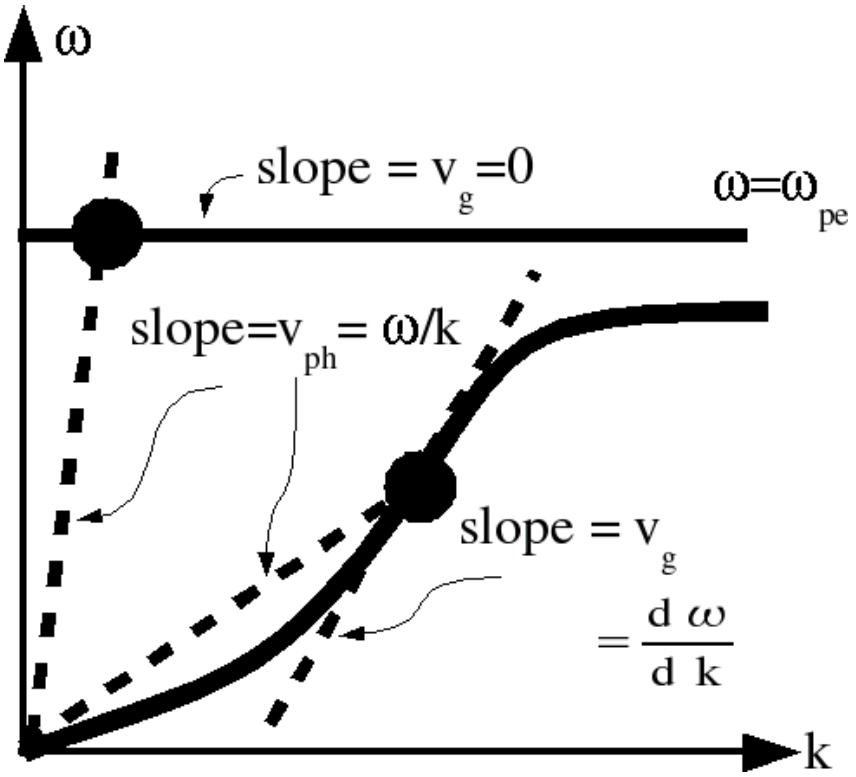

Figure B.1: Dispersion curves (solid) for plasma oscillations ($\omega = \omega_{pe} = \text{const}$) and whistler waves showing the corresponding phase and group speeds at specific (ω, k) points (filled circles).

For simple waves, such as light or sound waves in an ordinary gas, the dispersion relation is of the form

$$\omega = kc \tag{B.20}$$

and both the phase and group speeds are equal to c. In more complicated media, this is no longer the case. Consider the case of plasma oscillations introduced in Section 2.5.1 for which

$$\omega(k) = \omega_{pe} \tag{B.21}$$

Since ω_{pe} is a constant, the phase speed is simply $v_{ph} = \omega_{pe}/k$ and increases with decreasing k. As $k \to 0$ this phase speed can exceed the speed of light! However, this represents nothing more than the phasing between oscillations in neighbouring plasma regions, as though there were a set of pendulums suspended along a line. The speed with which a displacement appears to move along the line is determined only by the initial phases of the individual pendulums; no information nor energy is transferred from one to the other.

By contrast, for such plasma oscillations, the group speed is $v_g = \frac{d\omega_{pe}}{dk} = 0$. No information is transferred through the medium. A local set of oscillators continue to oscillate in place and do not send any signals beyond their locations. These properties are often illustrated by means of a dispersion diagram ω vs. k. The slope of the line from the origin to the relevant point on the dispersion curve $\omega(k)$ gives the phase speed $v_{ph} = \omega/k$ while the slope of tangent to the curve at that point is the group speed. These are illustrated in Figure B.1.

B.2.3 Waves in 3D

The analysis in the preceding sections is readily extended to the analysis of plane waves in three dimensions by the specification of three wavenumbers along the three cartesian directions, i.e., $\mathbf{k} = (k_x, k_y, k_z)$. Now our archetypal wave has disturbances which propagate according to

$$e^{i(\mathbf{k}\cdot\mathbf{x}-\omega t)} \tag{B.22}$$

where $\mathbf{x} = (x, y, z)$. The vector $\mathbf{k}$ is known as the wavevector. Points which have the same value of $\mathbf{k}\cdot\mathbf{x}$ at a given instant have the same phase, so $\mathbf{k}$ is directed perpendicular to the wave phase fronts and has a magnitude equal to 2π over the distance between successive fronts, i.e., $|\mathbf{k}| = 2\pi/\lambda$. In these cases the phase velocity $\mathbf{v_{ph}}$ is now a vector. Only the component along $\mathbf{k}$ is unique, since adding any velocity along the planar wave front yields a phase pattern which is indistinguishable from any other. Thus it is customary to think of $\mathbf{v_{ph}}$ as being directed along $\mathbf{k}$ so that

Phase Velocity	$\mathbf{v_{ph}} = \dfrac{\omega}{\lvert\mathbf{k}\rvert}\dfrac{\mathbf{k}}{\lvert\mathbf{k}\rvert}$	(B.23)

while the group velocity is now

Group Velocity	$\mathbf{v_g} = \dfrac{\partial\omega}{\partial\mathbf{k}}$	(B.24)

which is uniquely defined.

For example, an Alfvén wave propagating in a uniform medium in which the background magnetic field lies along the $\hat{z}$ direction has a dispersion relation given by

$$\omega(k) = k_z v_A \tag{B.25}$$

where v_A is a constant (see Equation (4.59)). For such waves, the phase velocity, as depicted in the Friedrichs diagram shown in Figure 4.8, is

$$\mathbf{v_{ph}} = \omega\frac{\mathbf{k}}{|\mathbf{k}|^2} = v_A\frac{k_z\mathbf{k}}{|\mathbf{k}|^2} \tag{B.26}$$

The phase velocity goes to zero at perpendicular propagation, and is less than the Alfvén speed unless $\mathbf{k}$ is aligned with the magnetic field.

On the other hand, the group velocity in this case is

$$\begin{aligned}
\mathbf{v_g} &= \frac{\partial\omega}{\partial\mathbf{k}} && \text{(B.27)}\\
&= \left(\frac{\partial k_z v_A}{\partial k_x}, \frac{\partial k_z v_A}{\partial k_y}, \frac{\partial k_z v_A}{\partial k_z}\right) && \text{(B.28)}\\
&= (0, 0, v_A) && \text{(B.29)}
\end{aligned}$$

showing that, regardless of the direction of $\mathbf{k}$, the energy transport in an Alfvén wave is always purely along the magnetic field at the Alfvén speed.

Index